Master's thesis

NTNU
Norwegian University of Science and Technology
Faculty of Natural Sciences
Department of Biomedical Laboratory Science

Lars Føleide

# Inducible CRISPR/dCas9 Targeting of CTCF-Associated Regulatory Sites Reduces MYC Expression in HCT116 Colorectal Cancer Cells

Master's thesis in Molecular Medicine
Supervisor: Kai Sandvold Beckwith
May 2026

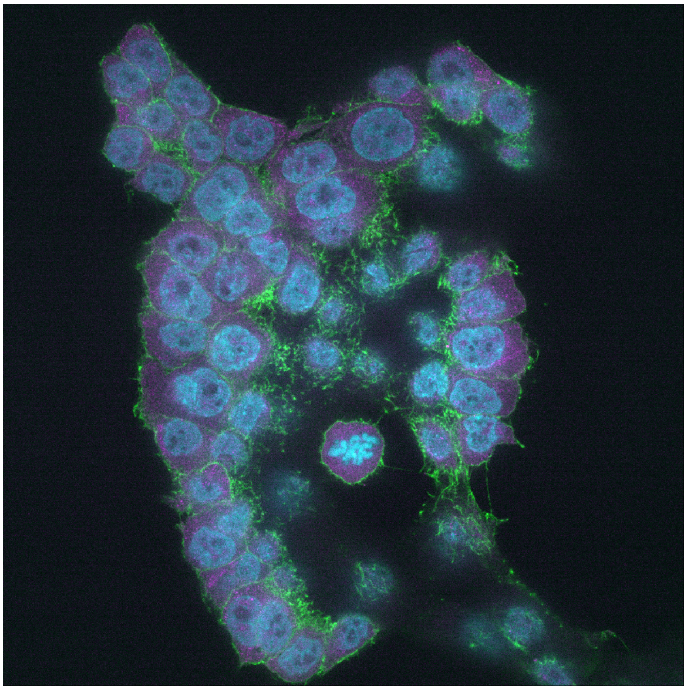

Fluorescence microscopy image of HCT116 colorectal cancer cells from the smRNA-FISH workflow, showing MYC RNA-FISH signal in magenta.

NTNU
Norwegian University of
Science and Technology

Lars Føleide

# Inducible CRISPR/dCas9 Targeting of CTCF-Associated Regulatory Sites Reduces MYC Expression in HCT116 Colorectal Cancer Cells

Master's thesis in Molecular Medicine
Supervisor: Kai Sandvold Beckwith
May 2026

Norwegian University of Science and Technology
Faculty of Natural Sciences
Department of Biomedical Laboratory Science

NTNU
Norwegian University of
Science and Technology

## Abstract

Three-dimensional genome organization contributes to gene regulation by shaping long-range enhancer–promoter communication. CTCF plays a central role in this process, but the functions of individual binding sites are difficult to test because global depletion affects thousands of sites simultaneously, whereas genomic deletion is irreversible and can introduce clonal artifacts. This thesis tested whether inducible CRISPR/dCas9 targeting of selected CTCF-associated regulatory sites at the MYC locus reduces MYC expression in HCT116 colorectal cancer cells, and whether any expression changes are accompanied by detectable changes in CTCF occupancy. The intended mechanism was steric interference with local CTCF function, but CTCF displacement was tested directly rather than assumed from downstream MYC expression changes.

An inducible dCas9-only platform was established in HCT116 cells using dual doxycycline/Shield-1 control. Single-guide RNAs were designed against a promoter-proximal CTCF-associated docking site near MYC and a distal CTCF-associated site within the broader 8q24 regulatory landscape. Bulk RT-qPCR, single-cell RNA-FISH, and CTCF ChIP-qPCR were combined to assess transcriptional output and target-site occupancy in the original H100 platform population and in a FACS-derived BFP-enriched subpopulation.

Guide-associated reductions in MYC output were identified across selected contexts and readouts. H100 RT-qPCR supported MYC-lowering patterns for guides A and D, although normalized effect sizes were interpreted cautiously because NT and reference-gene shifts affected fold-change estimates. RNA-FISH provided the strongest orthogonal expression-level support, showing reduced per-cell MYC for guides B and D in the FACS-derived population and for guide A and rescued guide D in H100. Direct CTCF ChIP-qPCR at the mapped promoter-proximal `mycP_CTCF` and distal `0SE_CTCF` assays did not detect guide-specific CTCF loss. Because the ChIP-qPCR runs were single-replicate, smaller or cell-heterogeneous occupancy changes could not be excluded.

Overall, this work establishes an inducible dCas9 framework for interrogating CTCF-associated regulation at MYC. The thesis supports expression-level perturbation of MYC by inducible dCas9 targeting of CTCF-associated regulatory sites, but does not validate the originally hypothesized steric CTCF-displacement mechanism. Direct dCas9 ChIP-qPCR at the guide target sites is therefore identified as the priority follow-up experiment needed to resolve the upstream target-engagement step.



**Keywords:** CRISPR/dCas9; CTCF; MYC; chromatin architecture; enhancer–promoter regulation; HCT116 colorectal cancer cells; RT-qPCR; ChIP-qPCR; RNA-FISH

# Contents

# Abbreviations

| Abbreviation | Full term |
|---|---|
| 8q24 | Cytogenetic band 8q24, the chromosomal region containing MYC and its distal regulatory landscape |
| A260, A280, A230 | NanoDrop absorbance readings at 260, 280, and 230 nm |
| AfeI | Type II restriction endonuclease (recognition site AGCGCT) |
| AgeI | Type II restriction endonuclease (recognition site ACCGGT) |
| ATP | Adenosine triphosphate |
| B2M | Beta-2-microglobulin (alternative qPCR reference gene) |
| BbsI / BpiI | Type IIS restriction endonuclease (used for sgRNA scaffold linearization) |
| BFP | Blue fluorescent protein (platform-positive cell marker) |
| BSA | Bovine serum albumin |
| CBS | CTCF binding site |
| CCAT1 / CCAT1-L | Colon cancer-associated transcript 1 / long isoform |
| CFD | Cutting Frequency Determination (CRISPOR specificity score) |
| ChIP | Chromatin immunoprecipitation |
| ChIP-qPCR | Chromatin immunoprecipitation followed by quantitative PCR |
| ConcA | Concanavalin A (membrane label used for RNA-FISH segmentation) |
| CRISPR | Clustered regularly interspaced short palindromic repeats |
| CRISPRd | CRISPR disruption (steric blocking by dCas9 without an effector) |
| CRISPRi | CRISPR interference |
| CRISPRoff | CRISPR-based heritable gene silencing via dCas9-DNMT3A-DNMT3L-KRAB |
| CTCF | CCCTC-binding factor |
| Cq | Quantification cycle (qPCR) |
| dCas9 | Catalytically inactive (dead) Cas9 |
| DAPI | 4',6-diamidino-2-phenylindole (nuclear counterstain) |
| dCq | Delta Cq (Cq target − Cq reference) |
| ddCq | Delta-delta Cq (dCq plus − dCq minus) |
| DD | Destabilization domain (FKBP12-derived; Shield-1-controlled) |
| DMEM | Dulbecco's Modified Eagle Medium |
| DNA | Deoxyribonucleic acid |
| DNMT3A / DNMT3L | DNA methyltransferase 3A / 3L (CRISPRoff effector elements) |
| Doench'16 | Doench-Root 2016 on-target activity score (CRISPOR) |
| dox | Doxycycline |
| DTT | Dithiothreitol |
| Eco32I | Type II restriction endonuclease (isoschizomer of EcoRV; site GATATC) |
| EDTA | Ethylenediaminetetraacetic acid |

| Abbreviation | Full term |
|---|---|
| FACS | Fluorescence-activated cell sorting |
| FC | Fold change |
| FBS | Fetal bovine serum |
| FKBP12 | FK506-binding protein 12 (degron parent protein for Shield-1) |
| FOV | Field of view (one microscope image position / stack in RNA-FISH analysis) |
| FSC-A / FSC-H | Forward scatter area / height (flow cytometry gating) |
| GAPDH | Glyceraldehyde-3-phosphate dehydrogenase (positive-control region for ChIP) |
| gDNA | Genomic DNA |
| H3K9me3 | Histone H3 trimethylated at lysine 9 |
| HCT116 | Human colorectal carcinoma cell line 116 |
| hg19, hg38 | Human reference genome assemblies (Genome Reference Consortium GRCh37 and GRCh38) |
| Hi-C | High-throughput chromosome conformation capture |
| hyPBase | Hyperactive PiggyBac transposase |
| IDT | Integrated DNA Technologies (oligonucleotide vendor) |
| IF | Immunofluorescence |
| IgG | Immunoglobulin G (negative-control IP) |
| IP | Immunoprecipitation |
| JASPAR | Open-access database of curated transcription-factor binding motifs |
| KpnI | Type II restriction endonuclease (recognition site GGTACC) |
| KRAB | Krüppel-associated box (transcriptional repressor domain) |
| LB | Luria-Bertani / lysogeny broth (bacterial growth medium) |
| lncRNA | Long non-coding RNA |
| MeCP2 | Methyl CpG-binding protein 2 (effector domain in PB-TRE-dCas9-Zim3-MeCP2) |
| MIT (specificity score) | MIT specificity score for sgRNA off-target risk |
| MNase | Micrococcal nuclease |
| mRNA | Messenger RNA |
| MYC | MYC proto-oncogene; central transcription factor at chromosome 8q24 |
| NEB | New England Biolabs |
| NRT | No-reverse-transcriptase control (RT-qPCR) |
| NT | Non-targeting (control sgRNA) |
| NTC | No-template control |
| OSE | Oncogenic super-enhancer |
| PAM | Protospacer-adjacent motif |
| PB | PiggyBac (transposon-compatible vector prefix) |

| Abbreviation | Full term |
|---|---|
| PBS | Phosphate-buffered saline |
| PCR | Polymerase chain reaction |
| PFA | Paraformaldehyde |
| PiggyBac | PiggyBac transposon system for stable transgene integration |
| Pol II | RNA polymerase II |
| qPCR | Quantitative polymerase chain reaction |
| RNA | Ribonucleic acid |
| RNA-FISH | RNA fluorescence in situ hybridization |
| rpm | Revolutions per minute |
| RT | Reverse transcription / room temperature (context-dependent) |
| RT-qPCR | Reverse transcription quantitative PCR |
| ScaI | Type II restriction endonuclease (recognition site AGTACT) |
| SD | Standard deviation |
| sgRNA | Single guide RNA |
| Shield-1 | Small-molecule stabilizer of the FKBP12 destabilization domain |
| SmaI | Type II restriction endonuclease (recognition site CCCGGG) |
| smRNA-FISH | Single-molecule RNA fluorescence in situ hybridization |
| SNR | Signal-to-noise ratio |
| TAD | Topologically associating domain |
| tagBFP | Tag blue fluorescent protein (used in CRISPRoff and the dCas9-Only platform) |
| TBE | Tris/Borate/EDTA buffer |
| Tet-On | Tetracycline-inducible expression system activated by doxycycline |
| TRE | Tetracycline response element |
| TSS | Transcription start site |
| WNT | Wingless/Int1 signaling pathway |
| YWHAZ | Tyrosine 3-monooxygenase/tryptophan 5-monooxygenase activation protein zeta (qPCR reference gene) |
| Zim3 | KRAB-domain protein used in the parental dCas9-Zim3-MeCP2 effector |

# List of Figures

# List of Tables

# 1 Introduction

## 1.1 Gene regulation is organized in three dimensions

Gene expression in mammalian cells is controlled by regulatory DNA elements such as promoters, enhancers, silencers, and insulators that operate within the physical constraints of chromatin packaged into the nucleus. While the linear genome provides the sequence "parts list," many regulatory decisions depend on three-dimensional (3D) proximity: enhancers can activate promoters over long genomic distances, and spatial genome folding can both facilitate and prevent such contacts.

High-throughput chromosome conformation capture methods (e.g., Hi-C) have revealed that genomes are partitioned into hierarchical structures. At megabase scales, chromosomes segregate into active and inactive compartments. At smaller scales, chromatin is organized into topologically associating domains (TADs), within which regulatory interactions are enriched and across which interactions are comparatively depleted (Dixon et al., 2012; Rao et al., 2014). These features provide a structural framework that helps explain how enhancers can act selectively on their target genes while limiting "off-target" activation of nearby genes.

A useful conceptual model is that 3D genome architecture acts as a moderator of chromosomal communication: it shapes the probability that any given enhancer and promoter will meet in space and therefore modulates transcriptional output (Dekker & Mirny, 2016). The resulting regulatory logic is particularly important at loci containing dense enhancer landscapes, where many potential enhancer–promoter pairings exist but only a subset are productive in a given cell type.

## 1.2 TADs, loops, and the loop extrusion model

Two prominent features observed in Hi-C maps are (i) TADs and (ii) focal chromatin loops. Many loops and TAD boundaries are enriched for binding sites of the architectural protein CCCTC-binding factor (CTCF) and for cohesin, a ring-shaped protein complex best known for its role in sister chromatid cohesion.

Mechanistic work and polymer modeling have converged on the loop extrusion model as a parsimonious explanation for TAD and loop formation. In this model, cohesin loads onto chromatin and enlarges loops by translocating along DNA until it is stalled by boundary elements. CTCF is a key boundary factor because it can halt extrusion in an orientation-dependent manner, producing corner peaks in contact maps that correspond to stable loops (Fudenberg et al., 2016; Sanborn et al., 2015). Consistent with this, the polarity of CTCF motifs strongly influences loop anchors: convergently oriented motifs preferentially form loop pairs, whereas altering motif orientation can rewire looping patterns (de Wit et al., 2015).

Together, these findings link sequence-defined binding sites to genome folding and, by extension, to gene regulation. Importantly, the presence of a loop or boundary does not guarantee a particular transcriptional outcome. Rather, architecture changes the odds that regulatory elements can find each other, creating an additional layer of control that can buffer or amplify signals depending on cellular context.

## 1.3 CTCF as a multifunctional architectural protein

CTCF is a ubiquitously expressed zinc-finger protein with diverse roles in transcription and genome organization. Three roles are particularly relevant to the work in this thesis. First, CTCF mediates *insulation and boundary formation* by stalling cohesin-mediated loop extrusion and anchoring the boundaries of topologically associating domains, thereby limiting enhancer activity to appropriate target promoters. Second, it supports *promoter and enhancer organization* by participating in long-range loops that bring distal regulatory elements into productive proximity with their target genes. Third, its function is *context-dependent*: CTCF binding sites can be constitutive or cell-type-specific, and their occupancy can vary with developmental stage, signaling state, or disease, giving genome architecture a dynamic sensitivity to cellular context.

CTCF binding is also sensitive to local sequence and epigenetic state. Classical work at imprinted loci demonstrated that DNA methylation can disrupt boundary function, enabling changes in enhancer access and gene expression programs (Bell & Felsenfeld, 2000). This methylation sensitivity is relevant to cancer, where altered methylation patterns can modify CTCF occupancy, weaken insulation, and contribute to aberrant enhancer-promoter rewiring.

## 1.4 MYC as a central oncogenic transcription factor

The MYC proto-oncogene encodes a transcription factor that regulates broad gene programs involved in growth, metabolism, ribosome biogenesis, and cell-cycle progression. Consequently, dysregulated MYC activity is a common feature of aggressive cancers and is often associated with poor prognosis (Dang, 2012). Unlike many oncogenes that are frequently mutated in their coding sequence, MYC is often deregulated through changes in its regulatory landscape, including copy number amplification and enhancer activation.

A major challenge in understanding and therapeutically targeting MYC is that its expression is controlled by large, complex noncoding regions. The MYC locus resides within a sizable regulatory neighborhood (often described as an extended domain around 8q24) that can harbor cancer-associated enhancers and super-enhancers. Super-enhancers are clusters of enhancers with unusually high levels of transcriptional co-activators and chromatin marks, and they are frequently

associated with genes that control cell identity and disease states (Hnisz et al., 2013; Whyte et al., 2013). In cancers, acquisition or activation of super-enhancers can drive high MYC expression without altering the MYC coding region.

For this thesis, MYC is therefore not only an oncogenic endpoint but also a mechanistically useful locus for testing whether perturbation of selected CTCF binding sites can shift enhancer communication and measurable transcriptional output.

## 1.5 The MYC locus as a model for enhancer–promoter specificity

The two CTCF sites perturbed in this thesis sit within the broader 8q24 regulatory landscape and are described in turn in the subsections that follow. Their relative positions and the targeting strategy of the four guides (A, B, D, NT) are summarized in Figure 1.1. Because CTCF-mediated looping depends on motif orientation and local anchor context (§1.2), guide placement relative to the CTCF motif is central to the experimental logic rather than a purely technical design detail.

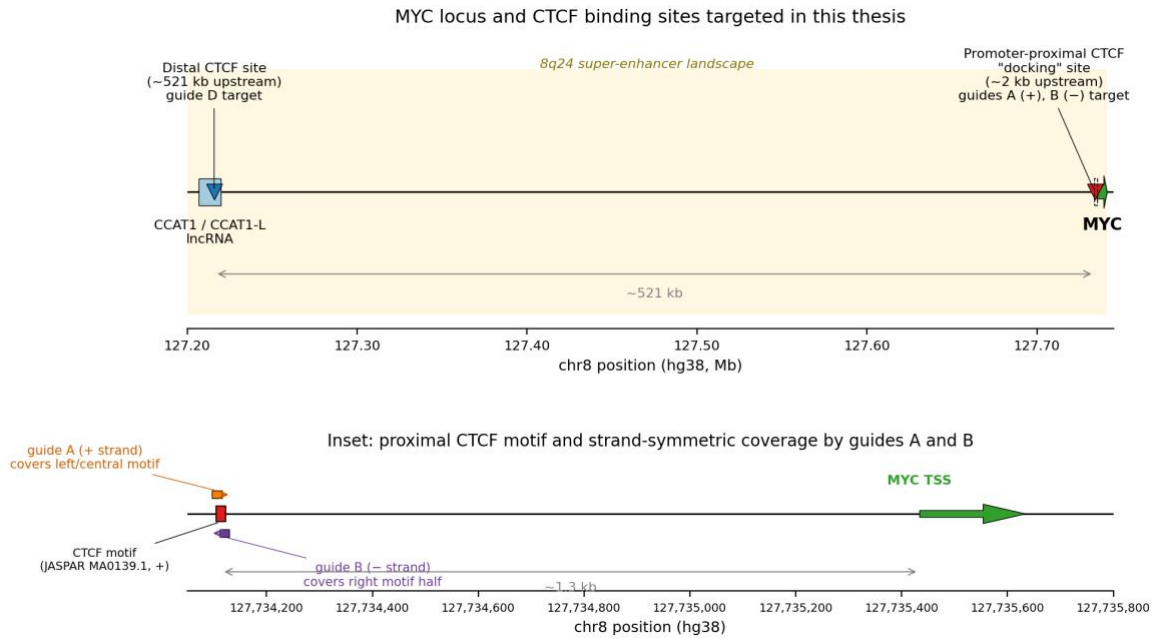


**Figure 1.1.** Schematic of the MYC locus and the CTCF binding sites targeted in this thesis (hg38 coordinates). Top: ~540 kb view of the 8q24 region around MYC. The promoter-proximal CTCF "docking" site (red triangle, ~2 kb upstream of MYC) is targeted by guides A and B. The distal CTCF site (blue triangle, ~521 kb upstream of MYC) lies near the long non-coding RNA *CCAT1* (colon cancer-associated transcript 1) and its long isoform CCAT1-L, and is targeted by guide D. The shaded region indicates the broader 8q24 super-enhancer landscape. The dashed rectangle marks the inset shown below. Bottom: zoom of the proximal CTCF site (JASPAR MA0139.1 motif at chr8:127,734,105–127,734,123, +). Guide A (orange, plus strand) covers the left/central portion of the motif; guide B (purple, minus strand) covers the right portion from the opposite strand, so the two guides tile the motif with strand-symmetric coverage. The motif center sits ~1.3 kb upstream of the MYC transcription start site (TSS, green). The non-targeting control guide (NT) is not shown.

### 1.5.1 Long-range regulation and the 8q24 gene desert

In colorectal cancer and other malignancies, MYC can be regulated by distal enhancer regions located hundreds of kilobases to megabases away. A well-studied contributor is the CCAT1/CCAT1-L locus, located approximately 0.5 Mb upstream of MYC, which is transcribed in colorectal cancer and participates in long-range chromatin interactions at 8q24 (Xiang et al., 2014). This region also harbors the distal CTCF site that guide D was designed to target in this thesis (§1.5.3, Figure 1.1). Such distal regions illustrate a common theme: noncoding transcription, enhancer activity, and chromatin looping can be intertwined in establishing an oncogenic regulatory state.

### 1.5.2 A promoter-proximal CTCF "docking" site for diverse cancer enhancers

A key insight relevant to this thesis is that distinct cancer-specific enhancer elements can converge on a shared architectural mechanism for engaging MYC. Using a comparative approach across multiple cancer models, Schuijers and colleagues identified a CTCF binding site approximately 2 kb upstream of the MYC promoter that functions as a shared "enhancer-docking" site (Schuijers et al., 2018). In their model, diverse super-enhancers within the MYC regulatory domain interact with the MYC gene through this conserved promoter-proximal CTCF site. This suggests that certain CTCF sites can act as regulatory hubs that integrate multiple enhancer inputs.

This promoter-proximal site is directly relevant to the present work, because guides A and B were designed against this docking region.

Complementary evidence comes from acute, global depletion strategies. Rapid loss of CTCF can disrupt enhancer–promoter looping at MYC and alter its regulatory contacts, emphasizing that CTCF contributes to maintaining specific long-range interactions at this locus (Hyle et al., 2019; Nora et al., 2017). Together, these studies support the idea that CTCF is not only an insulating boundary factor but can also participate in wiring enhancer communication to a key oncogene.

### 1.5.3 Noncanonical CTCF functions and signaling dependence

CTCF's contribution to MYC regulation may extend beyond static looping. In HCT116 colorectal cancer cells, a distal CTCF site embedded within an oncogenic super-enhancer (OSE) region has been shown to "gate" MYC output in response to canonical WNT signaling, through a mechanism involving nuclear periphery positioning and mRNA export (Chachoua et al., 2022). Notably, in this context, disrupting the CTCF motif did not necessarily abolish physical enhancer–promoter contact, underscoring that CTCF can influence gene output via additional layers of regulation.

A recent preprint further extends this model by proposing that the same distal CTCF site coordinates CCAT1 expression and MYC gating within a negative feed-forward circuit that increases cell-to-cell MYC expression heterogeneity, suggesting that this site may regulate not only average MYC output but also expression plasticity across the population (Gao et al., 2026).

This signaling-linked distal logic provides the main biological rationale for guide D in the present work. Unlike guides A and B, which were aimed at the promoter-proximal docking site, guide D was designed against a CTCF-associated site approximately 521 kb upstream of MYC in order to test a mechanistically distinct possibility: that perturbing a distal element within the broader 8q24 regulatory landscape could alter MYC output through context-dependent gating rather than direct promoter docking.

Collectively, these studies position the MYC locus as an excellent system for dissecting how specific CTCF binding sites shape enhancer communication and oncogenic transcriptional programs.

## 1.6 Disrupted genome architecture as a cancer mechanism

Disruption of architectural insulation can lead to pathological enhancer rewiring. For example, in IDH-mutant gliomas, altered DNA methylation can impair CTCF-dependent insulation, allowing enhancers to ectopically activate oncogenes that were previously insulated from those regulatory elements (Flavahan et al., 2016). This paradigm strengthens the case that individual CTCF sites can be causal nodes in cancer gene regulation and are therefore attractive targets for mechanistic study.

## 1.7 Tools to perturb CTCF binding sites and enhancer–promoter wiring

### 1.7.1 Limitations of global depletion and genomic deletion

A straightforward method to test CTCF function is global depletion (e.g., degron systems) or knockout approaches. These strategies have been powerful for discovering general principles of genome folding, but they confound locus-specific interpretation because CTCF binds tens of thousands of sites genome-wide. Acute degradation can also trigger secondary effects (e.g., altered cell state, compensatory transcriptional responses) that complicate attributing phenotypes to a single binding site (Nora et al., 2017).

Similarly, CRISPR-mediated deletion of a CTCF motif can yield clear outcomes but is irreversible and may create clonal selection biases. Deletions can also remove more sequence context than intended (e.g., nucleosome positioning signals), making it difficult to attribute effects solely to loss of CTCF occupancy.

### 1.7.2 dCas9-based programmable perturbation

Catalytically inactive Cas9 (dCas9) provides a programmable platform to modulate genomic function without introducing double-strand breaks. Foundational work

repurposed CRISPR systems for sequence-specific control of transcription and demonstrated that dCas9 can be targeted to promoters and regulatory elements with guide RNAs (Gilbert et al., 2013; Qi et al., 2013). The same programmable targeting can be extended beyond transcriptional repression/activation to disrupt binding of endogenous proteins. Shariati and colleagues introduced the term CRISPRd (CRISPR disruption) to describe this use of dCas9 to block binding of a transcription factor at a specific motif, thereby isolating the function of a single binding site without perturbing the transcription factor globally (Shariati et al., 2019). Compared with global depletion or motif deletion (§1.7.1), CRISPRd offers site specificity, reversibility, and modularity, which makes it well suited for testing whether defined CTCF sites at MYC function primarily as insulators, enhancer-docking anchors, context-dependent gates, or some combination thereof.

Effector-based dCas9 variants such as dCas9-KRAB and CRISPRoff can repress regulatory regions, but they also introduce chromatin-modifying activities that may spread beyond the targeted motif or persist after induction. Because this thesis asks whether local steric targeting of CTCF-associated sites is sufficient to alter MYC output, an effector-free dCas9-only strategy provides the cleanest conceptual test.

For this comparison to be informative, however, the off state must be genuinely off. Conventional Tet-On dCas9 systems can show substantial leaky expression in the absence of doxycycline, and this leakiness is particularly pronounced in HCT116 cells, where basal activity has been reported to be high enough that doxycycline induction produces little additional effect (Srinivasan et al., 2026). Adding an FKBP12-based destabilization domain to dCas9 keeps the protein unstable until the small-molecule stabilizer Shield-1 is supplied, so a dual doxycycline-plus-Shield-1 induction design recovers a tight off/on contrast. The HCT116 platform built for this thesis was therefore engineered around this dual-control logic (§2.3.1, §2.4.4) rather than relying on doxycycline alone.

Prior studies support the feasibility of dCas9-based targeting to interfere with endogenous CTCF occupancy, but also show that displacement is guide- and locus-dependent. Tarjan et al. tested dCas9-KRAB at endogenous CTCF-bound insulators and found that CTCF could be selectively reduced when guide RNAs were positioned directly over the CTCF motif; they also tested dCas9 lacking the KRAB domain at two CTCF motifs and observed reduced CTCF binding, although less strongly than with dCas9-KRAB (Tarjan et al., 2019). Moore et al. later extended the programmable targeting concept using KRAB-dCas9 CRISPRi with truncated guides across thousands of CTCF motif sites, showing broad CTCF disruption in that effector-based system (Moore et al., 2025). Together, these studies support the plausibility of dCas9-positioned CTCF-site interference, while emphasizing that dCas9-only steric displacement cannot be assumed and must be validated directly at each locus.

Additional sources of guide-specific behavior — seed-sequence off-target activity (Rohatgi et al., 2024) and dCas9 occupancy acting as a transcriptional roadblock depending on placement and orientation (Zukher et al., 2023) — further strengthen the need for non-targeting controls, matched induction conditions, and orthogonal expression and occupancy readouts.

Whether dCas9 can outcompete CTCF at any specific motif must be tested empirically, which is why ChIP-qPCR validation is part of the workflow rather than an optional follow-up. Chromatin immunoprecipitation followed by quantitative PCR (ChIP-qPCR) provides this readout: a CTCF antibody pulls down chromatin fragments containing CTCF, and locus-specific primers then quantify recovery at the targeted site against an input reference. A successful steric block would be expected to reduce CTCF signal at its target site upon induction without affecting unrelated control regions, but unchanged bulk CTCF signal would not by itself exclude functional interference. The work in this thesis therefore couples RT-qPCR (downstream MYC expression) with ChIP-qPCR (upstream CTCF occupancy) to interrogate both ends of the perturbation chain (§2.10).

## 1.8 Rationale, knowledge gap, and thesis scope

Despite extensive evidence that CTCF contributes to genome folding, three concrete questions about MYC regulation remain difficult to address with the methods most commonly used in the field. First, *can site-specific, inducible perturbation of an individual CTCF site at MYC change MYC expression at all?* Global CTCF depletion in HCT116 has effects on MYC (Hyle et al., 2019), but those effects are confounded with the thousands of other CTCF sites simultaneously lost. Second, *if expression does change, in which direction, and why?* The architectural literature predicts opposite effects depending on whether a site primarily acts as a productive docking or gating element (in which case disruption should lower MYC) or as an insulating boundary (in which case disruption should raise MYC by allowing new enhancer access). Distinguishing these two regimes requires single-site, controlled perturbation rather than global loss. Third, *what is the cleanest, reversible way to test this experimentally?* CRISPR-mediated motif deletion is irreversible and creates clonal selection biases; degron-based global depletion is reversible but not site-specific. Connecting individual CTCF sites to quantitative gene-expression changes in a way that is both mechanistically interpretable and experimentally tractable therefore remains an open challenge.

At the MYC locus, multiple lines of evidence position two specific sites as the most informative targets to address these questions: a conserved promoter-proximal CTCF site that serves as a focal point for enhancer engagement (Schuijers et al., 2018), and a distal CTCF site embedded in an oncogenic super-enhancer region that gates MYC output in response to WNT signaling (Chachoua et al., 2022). Existing

perturbation strategies cannot cleanly isolate either site: they either remove CTCF globally, which weakens locus-specific interpretation, or alter the underlying DNA sequence permanently, which introduces clonal artifacts and limits temporal analysis. The experimental work in this thesis is designed to fill that methodological gap at the MYC locus specifically.

To do so, it focuses on two classes of MYC-associated CTCF sites: a promoter-proximal docking site approximately 1.3 kb upstream of the MYC TSS and a distal CTCF-associated site approximately 521 kb upstream of MYC. This design makes it possible to compare perturbation of a candidate shared docking site with perturbation of a more distal signaling-linked site within the same overall locus.

At the MYC locus studied here, the expected direction of effect was not completely open-ended. If the targeted CTCF sites primarily function as productive docking or gating elements, steric disruption would be expected to reduce MYC output. A marked increase in MYC would instead be more consistent with local insulation weakening and new enhancer access. Because this system did not center on a comparably strong nearby enhancer poised to engage the promoter, the working expectation at MYC was that disruption of productive CTCF-supported interactions would be more likely to lower MYC than to raise it. This expectation is locus-specific and does not imply that the same directional logic must hold at other genomic regions.

To provide a clear bridge between the biological rationale and the experimental work, the project follows a straightforward perturbation-and-readout workflow. Single-guide RNAs (sgRNAs) are designed to target defined CTCF binding motifs at the MYC locus and are cloned into sgRNA expression vectors for delivery into cells expressing inducible dCas9. After selection and induction, functional consequences were assessed primarily by bulk RT-qPCR, with single-molecule RNA fluorescence in situ hybridization (RNA-FISH) included as an orthogonal single-cell readout of MYC expression and ChIP-qPCR used to test whether guide targeting altered CTCF occupancy at the selected sites.

RNA-FISH detects individual mRNA molecules in fixed cells as discrete fluorescent puncta, so transcript abundance can be quantified per segmented cell (Femino et al., 1998; Raj et al., 2008; Mueller et al., 2013). This makes it complementary to bulk RT-qPCR: RT-qPCR estimates average transcript abundance across a population, whereas RNA-FISH preserves cell-to-cell variation and allows technical image quality to be assessed at the field-of-view level. For this thesis, the single-cell readout was included to check whether guide-associated MYC patterns persisted when measured independently of bulk reference-gene normalization, RNA-preparation artifacts, and population averaging. This approach preserves cell-to-cell

variation while keeping CTCF ChIP-qPCR as the direct occupancy-oriented test of the upstream mechanism.

## 1.9 Hypothesis and research aims

The overall objective of this thesis is to characterize whether inducible dCas9 targeting of CTCF-associated regulatory sites reduces MYC expression in a colorectal cancer model and whether any expression changes are accompanied by detectable changes in CTCF occupancy.

The central hypothesis was that inducible dCas9 targeting of selected CTCF-associated regulatory sites at MYC would reduce MYC mRNA output if these sites support productive enhancer docking or distal regulatory gating. CTCF ChIP-qPCR was used to test whether any expression changes were accompanied by detectable loss of CTCF occupancy.

To test this hypothesis, this thesis pursued four aims:

- Aim 1: Establish an inducible, effector-free dCas9 platform in HCT116 cells with tight off/on control. Can a stable, doxycycline- and Shield-1-controlled degron-tagged dCas9 platform be established in HCT116 cells that supports reproducible targeting of noncoding regulatory elements with low basal activity in the uninduced state?
- Aim 2: Test whether sgRNA-guided dCas9 targeting produces detectable CTCF occupancy changes at promoter-proximal and distal MYC-associated CTCF sites. Does sgRNA-guided recruitment of dCas9 to selected CTCF-associated sites produce measurable changes in CTCF recovery by ChIP-qPCR?
- Aim 3: Quantify whether inducible dCas9 targeting reduces MYC mRNA expression using bulk RT-qPCR and single-cell RNA-FISH. Is the direction of any MYC expression change more consistent with disruption of productive enhancer docking or gating than with boundary leakage?
- Aim 4: Integrate expression and occupancy readouts to determine whether MYC expression changes are consistent with site-specific disruption of CTCF-associated regulatory function. Are MYC expression changes accompanied by detectable CTCF occupancy changes, and are the combined results consistent with site-specific disruption of CTCF-associated MYC regulation?

More broadly, if inducible dCas9 targeting can be used to perturb individual architectural sites without editing the underlying DNA sequence, the same strategy could be applied to other oncogene-associated regulatory landscapes. This would provide a reversible framework for testing whether specific CTCF-associated sites act as productive enhancer-docking elements, insulating boundaries, or context-dependent regulatory gates, while keeping CTCF displacement as a mechanism to be tested directly rather than assumed.

## 1.10 Chapter overview

The remainder of the thesis is organized as follows. **Chapter 2** describes the experimental design and methods used to establish and evaluate the inducible dCas9 platform, including cell culture, sgRNA cloning, RT-qPCR, RNA-FISH, and CTCF ChIP-qPCR workflows.

**Chapter 3** presents the experimental results, beginning with platform validation and sgRNA generation, followed by the RT-qPCR expression series, ChIP-qPCR optimization and occupancy testing, RNA-FISH single-cell MYC analysis, and an integrated cross-readout guide summary.

**Chapter 4** interprets the findings across assays and cell populations, with emphasis on guide-associated MYC expression effects, the unresolved CTCF-occupancy mechanism, technical limitations, and future validation experiments.

**Chapter 5** summarizes the main conclusions and outlines the most important next step. The appendices provide supporting material for RNA quality control, qPCR plate layouts and Cq values, ChIP-qPCR layouts and summaries, sgRNA Sanger verification, and RNA-FISH setup and image-QC documentation.

# 2 Materials and Methods

## 2.1 Experimental design

This study used inducible CRISPR/dCas9 targeting to test whether selected CTCF-associated regulatory sites at the MYC locus influence MYC expression in HCT116 colorectal cancer cells. The intended perturbation model was steric interference with local CTCF function; whether that interference produced detectable changes in CTCF occupancy is treated as an experimental question rather than an assumption, and is tested directly by CTCF ChIP-qPCR in §3.3. The workflow consisted of four experimental parts: generation of an inducible dCas9 cell platform, introduction of sgRNA constructs, RT-qPCR measurement of MYC expression, and ChIP-qPCR assay development and occupancy testing.

Matched minus and plus conditions were used throughout the targeting experiments. The minus condition denotes uninduced cells, whereas the plus condition denotes cells treated with doxycycline and Shield-1. Doxycycline was used to activate the inducible CRISPR/dCas9 system, and Shield-1 was used to stabilize the degron-controlled dCas9 component. This dual-control design follows the logic of chemically controlled CRISPR systems in which degron-based regulation reduces basal activity in Tet-inducible platforms (Srinivasan et al., 2026).

The three readout classes were interpreted hierarchically. RT-qPCR was used as the bulk expression readout (§2.8), RNA-FISH as an orthogonal single-cell expression readout (§2.11–§2.12), and CTCF ChIP-qPCR as the occupancy-oriented test of the upstream mechanism (§2.10). Because the thesis combined assay development with biological readouts, datasets with limited replication or failed controls were interpreted descriptively rather than by formal inferential statistics.

## 2.2 Cell culture and experimental cell populations

The project used HCT116 colorectal cancer cells and engineered HCT116-derived populations carrying the inducible dCas9 platform. HCT116 cells were cultured in high-glucose Dulbecco's Modified Eagle's Medium (DMEM; Sigma-Aldrich/Merck, Cat. No. D6429) supplemented with 10% fetal bovine serum (FBS) and 1% penicillin/streptomycin, and maintained at 37 °C in 5% $CO_2$. Cells were passaged at approximately 70–90% confluency using an in-house-prepared 0.5% trypsin-EDTA solution.

Two HCT116-derived platform populations were used for the main RT-qPCR series. The H100 platform population refers to the HCT116-derived inducible dCas9 population generated under 100 µg/mL hygromycin selection (§2.4.2); the name "H100" is a hygromycin-selection label, not a separate cell line. This H100 population was used directly in the March 27, April 21, and May 1 RT-qPCR

experiments and also served as the starting material for fluorescence-activated cell sorting based on the blue fluorescent protein (BFP) reporter integrated into the platform (§2.4.3). The FACS-derived population was obtained by sorting and re-expanding a small BFP-positive fraction from H100 and was used in the March 31, April 1, and April 19 RT-qPCR experiments.

Cell concentration and viability were measured before extraction using Countess automated cell counters, including both Countess 1 and Countess 3. These measurements provided an estimate of viable-cell input before RNA extraction and were recorded together with later RNA quantification data for each experimental series. Countess values were not treated as strict quantitative endpoints. Readouts from Countess 1 were interpreted more cautiously than readouts from Countess 3, because repeated use suggested that Countess 1 tended to report lower cell numbers and less stable viability values, particularly at higher cell densities.

## 2.3 Plasmids, cloning, and construct verification

Three vectors were prepared and verified before mammalian-cell work: the dCas9 platform vector, the PiggyBac transposase support plasmid (hyPBase), and a panel of sgRNA expression vectors (guides A, B, D, and NT). All restriction digests used FastDigest enzymes (Thermo Fisher) or NEB enzymes in the buffers specified below. All gel purifications used a Monarch DNA Gel Extraction Kit (New England Biolabs, T1020G); agarose percentage and running buffer are specified for each digest below.

### 2.3.1 dCas9 platform vector

The original PiggyBac platform vector recommended for this project was `PB-TRE-dCas9-Zim3-MeCP2` (Addgene #220143), a doxycycline-inducible dCas9 fused to a Zim3-KRAB and MeCP2 dual-effector cassette, with hygromycin resistance for mammalian selection. Before the present cloning, a fellow master's student in the supervising lab (A. Iliadou) modified this vector by Gibson assembly to add two elements: (i) an FKBP12-based destabilization domain (DD) onto dCas9, giving a degron-tagged variant whose dCas9 protein is degraded in the absence of the small-molecule stabilizer Shield-1 (§2.4.4); and (ii) a tagBFP marker derived from `CRISPRoff-v2.1` (Addgene #167981) to allow flow-cytometric monitoring of platform-positive cells (used in §2.4.3 and §2.5.1). The resulting parental vector for the present work was `PB-TRE-DD-BFP-dCas9-Zim3-MeCP2`. The FKBP12 + Shield-1 system is the same one shown to suppress Tet-On Cas9 leakiness in HCT116 cells in Srinivasan et al. (2026).

For the present work, the Zim3-KRAB-MeCP2 effector cassette was removed from `PB-TRE-DD-BFP-dCas9-Zim3-MeCP2` so that the platform would deposit an effector-free degron-tagged dCas9 at target sites and act through steric interference rather than effector-driven transcriptional repression. The DD and BFP elements were

retained. The effector cassette was excised by AgeI (NEB R0552) + KpnI (NEB) double digest in 1× CutSmart buffer, 37 °C, 2 h. The linearized backbone was resolved on a 0.8% TBE agarose gel and gel-purified. The 5' overhangs were blunted with T4 DNA polymerase (NEB) in 1× T4 DNA ligase buffer supplemented with 1 µL of 10 mM dNTPs (20 µL reaction, ~200 ng input DNA, 10 min at room temperature) and stopped with 0.5 M EDTA. The reaction was cleaned up using a DNA Clean & Concentrator-5 kit (Zymo Research, D4013) to remove EDTA and enzymes prior to ligation. The blunted backbone was self-ligated with T4 DNA ligase (NEB) at room temperature, transformed into competent *E. coli*, plated on LB + ampicillin (100 µg/mL), and grown overnight at 30 °C. The resulting platform vector, `PB-TRE-DD-BFP-dCas9`, hereafter referred to as the dCas9-Only vector, was used in all downstream experiments.

Backbone identity was confirmed by diagnostic AgeI + KpnI digest: the parental `PB-TRE-DD-BFP-dCas9-Zim3-MeCP2` releases a ~1.2 kb Zim3-MeCP2 effector fragment, whereas the dCas9-Only vector retains only the linearized backbone. Selected clones were further confirmed by Sanger sequencing across the deletion junction.

### 2.3.2 hyPBase support plasmid

The PiggyBac transposase support plasmid `pCMV_hyPBase_P2A_mCherry_v2` (6,544 bp) was constructed in-house for this project by Gibson assembly. The hyperactive PiggyBac transposase (hyPBase) coding sequence is not deposited on Addgene because of licensing restrictions on the source enzyme; it was therefore ordered as a custom GeneArt synthetic gene string (Thermo Fisher) with overhangs homologous to the cloning site of `pCre-P2A-mCherry` (Addgene #212105). The acceptor backbone was prepared by SmaI + AfeI double digest of `pCre-P2A-mCherry-212105`, releasing the Cre coding sequence, and purified using a Monarch PCR & DNA Cleanup Kit (5 µg; New England Biolabs, T1030G). The hyPBase synthetic insert was then Gibson-assembled into the digested backbone in place of Cre, upstream of the existing P2A-mCherry cassette. The resulting `pCMV_hyPBase_P2A_mCherry_v2` plasmid co-expresses hyPBase and mCherry from a single bicistronic transcript, with mCherry serving as a transfection-uptake indicator during early lipofection optimization (§2.5.3).

Because the hyPBase plasmid shares most of its backbone with the parental `pCre-P2A-mCherry-212105`, preparations were verified by diagnostic SmaI + Eco32I double digest, where Eco32I is an EcoRV isoschizomer. The engineered construct was identified by the expected single 6,544 bp linear band and by the absence of the parental 511 bp Cre-plasmid fragment.

### 2.3.3 sgRNA expression vectors

sgRNAs were cloned into the PiggyBac-compatible scaffold `PB_gRNA_S.pyogenes_scaffold_BB` (Addgene #226429; linearized backbone ~6.4

kb), which carries puromycin resistance for mammalian selection, at the U6-promoter-flanking BpiI/BbsI cloning site, following a Zhang-lab-style oligo-cloning protocol.

Guide oligo pairs (annealing top + bottom strands) were ordered as dry commercial oligos and resuspended in 1× TE to 100 µM stocks. Four pairs were prepared: guide A, guide B, guide D, and a non-targeting (NT) control. Spacer sequences and genomic coordinates for all four are listed in Table 2.2. The NT control was a published scrambled sequence with no match in the human genome, used previously as a non-targeting control in BbsI-cloned sgRNA scaffolds. Each pair was phosphorylated and annealed in a single 10 µL reaction containing 1 µL forward oligo (100 µM), 1 µL reverse oligo (100 µM), 1 µL 10× T4 DNA ligase buffer (with ATP), 0.5 µL T4 polynucleotide kinase, and 6.5 µL nuclease-free water. The phosphorylation/annealing program was 37 °C for 30 min, 95 °C for 5 min, followed by cooling to 25 °C at 5 °C/min. Annealed duplexes were diluted 1:200 in nuclease-free water before ligation.

The backbone was prepared by one-pot BpiI digestion and dephosphorylation: 1 µg of `PB_gRNA_S.pyogenes_scaffold_BB` plasmid was incubated with 1 µL FastDigest BpiI (Thermo) and 1 µL FastAP (Thermo) in 1× FastDigest Green buffer in a 20 µL reaction, 37 °C for 30–60 min. The linearized ~6.4 kb backbone was gel-purified from a 0.8% TBE agarose gel.

Ligations combined cut backbone with diluted annealed duplex using T4 DNA ligase (NEB) in 1× T4 ligase buffer at room temperature, then transformed into competent *E. coli*, plated on LB + ampicillin (100 µg/mL), and grown overnight at 30 °C. A vector-only no-ligase plate was included as a background control.

### 2.3.4 Plasmid recovery and verification

Three to six well-isolated colonies per ligation were picked from the LB + ampicillin plates and transferred into 5–5.5 mL LB + ampicillin (1:1000 dilution from a 100 mg/mL ampicillin stock). Cultures were grown overnight at 30–37 °C with shaking at 220–250 rpm. Glycerol stocks were prepared from sequence-relevant clones in 25% glycerol and stored at −80 °C.

Plasmid DNA was purified from the remaining culture using a ZymoPURE Plasmid Miniprep Kit (Zymo Research, D4210) on a vacuum manifold, eluted in 25–50 µL pre-warmed Elution Buffer, and quantified by NanoDrop. For sgRNA constructs, identity was confirmed by Sanger sequencing across the U6–spacer junction using a hU6-sequencing primer; for the hyPBase plasmid, sequencing across the Gibson junctions used the M13_seq_F and M13_seq_R primers.

Sanger reactions were prepared in the Eurofins LightRun format using 5 µL plasmid DNA at 80–100 ng/µL and 5 µL sequencing primer at 5 µM in nuclease-free water.

Diagnostic restriction digests used the same FastDigest enzyme set described in §2.3.2, with 1 µL plasmid DNA added to 9 µL digest master mix, incubated at 37 °C for 10 min, and electrophoresed on a 1% TBE agarose gel pre-stained with GelRed Nucleic Acid Stain at 2 µL per 20 mL gel at 100 V for 40 min (GelRed: 10,000× in water; Biotium, cat. no. 41003).

Sanger sequencing confirmed the sgRNA inserts in the constructs used downstream: A4/JTJ522 for guide A, B2/JTJ512 for guide B, D1/JTJ519 for guide D, and NT2/JTJ523 and NT3/JTJ524 for the non-targeting controls. Clones with unreadable, partially readable, or deletion-containing inserts were not used for downstream experiments.

Guide A required additional verification because the first 2025 Sanger reads for A1/JTJ508 and A2/JTJ507 were unreadable. Repeat screening in 2026 identified sequence-confirmed guide A clones, and A4/JTJ522 was selected for downstream experiments. The constructs taken forward to mammalian-cell work are summarized in Table 2.1; the full per-clone Sanger trace, including replated 2025 colonies, the unselected 2026 sequence-confirmed clones, and the excluded or unreadable clones with their NanoDrop quality values, is given in Appendix E (Table E.1).

**Table 2.1. sgRNA clones used downstream (Sanger-confirmed, Eurofins LightRun service).** Compact summary; the full per-clone trace including replated and excluded clones is given in Appendix E (Table E.1).

| Guide | Clone used | LightRun ID | Status |
|---|---|---|---|
| A | A4 | JTJ522 | Used; sequence-confirmed (replated 2026 colony from 2025 batch) |
| B | B2 | JTJ512 | Used; sequence-confirmed |
| D | D1 | JTJ519 | Used; sequence-confirmed |
| NT | NT2 | JTJ523 | Used; sequence-confirmed |
| NT | NT3 | JTJ524 | Used; sequence-confirmed |
| Excluded (A, D) | A2, D2 | JTJ526, JTJ520 | One-nucleotide deletion; not used |

## 2.4 Generation of the inducible dCas9 platform

### 2.4.1 DNA transfection

DNA transfection was performed using Lipofectamine 3000 Transfection Reagent (Invitrogen, L3000015). HCT116 cells were transfected with PiggyBac-compatible dCas9 transposon DNA and hyPBase support plasmid DNA. In the H100 platform-generation setup, 1.0 µg total DNA was used per well in 12-well format at an approximately 3:1 transposon-to-transposase mass ratio. P3000 reagent was included according to the Lipofectamine 3000 workflow.

Guide construct delivery into the established dCas9 receiver line was later performed in 24-well format. A typical guide-delivery setup used 500 ng total DNA per well, consisting of 375 ng sgRNA PiggyBac donor and 125 ng hyPBase plasmid, together with 1.0 µL P3000 and 1.5 µL Lipofectamine 3000 in Opti-MEM. Cells were transfected in 450 µL complete medium with 50 µL transfection complex added per well.

The reagent lot used in this project (lot 2476275; manufacturer expiration 2023-05-23) was beyond its manufacturer-printed shelf life during these experiments. Its continued practical performance was assessed empirically by mCherry uptake (§2.5.3) and subsequent hygromycin selection (§2.4.2).

### 2.4.2 Antibiotic selection and expansion

After platform transfection, hygromycin B (50 mg/mL; Roche) selection was used during generation of the dCas9 platform. Two hygromycin concentrations were tested during HCT116 optimization: 100 µg/mL (the source of the H100 platform population used in this thesis) and 200 µg/mL (the H200 condition, retained for reference but not used as the source of the main RT-qPCR populations). The labels “H100” and “H200” therefore refer to the hygromycin concentration used during platform selection, not to independent cell lines. Guide-delivery experiments used puromycin selection, with 1 µg/mL puromycin (10 mg/mL; Sigma-Aldrich, P4512) applied to recover guide-positive pools. Selection controls without transfected DNA were included when setting up antibiotic selection. After antibiotic selection and expansion, the H100 platform population, the FACS-derived H100 subpopulation, and all derived sgRNA-carrying guide populations were cryopreserved as working stocks in complete DMEM containing 5% DMSO, using controlled cooling in an isopropanol freezing container before storage at −80 °C.

### 2.4.3 FACS-based enrichment

Fluorescence-based enrichment was performed by FACS, using the H100 platform population (§2.2) as the starting material to obtain a more defined platform-positive subpopulation. Cells were prepared as single-cell suspensions, filtered before sorting, and maintained in cold sort buffer. Sorting was performed on a BD FACSAria II cell sorter using the violet 405 nm laser and the DAPI 450/40 channel for BFP detection. Platform-positive cells were enriched by sequential gating of the main cell population, singlets, and BFP-positive events; a wild-type HCT116 sample was acquired in parallel on the same gates as a no-BFP reference. The sorted BFP-positive fraction was collected into medium and re-expanded as the FACS-derived BFP-enriched H100 subpopulation used in later RT-qPCR experiments. The quantitative enrichment outcome is reported in §3.1 and discussed in §4.3.

### 2.4.4 Induction conditions

Induction used doxycycline and Shield-1 together. Doxycycline activated transcription of the inducible CRISPR system, while Shield-1 stabilized the degron-tagged dCas9 platform and thereby suppressed leakiness in the uninduced state. This dual-control logic is consistent with recent work showing that conventional Tet-On Cas9 systems can exhibit substantial basal activity, including in HCT116 cells, and that degron-based control can markedly improve the contrast between off and on states (Srinivasan et al., 2026). In the induced condition, doxycycline and Shield-1 were therefore used together to permit accumulation of the active dCas9-based machinery. The minus/plus comparison in the RT-qPCR experiments analyzed in this thesis should be understood as the combined induction state of the system rather than as a doxycycline-only contrast.

For sorting-associated induction, cells were exposed for approximately 24 h before FACS. The recorded working setup used Shield-1 at 1:1000 from a 1 mM stock, giving 1 µM final Shield-1, and doxycycline at an overall 1:200,000 dilution from a 20 mg/mL stock, giving 100 ng/mL final doxycycline.

## 2.5 Platform validation and quality-control assays

### 2.5.1 Flow cytometry

Flow cytometry was used to assess the BFP-positive platform-associated population during FACS enrichment. Gating used forward and side scatter to define the main cell population, FSC-A versus FSC-H to remove doublets, and BFP fluorescence to define platform-positive events.

### 2.5.2 Anti-Cas9 immunofluorescence

Anti-Cas9 immunofluorescence was performed in 96-well glass-bottom format. Cells were fixed with 4% paraformaldehyde, permeabilized with 0.1% Triton X-100, and blocked in 1% BSA. A mouse anti-Cas9 monoclonal antibody was used at 1:500 dilution overnight at 4 °C (Invitrogen, MA1-201, clone 7A9-3A3), followed by goat anti-mouse Alexa 555 secondary antibody at 1:1000. DAPI was used as a nuclear counterstain in wells where the blue channel was not needed for BFP imaging. Imaging was performed after secondary staining. The assay was used as qualitative supporting evidence of dCas9 expression. A representative field is shown in Figure 2.1.

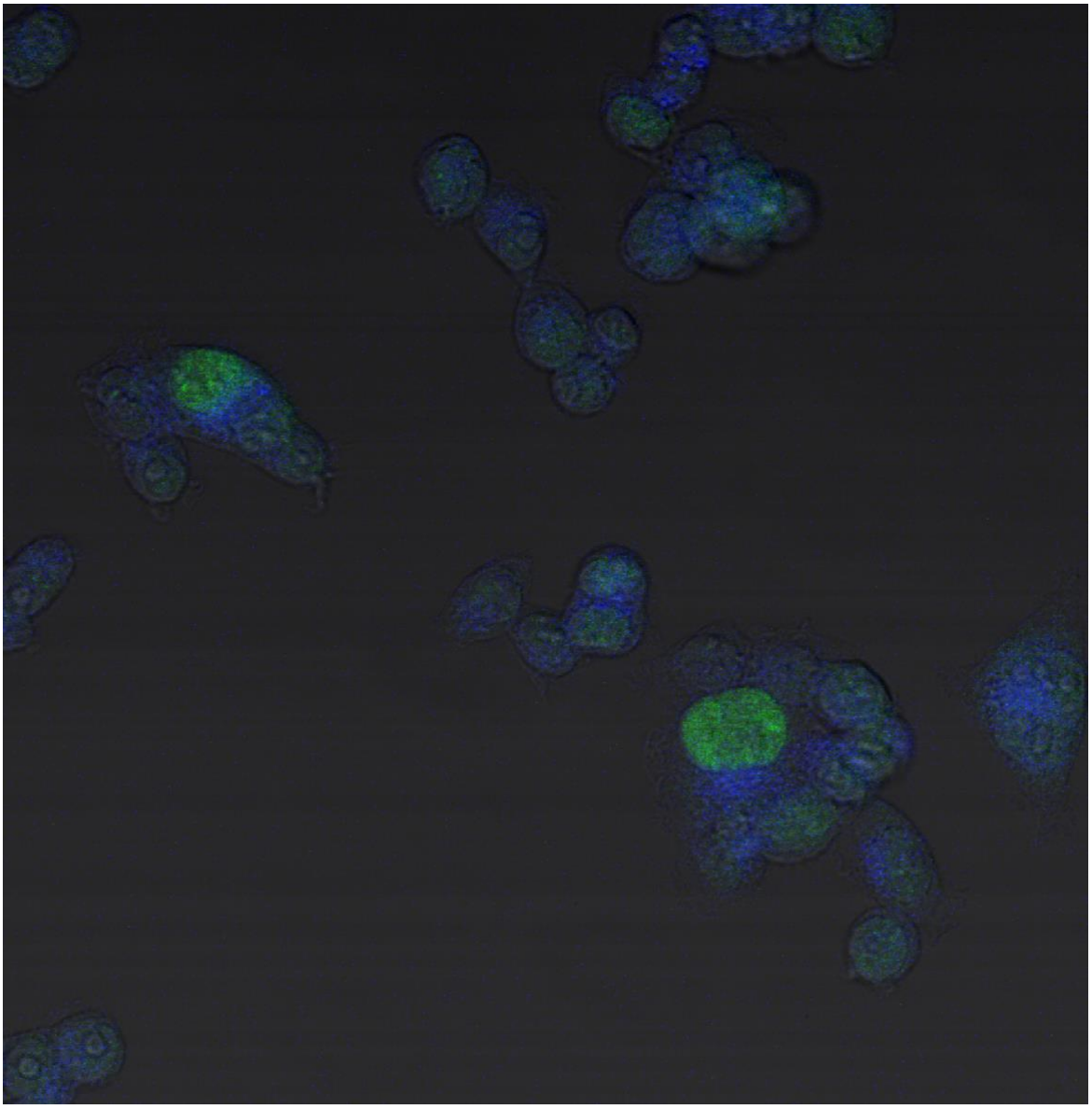

**Figure 2.1.** Representative anti-Cas9 immunofluorescence image of HCT116-derived dCas9 platform cells. Blue shows DAPI-stained nuclei, gray shows transmitted-light/DIC morphology, and green shows Cas9-antibody fluorescence. The image was acquired as a single optical plane using a 20×/0.8 NA Plan-Apochromat objective. Cas9-associated signal was detectable in a subset of cells and was interpreted qualitatively rather than as a quantified single-cell positivity readout.

### 2.5.3 Additional microscopy

mCherry fluorescence was checked after transfection to assess uptake of hyPBase-containing plasmids. This microscopy check was performed on a Zeiss LSM510 confocal microscope using a 10×/NA 0.30 Fluar objective; mCherry was excited with a 561 nm DPSS laser, and a transmitted-light/brightfield channel was acquired in parallel. A representative field is shown in Figure 2.2; mCherry signal in transfected HCT116 cells served as the empirical transfection-success readout used in §2.4.1, before hygromycin-based platform selection and downstream FACS enrichment.

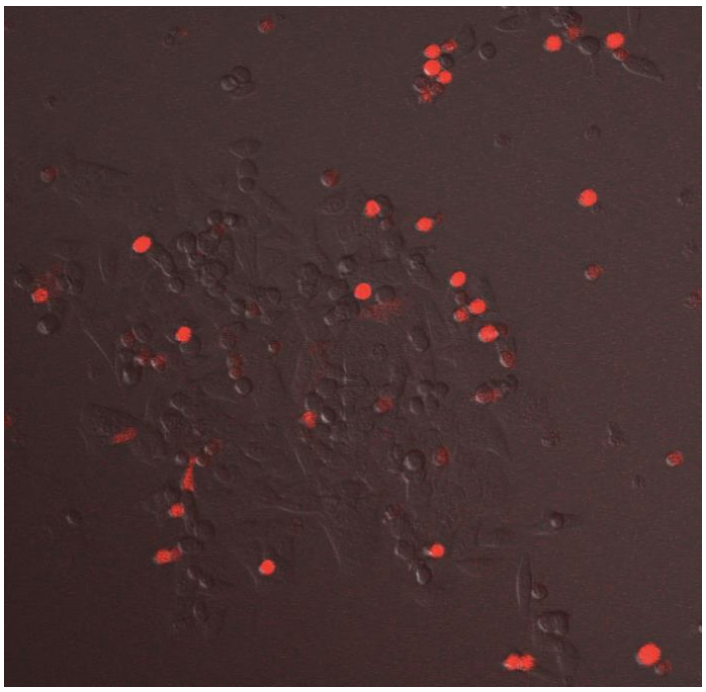

**Figure 2.2.** Representative brightfield/mCherry overlay of HCT116 cells after transient transfection with the pCre-mCherry construct, imaged on a Zeiss LSM510 confocal microscope (10×/NA 0.30 Fluar objective; 561 nm DPSS-laser excitation for mCherry with a transmitted-light/brightfield channel acquired in parallel). Bright red signal marks mCherry-positive cells against the brightfield view of the surrounding non-fluorescent cells. This empirical mCherry-uptake check was used as the primary transfection-success readout for the hyPBase/mCherry-containing transfections described in §2.4.1, prior to hygromycin-based platform selection (§2.4.2) and FACS-based BFP enrichment (§2.4.3).

BFP-channel imaging was also performed on guide-B-carrying H100 cells before and after doxycycline/Shield-1 induction, providing a qualitative microscopy view of inducible platform behavior at the cellular level. Figure 2.3 shows representative brightfield/BFP overlay images of uninduced (−B) and induced (+B) cells. Although blue-channel signal was detectable even in the uninduced condition, induction produced larger and more prominent blue-positive regions, consistent with platform activation. The uninduced signal could reflect autofluorescence, imaging background, or low basal reporter expression. Because the destabilization-domain/Shield-1 design (§2.3.1, §2.4.4) was specifically intended to suppress basal dCas9 accumulation, the uninduced signal was not interpreted as direct evidence of platform leakiness. However, it supports interpreting BFP-channel microscopy qualitatively rather than as a definitive single-cell BFP-positive classification readout.

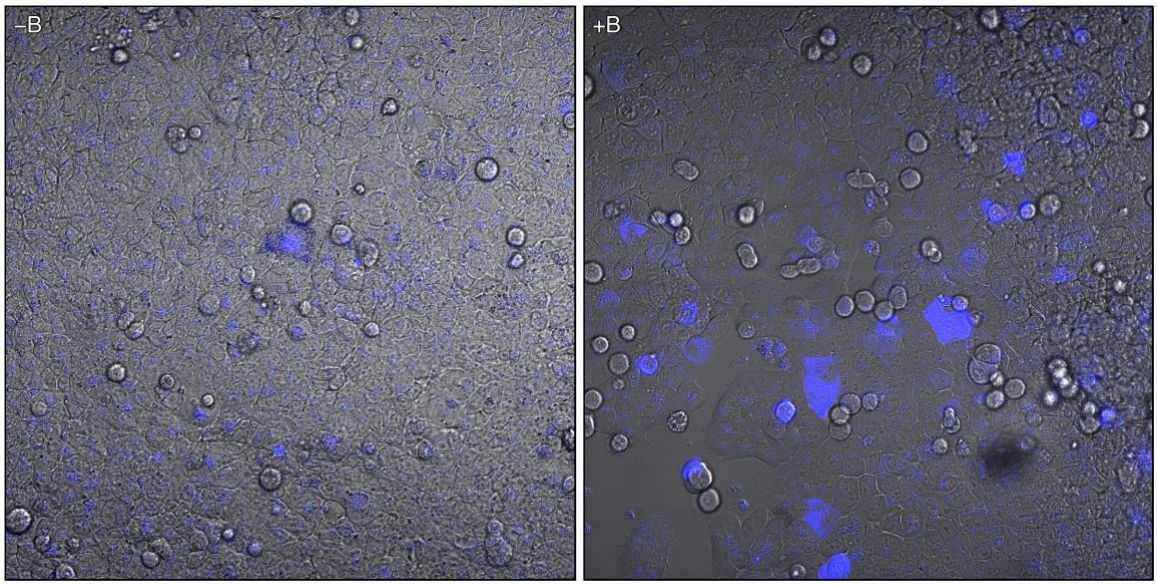


**Figure 2.3.** BFP-channel background and induction-associated blue fluorescence in guide-B-carrying H100 cells. Brightfield/BFP overlay images of uninduced (−B, left) and doxycycline/Shield-1-induced (+B, right) cells, imaged on a Zeiss LSM510 confocal microscope (20×/NA 0.8 Plan-Apochromat objective; glass-bottom 96-well plate; 405 nm excitation with 420–480 nm emission detection for the BFP channel; transmitted-light/brightfield channel acquired in parallel). The −B condition showed detectable punctate and diffuse blue-channel signal, whereas the +B condition showed larger and more prominent blue-positive regions after induction. Because blue-channel signal was present even in the uninduced condition, microscopy was interpreted as qualitative support for induction-associated fluorescence rather than as a definitive single-cell BFP-positive classification readout.

## 2.6 sgRNA design and cloning

The sgRNA panel consisted of guide A, guide B, guide D, and a non-targeting control. Guides A and B were both designed against the same promoter-proximal CTCF motif (JASPAR MA0139.1; consensus `CTGCCAGTAGAGGGCACAC` at chr8:127,734,105–127,734,123, ~2 kb upstream of MYC) but on opposite strands, so that they would tile the motif from both faces and provide strand-symmetric steric coverage of the binding site (Figure 1.1, inset). Guide D targeted a distal oncogenic super-enhancer (OSE) / CCAT1-associated CTCF site approximately 521 kb upstream of MYC. NT was used as a non-targeting control.

The biological target regions were selected from prior studies of MYC regulation, but the exact dCas9-compatible protospacers used here were chosen specifically for this project. An exploratory HCT116 CTCF ChIP-seq–based design pipeline was used during initial guide development, followed by final guide selection with CRISPOR, CHOPCHOP, and IDT to identify motif-overlapping guides suitable for dCas9-only targeting. For the promoter-proximal site, this led to the strand-symmetric guide A/guide B pair used in the final panel; for the distal arm of the study, the final panel

was redirected to the upstream OSE/CCAT1-associated CTCF site described by Chachoua et al. (2022), yielding guide D.

Guide candidates were evaluated with CHOPCHOP, CRISPOR, and IDT design/scoring tools (Table 2.3). Selection prioritized direct overlap with the CTCF motif, compatibility with SpCas9 NGG protospacer-adjacent motif (PAM) requirements, and acceptable predicted on-target / off-target characteristics.

For the promoter-proximal motif, guide design was informed by the MYC_CTCF oligo reported by Schuijers et al. (2018) in Table S4 and refined using project-specific CRISPOR, CHOPCHOP, and IDT guide-design scoring. This produced guide A, which overlaps the reported MYC_CTCF oligo, and guide B, an opposite-strand, motif-overlapping partner. Together, guides A and B tiled the same promoter-proximal CTCF motif from opposite strands and were ordered as a strand-symmetric pair (Figure 1.1). On *specificity*, all three tools agreed that guide B was the stronger candidate (CRISPOR MIT 82 vs. 67; CFD 92 vs. 85; IDT specificity 62 vs. 32). On *predicted on-target activity*, the tools disagreed — CHOPCHOP and CRISPOR Doench'16 rated guide A higher, whereas IDT's algorithm rated guide B higher. This interpretation is consistent with the use of dCas9/CRISPRd as an occupancy-based strategy for perturbing transcription factor binding sites, where guide choice should consider target-site specificity as well as predicted activity (Mohr et al., 2016; Shariati et al., 2019). Guide B was therefore carried forward as the primary promoter-proximal guide and guide A as its strand-symmetric partner. Guides A and B were cloned as 20-nt protospacers.

For the distal CTCF site, guide D was designed to overlap the OSE CTCF motif identified in HCT116 cells by Chachoua et al. (2022) at chr8:128,227,330–128,227,353 (hg19; ~520 kb upstream of MYC, hg38 conversion in Table 2.2). The chosen protospacer was Rank 1 in both CHOPCHOP and CRISPOR, with strong specificity (CRISPOR MIT 88, CFD 93; IDT 71/68) and ~18 bp overlap with the 24-bp motif. Guide D was ordered as a 20-mer.

The promoter-proximal guide A and guide B cloning oligos were ordered from Invitrogen (cat. no. 10336-022). The same order included the hU6 sequencing primer used for Sanger verification of guide inserts. Oligo identifiers and full cloning-oligo sequences for guides A and B are listed in Table 2.4.

**Table 2.2. sgRNA target summary.** Cloned spacers are what was ordered and inserted into the PiggyBac sgRNA scaffold (`PB_gRNA_S.pyogenes_scaffold_BB`, Addgene #226429). The target-region column gives the ChIP-qPCR assay name used elsewhere in the thesis (Table 2.7). All hg38 spans are reported on the same reference build as the rest of the thesis. For guide D, the approximate hg38 liftOver is shown in the table, while the original hg19 source span is retained below for traceability to Chachoua et al. (2022).

| Guide | Target region | Cloned spacer (5'→3'; nt) | Strand | Genomic span | Motif overlap | Role |
|---|---|---|---|---|---|---|
| A | `mycP_CTCF` | TGATCTCT GCTGCCA GTAGA (20) | + | chr8:127,734 ,097– 127,734,116 (hg38) | 11–12 bp, left/central part of MA0139.1 motif | Promoter-proximal guide (+ strand) |
| B | `mycP_CTCF` | AAAGTAAG TGTGCCCT CTAC (20) | – | chr8:127,734 ,111– 127,734,130 (hg38) | ~13 bp, right part of the same MA0139.1 motif | Promoter-proximal guide (– strand) |
| D | `OSE_CTCF` | TAAACCTC CTCACCAT TGGA (20) | + | chr8:127,215 ,879– 127,215,898 (hg38, approximate liftOver) | ~18 bp of distal OSE/CCAT 1-associated CTCF motif | Distal OSE/CCAT1-associated guide |
| NT | n/a | TATTACTG ATATTGGT GGG (19) | n/a | n/a | No human genome target | Non-targeting control |

**Table note.** Guide D source span: chr8:128,227,328–128,227,347 (hg19). The published OSE/CCAT1-associated CTCF motif is reported at chr8:128,227,330–128,227,353 (hg19) by Chachoua et al. (2022). The non-targeting control was ordered as a 19-nt spacer following the Beckwith-laboratory standard NT design; guides A, B, and D were ordered as 20-nt protospacers. NT spacer identity was Sanger-verified in NT2/JTJ523 and NT3/JTJ524.

**Table 2.3. sgRNA design-tool scores.** CHOPCHOP efficiency (0–100); CRISPOR Doench'16 on-target score; CRISPOR MIT and CFD specificity scores (0–100, higher = more specific); IDT proprietary activity and specificity scores (0–100 each).

| Guide | CHOPCHOP | Doench'16 | MIT | CFD | IDT activity | IDT specificity |
|---|---|---|---|---|---|---|
| A | 50 | 50 | 67 | 85 | 37 | 32 |
| B | 39 | 39 | 82 | 92 | 66 | 62 |
| D | 63 | 63 | 88 | 93 | 71 | 68 |
| NT | n/a | n/a | n/a | n/a | n/a | n/a |

**Table 2.4. Ordered sgRNA cloning oligos and sequencing primer.**

| Name | ID | Sequence (5'→3') |
|---|---|---|
| sg_dCas_CTCF_MYCprom_A_F | J1132B04 | CACCGTGATCTCTGCTGCCAGTAGA |
| sg_dCas_CTCF_MYCprom_A_R | J1132B05 | AAACTCTACTGGCAGCAGAGATCAC |
| sg_dCas_CTCF_MYCprom_B_F | J1132B06 | CACCGAAAGTAAGTGTGCCCTCTAC |
| sg_dCas_CTCF_MYCprom_B_R | J1132B07 | AAACGTAGAGGGCACACTTACTTTC |
| hU6_seq_F | J1132B08 | GAGGGCCTATTTCCCATGATT |

## 2.7 RNA extraction and quantification

RNA used for downstream RT-qPCR was extracted with the Lybe Scientific NAxtra Cells total nucleic acid extraction kit, 96-prep format (catalog LSNXC0096). Magnetic bead separation was used, and RNA was eluted in RNase-free water. DNase treatment was not applied uniformly across all runs: the March 27 run was performed without DNase treatment, whereas DNase was included in later extraction workflows where recorded.

RNA concentration and purity were measured with NanoDrop. RNA-40 readings were used for final RNA concentration calculations. DNA-50 readings were initially recorded by mistake for some samples and were not used directly for final RNA loading calculations because the DNA-50 setting is not calibrated for RNA and can overestimate RNA concentration. Where early-run loading had to be reconstructed from DNA-50 records, the resulting estimates were treated as approximate and interpreted cautiously. NanoDrop 260/280 and 260/230 ratios were recorded as supporting quality indicators. NanoDrop concentrations below approximately 25 ng/µL were treated as approximate, since the instrument is more susceptible to baseline noise and salt-carryover effects in this range. Per-run NanoDrop and Countess values, including viability and 260/280 and 260/230 ratios for each sample, are recorded in the project documentation folder and were used to flag prep-stage quality issues for downstream interpretation rather than as strict acceptance criteria.

For the May 1 H100 rerun, all 16 RNA samples were treated with TURBO DNA-free before RT-qPCR, re-quantified by NanoDrop, and diluted to a common 10 ng/µL working concentration for 20 ng RNA input per reaction.

## 2.8 RT-qPCR setup and analysis

RT-qPCR was performed on a Bio-Rad CFX96 system and analyzed in CFX Maestro. The chemistry was One-step NZYSpeedy RT-qPCR Green kit (NZYTech, MB34602; 500 reactions). Reactions were prepared in 20 µL total volume.

Standard RT-positive reactions contained 10.0 µL 2× NZYSpeedy Green master mix, 0.8 µL forward primer, 0.8 µL reverse primer, 0.8 µL NZYRT mix, RNA template, and

RNase-free water to 20 µL. No-reverse-transcriptase (NRT) controls replaced NZYRT mix with water. No-template controls (NTC) replaced RNA template with water. The standard cycling program was 50 °C for 15 min, 95 °C for 2 min, followed by 40 cycles of 95 °C for 5 s and 60 °C for 30 s, with fluorescence acquisition at the 60 °C step. A post-amplification melt curve was acquired from 65 to 95 °C in 0.5 °C increments.

MYC was the primary target gene, amplified with the "MYC span" primer pair (forward 20 nt, reverse 25 nt; Invitrogen). YWHAZ was the main reference gene used for normalized interpretation, and B2M was included as an alternative reference gene in selected plate designs. GAPDH and ACTB were not used as RT-qPCR reference genes in this thesis. The choice of YWHAZ + B2M instead of the more commonly assumed GAPDH/ACTB pair follows Hu et al. (2023), who screened eight candidate reference genes (GAPDH, ACTB, 18S, PPIA, B2M, SDHA, GUSB, YWHAZ) across one normal colonic epithelial line (NCM460) and seven colorectal cancer cell lines including HCT116 using geNorm, NormFinder, and BestKeeper. That study found GAPDH and ACTB to be less stable than YWHAZ and B2M across most of the tested lines, identified YWHAZ + B2M as the optimal two-gene reference panel for HCT116 (and for five of the eight lines overall), and validated the panel by showing that normalizing APC expression against YWHAZ + B2M produced more statistically defensible expression differences than normalizing against GAPDH, ACTB, or a GAPDH + ACTB pair. The present thesis therefore inherited this colorectal-cancer-cell-line panel rather than the conventional GAPDH default. The lab also carried validated stock primers (`HuRef_YWHAZ_F/R` and `HuRef_B2M_F/R`; Table 2.5) for both members of the panel, and pilot runs showed Cq values close to the MYC sample Cq window for both.

Within the YWHAZ + B2M panel, YWHAZ was treated as the preferred descriptive reference and B2M as a cross-checking secondary reference rather than as a co-averaged normalizer. Formal reference-gene-stability ranking by geNorm/NormFinder was not performed inside this thesis (the Hu et al. 2023 ranking was used as the prior); reference-gene behavior was instead audited per run by inspecting NT +/− shifts and by checking that normalized and raw-MYC contrasts moved in the same direction (§3, §4.4). The data collected during the thesis support YWHAZ as the more usable member of the panel for descriptive normalization in several runs: technical-duplicate Cq SDs were tighter for YWHAZ than for B2M on plates where both were run in duplicate (Appendix C), and plate-wide Cq variance across guides and induction conditions was lower for YWHAZ than for B2M. However, May 1 required a run-specific interpretation because YWHAZ was run as a single well per sample, the -NT2 YWHAZ well was non-interpretable, and B2M Cq became ~1.0–1.3 cycles earlier in the +dox NT samples than the matched -dox NT

samples (-NT1 23.79 → +NT1 22.54; -NT2 22.64 → +NT2 21.85; §3.2.3, §4.4). Under that NT plus-shift, reference normalization can inflate apparent +dox MYC reductions in the NT controls themselves. For May 1, raw MYC fold change is therefore used as the clearest directional readout, while YWHAZ- and B2M-normalized fold changes are retained as normalization diagnostics rather than standalone guide-specific effect sizes. dCas9 was included in a limited number of wells as a platform-induction check using a Cas9 qPCR primer pair ordered from Invitrogen (primer names `Cas9_qPCR_F` and `Cas9_qPCR_R`). RT-qPCR primer sequences for MYC, YWHAZ, B2M, and Cas9 are listed in Table 2.5.

An initial unperturbed-HCT116 pilot in December 2025 was used to test candidate RT-qPCR primer sets before the guide-targeting series. The pilot revealed unacceptable NTC amplification with an earlier alternative MYC primer pair and lacked definitive melt-curve verification, leading to selection of the "MYC span" pair as the headline MYC assay and motivating the stricter NTC/NRT and melt-curve QC discipline used throughout the main RT-qPCR series. Formal serial-dilution standard curves were not run for the MYC, YWHAZ, B2M, or Cas9 primer pairs in this thesis, so per-primer efficiency values are not reported; the ddCq → fold-change calculation in §2.8 therefore assumes E ≈ 100 % for all assays. YWHAZ-normalized MYC fold change was treated as the preferred normalized RT-qPCR expression readout where NT and reference-gene behavior were acceptable. Raw MYC fold change and B2M-normalized fold change were retained as sensitivity checks, and raw MYC was promoted to the main directional readout in the May 1 H100 DNase rerun because the NT reference-gene shifts made normalized fold changes non-specific (§3.2.3).

Per-well acceptance criteria were defined before run interpretation. A well was accepted as MYC-specific only if the CFX Maestro melt-curve caller returned a single peak inside the 88.5–90.5 °C MYC amplicon window (rationale and re-scoring procedure in §3.2.1); wells with peaks outside this window were treated as non-MYC-specific even when CFX returned a Cq. For YWHAZ and B2M, the expected melt windows were 82.0–83.5 °C and 80.0–80.5 °C respectively, scored by the same single-peak-inside-window rule. NTC and NRT wells were required to fall outside the corresponding sample-target melt window or to remain undetected; same-window NTC or NRT amplification disqualified the corresponding sample-target combination from melt-supported interpretation. Technical-replicate Cq values with within-replicate SD > 1.0 cycle were re-inspected; where one replicate clearly fell outside the run-level distribution while the partner replicate fit the rest of the panel, the outlier well was excluded and the partner used as the per-sample Cq (the exclusions made under this rule are documented case-by-case in §3.2.3 and Appendix C).

**Table 2.5. RT-qPCR primer sequences.**

| Assay | Primer | Sequence (5'→3') | Source |
|---|---|---|---|
| MYC span | Forward | CCTCAGAGTGCATCGACCCC | Invitrogen |
| MYC span | Reverse | TCTTCTTGTTCCTCCTCAGAGTCG | Invitrogen |
| YWHAZ | Forward (HuRef_YWHAZ_F) | GGAGCCCGTAGGTCATCTTG | Lab stock (ID J4201D11) |
| YWHAZ | Reverse (HuRef_YWHAZ_R) | CGGCAACCTCAGCCAAGTAA | Lab stock (ID J4201D12) |
| B2M | Forward (HuRef_B2M_F) | GTTAAGTGGGATCGAGACATGTAAG | Lab stock (ID J4201D09) |
| B2M | Reverse (HuRef_B2M_R) | TCAAACATGGAGACAGCACTC | Lab stock (ID J4201D10) |
| Cas9 | Forward (Cas9_qPCR_F) | TGATGAGCACCACCAAGACT | Invitrogen (ID J2414A05) |
| Cas9 | Reverse (Cas9_qPCR_R) | ATTGTCGAAAGTGCGCTGTT | Invitrogen (ID J2414A06) |

For normalized analyses, dCq was calculated as:

`dCq = Cq(MYC) - Cq(reference)`

The matched induction contrast was calculated as:

`ddCq = dCq(+dox) - dCq(-dox)`

Fold change was calculated as:

`fold change = 2^-ddCq`

Values below 1 indicate lower normalized MYC in the plus condition relative to the matched minus condition.

## 2.9 RT-qPCR run formats

The main RT-qPCR runs used in the thesis are summarized below.

**Table 2.6. RT-qPCR run formats used in the thesis.** "H100" denotes the H100 platform population and "FACS-derived" denotes the FACS-derived BFP-enriched H100 subpopulation, both as defined in §2.2.

| Date | Population and guides | RNA input | Main assays |
|---|---|---|---|
| March 27, 2026 | H100; A, B, D, NT | Fixed-volume / reconstructed input | MYC, YWHAZ |
| March 31, 2026 | FACS-derived; A, B, D, NT | Fixed-volume loading | MYC, YWHAZ, B2M, dCas9 |
| April 1, 2026 | FACS-derived; B only | 8 ng equal-mass loading | MYC, YWHAZ |
| April 19, 2026 | FACS-derived; A, B, D, NT | 8 ng equal-mass loading | MYC, YWHAZ |
| April 21, 2026 | H100; A, B, D, NT | 20 ng equal-mass loading | MYC, YWHAZ, B2M |
| May 1, 2026 | H100; A, B, D, NT | 20 ng equal-mass loading after DNase treatment | MYC, YWHAZ, B2M |

Technical duplicates were used for the main RT-qPCR assays where plate space allowed. Larger plate formats included NTC and NRT controls. On the May 1 plate, MYC and B2M were run in duplicate for all 16 samples, YWHAZ was run as a single secondary-reference well per sample, and four spare MYC wells were used as old-dilution diagnostic wells rather than as additional main-result replicates. Melt-curve output, endpoint fluorescence, technical duplicate agreement, and control behavior were reviewed before interpretation.

Samples were grouped by guide identity and induction status. The main guide categories were A, B, D, and NT, each analyzed in paired minus and plus conditions. On some plates, additional labels such as B1 and B2 were used within a guide group. These labels did not represent different guide designs or different biological conditions. Instead, they referred to parallel culture wells that had been seeded at the same time and processed separately through extraction and RT-qPCR. In later experiments, B1 and B2 were therefore treated as distinct matched sample pairs within guide B, but not as biologically different perturbations.

## 2.10 ChIP-qPCR workflow

ChIP-qPCR was developed as an occupancy-oriented assay for testing CTCF binding at targeted sites. The workflow used the Thermo Scientific Pierce Magnetic ChIP Kit (Cat. No. 26157). Cells were crosslinked with 1% formaldehyde for 10 min at room temperature and quenched with glycine before nuclei isolation.

### 2.10.1 Chromatin preparation and fragmentation

Cell pellets were resuspended in 200 µL Membrane Extraction Buffer supplemented with 1× Halt Protease/Phosphatase Inhibitor Cocktail, vortexed, incubated on ice for 10 min, and pelleted at 9,000 × g for 3 min. Nuclei were resuspended in 200 µL micrococcal nuclease (MNase) Digestion Buffer Working Solution containing 1 mM DTT, 2 µL diluted MNase was added per condition, and the suspension was incubated at 37 °C for 15 min with mixing every 5 min. Digestion was stopped with 20 µL MNase Stop Solution, samples were chilled on ice for 5 min, and nuclei were pelleted at 9,000 × g for 5 min.

Pellets were resuspended in 200 µL 1× IP Dilution Buffer with inhibitors and transferred to 1.5 mL Bioruptor Pico tubes. Sonication used 30 s ON / 30 s OFF cycles at the working condition S5 (5 cycles). MNase titration during optimization tested 0, 1, 2, 4, and 6 µL MNase per 100 µL nuclei suspension, with an additional 2 µL S3 comparison. The preferred fragmentation condition taken forward was 2 µL MNase combined with S5, targeting fragments in the approximate 200–1000 bp range. Fragmentation was assessed on a 2% agarose gel in 1× TAE pre-stained with 2 µL GelRed Nucleic Acid Stain (10,000× in water; Biotium, cat. no. 41003; added to ~25 mL of molten agarose before casting), loaded with 500 ng of reverse-crosslinked QC material per lane and run for 45 min alongside NEB 100 bp DNA Ladder (N3231L) for size reference (Figure 3.8). After sonication, chromatin was clarified at 9,000 × g for 5 min and the supernatant transferred to a fresh chilled tube.

### 2.10.2 Immunoprecipitation

10% of the clarified chromatin volume was set aside as the matched input sample. The remaining chromatin was split equally between a CTCF immunoprecipitation and a matched IgG immunoprecipitation, each brought to 300 µL final volume in 1× IP Dilution Buffer with inhibitors. Antibodies were added at:

- **CTCF IP:** 4 µL rabbit monoclonal anti-CTCF antibody (Abcam ab128873, clone EPR7314(B), ChIP grade). This clone was selected because the manufacturer lists it as ChIP-grade and reports knockout-validated reactivity for CTCF, and because the same clone has been used for CTCF ChIP-qPCR in published locus-specific work. Antibody validation is application-specific rather than transferable between formats (Uhlen et al., 2016), so the in-house validation step taken here was the April 20 IP-optimization plate (§3.3), which compared CTCF IP against matched IgG and input at the three CTCF-site assays on shared HCT116-derived chromatin.
- **IgG IP:** 1 µL Normal Rabbit IgG per IP, supplied with the Thermo Scientific Pierce Magnetic ChIP Kit (Cat. No. 26157) as part of the ChIP Kit subassembly (REF 1862739, lot 3214644).

In the April 20 optimization plate, an additional anti-RNA polymerase II (Pol II) immunoprecipitation was included as a positive-control IP at the active GAPDH locus only, in parallel with the anti-CTCF and IgG IPs at the three CTCF-site assays. The B/NT2 follow-up used only anti-CTCF and matched IgG IPs. The A/D/NT3 follow-up used a matched design across A-, A+, D-, D+, NT3-, and NT3+, with a 10% input, anti-CTCF IP, and matched IgG IP for each condition.

IP reactions were rotated overnight at 4 °C. The next day, 20 µL Protein A/G magnetic beads were added per IP and rotated at 4 °C for 2 h. Beads were collected on a magnet and washed four times with 1 mL IP Wash Buffer 1 (5 min mixing per wash), followed by one wash with 1 mL IP Wash Buffer 2. Bound material was eluted in 150 µL 1× IP Elution Buffer at 65 °C for 30 min on an Eppendorf ThermoMixer at 400 rpm.

### 2.10.3 Reverse crosslinking and DNA cleanup

IP eluates and matched 10 % inputs were reverse-crosslinked at 65 °C for 1.5 h with NaCl and Proteinase K on an Eppendorf ThermoMixer at 400 rpm, and the DNA was purified on the Pierce kit's DNA cleanup columns, quantified by NanoDrop, and stored at −20 °C. Buffer volumes and column wash/elution steps are tabulated in Appendix D.7.

### 2.10.4 qPCR readout and analysis

Locus-specific qPCR assays included mycP_CTCF (proximal CTCF docking site; this label is used throughout the thesis, including Tables 2.7–2.8, plate-layout figures, and §3.3; the primer-tube records use the alternative label mycProm_CTCF for the same primer pair), OSE_CTCF (distal OSE/CCAT1-associated CTCF site), GAPDH (positive control region), and negC_CTCF (negative-region control). Amplification used Invitrogen Platinum Direct PCR Universal Master Mix (A44647100) supplemented with 10× SYBR Green I working solution. The executed cycling program was an initial denaturation at 95 °C for 3 min, followed by 40 cycles of 95 °C for 5 s and 60 °C for 20 s, with fluorescence acquisition at the 60 °C step. A post-amplification melt curve was acquired from 65 to 95 °C in 0.5 °C increments. The executed conditions are the ones reported here for reproducibility.

Acceptance criteria for individual wells were defined before interpretation. A well was accepted as a specific amplification only if (i) the CFX Maestro melt-curve caller returned a single peak within ±1.0 °C of the expected assay-specific product temperature — 88.0–88.5 °C for mycP_CTCF, 83.5 °C for OSE_CTCF — and (ii) the matched NTC well for the same assay did not produce a called peak inside the same ±1.0 °C window. The negC_CTCF assay failed this criterion in both occupancy runs because sample and NTC wells amplified in the same Cq range without a called melt peak (§3.3), and is therefore reported but not used for guide interpretation.

ChIP-qPCR primer pairs were selected to test CTCF occupancy at the distal OSE-associated CTCF site, the promoter-proximal MYC CTCF docking site, and a negative-control CTCF region. The distal `OSE_CTCF` assay and the negative-control assay were taken from Supplementary Table I of Chachoua et al. (2022). UCSC In-Silico PCR against GRCh38/hg38 mapped these assays to chr8:127,215,027–127,215,169 (143 bp) and chr2:5,791,569–5,791,703 (135 bp), respectively. For the promoter-proximal MYC CTCF site targeted by guides A and B, the `mycP_CTCF` primer pair (also tagged `mycProm_CTCF` in the primer-tube records) was designed to flank the CTCF motif at chr8:127,734,105–127,734,123 and mapped to chr8:127,734,021–127,734,151 (131 bp), fully covering the motif. The `GAPDH` positive-control primer pair was supplied as a ready-to-use component of the Thermo Scientific Pierce Magnetic ChIP Kit (Cat. No. 26157, §2.10.1); the manufacturer does not disclose the exact sequences, so they are not listed in Table 2.8. Assay-level status and amplicon mapping are summarized in Table 2.7, and full primer sequences for the custom-ordered pairs are listed in Table 2.8.

**Table 2.7. ChIP-qPCR assay status and amplicon mapping (UCSC In-Silico PCR, GRCh38/hg38).**

| Assay | Status | Amplicon (GRCh38/hg38) | Size |
|---|---|---|---|
| `OSE_CTCF` | Mapped (published, Chachoua et al., 2022) | chr8:127,215,027–127,215,169 | 143 bp |
| `negC_CTCF` | Mapped (published, Chachoua et al., 2022) | chr2:5,791,569–5,791,703 | 135 bp |
| `mycP_CTCF` | Mapped (Primer3-designed; primer-tube alias `mycProm_CTCF`) | chr8:127,734,021–127,734,151 | 131 bp |
| `GAPDH` | Positive-control / Pol II; primers supplied with Pierce Magnetic ChIP Kit (Cat. No. 26157) | not mapped here | — |

**Table 2.8. ChIP-qPCR primer sequences.**

| Assay | Primer | Sequence (5'→3') | ID |
|---|---|---|---|
| OSE_CTCF | Forward (OSE_CTCF_qPCR_F) | AGAGCCGAGATTTGAGCCCAGT | J4201D01 |
| OSE_CTCF | Reverse (OSE_CTCF_qPCR_R) | GGTCCCTGCCCTTGATTTGCTG | J4201D02 |
| negC_CTCF | Forward (negCtrl_CTCF_qPCR_F) | CCCAACATTGCAGCCTCTGA | J4201D03 |
| negC_CTCF | Reverse (negCtrl_CTCF_qPCR_R) | GGGCTGTCCTCCACCTCTGA | J4201D04 |
| mycP_CTCF | Forward (mycProm_CTCF_qPCR_F) | GCTGGAAACCTTGCACCTC | J4201D05 |
| mycP_CTCF | Reverse (mycProm_CTCF_qPCR_R) | GCGTTCAGGTTTGCGAAAGT | J4201B02 |
| GAPDH | Forward + reverse pair | Supplied with Pierce Magnetic ChIP Kit (proprietary) | Pierce kit Cat. No. 26157 |

For qPCR, the saved 10% inputs were diluted 1:10 in nuclease-free water before loading, so input wells contained approximately 1% of the starting chromatin. This 100-fold dilution relative to total starting chromatin was accounted for when calculating recovery: percent input was calculated as 100 × 2^(Cq_input,adjusted − Cq_IP), where Cq_input,adjusted = Cq_input − log2(100) ≈ Cq_input − 6.64. Fold enrichment over IgG was calculated as 2^(Cq_IgG − Cq_IP). During the April 20 optimization run, a subset of inputs was amplified at both undiluted and 1:10-diluted concentration to verify the dilution step (see §3.3).

## 2.11 RNA-FISH sample preparation, hybridization, and imaging

Single-molecule RNA fluorescence in situ hybridization (smRNA-FISH) was used to quantify MYC RNA abundance at single-cell resolution, with GAPDH co-detected as a technical QC transcript. Two smRNA-FISH experiments were carried out, one in each of the two HCT116-derived populations defined in §2.2 (Table 2.9). The first experiment was performed in the FACS-derived BFP-enriched H100 subpopulation (§2.4.3) and compared guides D and B against the non-targeting control on a single six-channel ibidi µ-slide using overnight hybridization at high probe concentration. The second experiment was performed in the H100 platform population and introduced guide A; it used a longer four-day hybridization at lower probe concentration, following the protocol rationale that extended hybridization can preserve probe-target binding while reducing nonspecific background.

In the second experiment, guide A, guide B, and the −dox NT control were prepared on a fresh six-channel ibidi slide, while guide D and a complete −dox/+dox NT pair were prepared in matched wells of a 96-well glass-bottom plate to recover the +dox NT condition that was lost from the ibidi slide (Appendix F.2). Both experiments used

the same cell-handling, fixation, post-hybridization, and imaging workflow, and differed in the cell population, the layout, the primary-hybridization probe concentration, and the hybridization duration. Quantitative single-cell results from both experiments are reported in §3.4.1 (first experiment) and §3.4.2 (second experiment).

**Table 2.9. Overview of the two smRNA-FISH experiments.** "Population" follows the §2.2 definitions: FACS-derived = FACS-derived BFP-enriched H100 subpopulation; H100 = H100 platform population. Channel codes C1–C6 refer to the channels of the ibidi µ-Slide VI 0.5 Glass Bottom; well codes (e.g. B2, E3) refer to wells of the 96-well glass-bottom plate used in the second experiment for the guide D and complete NT pair. The +NT channel was lost from the second-experiment ibidi slide because of a contamination in C6 of the previously opened slide that caused the +NT cells to die before fixation; the +dox NT condition was recovered on the 96-well plate. Hybridization conditions reflect the tradeoff between probe concentration and incubation time.

| Experiment | Population | Guides included | Layout | Hybridization probe concentration | Hybridization duration |
|---|---|---|---|---|---|
| 1 | FACS-derived | D, B, NT | ibidi 6-channel: C1 D−, C2 D+, C3 B−, C4 B+, C5 NT−, C6 NT+ | 10 nM per target | overnight at 37 °C |
| 2 | H100 | A, B (ibidi); D, NT (96-well) | ibidi 6-channel: C1 B−, C2 B+, C3 A−, C4 A+, C5 NT−, C6 not used (contamination); 96-well glass-bottom plate: B2 D−, B3 D+, E2 NT−, E3 NT+ | 1 nM per target | 4 days at 37 °C (Thursday → Monday) |

**Table 2.10. Imaging and acquisition metadata for the two smRNA-FISH experiments.** Per-experiment values consolidate the parameters described in prose below. Probe identity refers to the Beckwith-laboratory imager assignment (D1 = GAPDH, D2 = MYC). "Matched" indicates that exposure, laser power, and gain were held matched between the paired −dox and +dox conditions within an experiment but were not exported as numerical settings; absolute values were not tabulated. Channel-by-channel imager information is given in the prose.

| Parameter | Experiment 1 | Experiment 2 |
|---|---|---|
| Cell population | FACS-derived BFP-enriched H100 subpopulation | H100 platform population |
| Sample carrier | ibidi µ-Slide VI 0.5 Glass Bottom (6 channels) | ibidi µ-Slide VI 0.5 Glass Bottom + 96-well glass-bottom plate |
| Carrier layout | 6 channels: C1–C6 (D, B, NT × −/+ dox) | ibidi: C1–C5 (B, A, NT−); 96-well: B2/B3 (D−/D+), E2/E3 (NT−/NT+) |
| Target confluency at fixation | ~70–80 %; intended target ~120,000 cells / channel, depending on glass attachment | ~70–80 %, equivalent areal density per well |
| Probe libraries (probe set assignment) | D1 = GAPDH, D2 = MYC (Beckwith-lab probe libraries) | D1 = GAPDH, D2 = MYC (same probe libraries) |
| Primary-hybridization probe concentration | 10 nM per target | 1 nM per target |
| Primary-hybridization duration | overnight at 37 °C | 4 days at 37 °C |
| Imager oligo concentration (D1/D2 readout) | 20 nM in 2× SSC + Tween-20 (from 50 µM stocks); ~4 min per round | 20 nM in 2× SSC + Tween-20 (from 50 µM stocks); ~4 min per round |
| DAPI counterstain | 1:1000 in 2× SSC + Tween-20 | 1:1000 in 2× SSC + Tween-20 |
| Microscope | Nikon CrestOptics X-Light V3 spinning-disk confocal | Nikon CrestOptics X-Light V3 spinning-disk confocal |
| Cameras | 2 × Photometrics Kinetix back-illuminated sCMOS | 2 × Photometrics Kinetix back-illuminated sCMOS |
| Objective | 100× silicone-oil, NA 1.35 | 100× silicone-oil, NA 1.35 |
| Channels acquired | C0 RNA-FISH (D1 then D2), C1 ConcA-Alexa488, C2 DAPI | C0 RNA-FISH (D1 then D2), C1 ConcA-Alexa488, C2 DAPI |
| Z-stack | 41 sections × 0.3 µm step (~12 µm total) | 41 sections × 0.3 µm step (~12 µm total) |
| FOVs per condition | 10 per ibidi channel (60 stacks total) | 10 per ibidi channel and 10 per well of the 96-well plate |
| Exposure / laser power / gain | matched within experiment; numerical settings not exported | matched within experiment; numerical settings not exported |

The smRNA-FISH workflow followed the Beckwith-laboratory single-molecule RNA-FISH standard operating procedure. All reagents downstream of fixation were RNase-free, and vanadyl ribonuclease complex (VRC) was included in longer incubation steps from fixation through completion of primary probe hybridization.

The standard planned seeding schedule was a three-day cycle: cells were seeded on day 1, medium was replaced on day 2 with matched −dox or +dox induction medium, and cells were fixed on day 3 after approximately 24 h of induction. The second experiment followed this standard schedule (seed Monday → induce Tuesday → fix Wednesday). The first experiment was seeded earlier in the week, with cells seeded Sunday and originally intended for Monday induction and Tuesday fixation. In practice, the schedule was extended: medium was changed to ±dox/Shield-1 on Wednesday (day 4), cells were fixed on Thursday (day 5), and post-hybridization imaging was carried out on Friday (day 6). The induction-to-fixation interval was therefore still ~24 h, but cells in the first experiment had ~3 extra days of attachment time on glass before induction.

Confluency at fixation in the first experiment was nevertheless lower than the intended ~120,000-cells-per-channel target. Two practical issues contributed. First, HCT116 cells attached more slowly to glass-bottom carriers than to standard tissue-culture plastic, which motivated earlier seeding on glass-bottom formats. Second, seeding produced an initial cell-density gradient across the slide. Cell-suspension density was measured on the Countess 3 immediately before seeding. Channels C1–C4 were seeded directly from that suspension without resuspending the Eppendorf in between, but enough time had elapsed by the time C5 and C6 were due that the suspension was re-pipetted before seeding those channels. This produced a higher initial cell density in C5 and C6 (the NT channels) than in C1–C4 at seeding. By fixation, this seeding-day gradient had largely disappeared, so confluency at fixation was no longer obviously different between C5/C6 and C1–C4.

The second experiment used the standard day-1 / day-2 / day-3 schedule and did not show the seeding-day gradient. Cells were seeded into the ibidi channels (~120 µL per channel) with the aim of reaching approximately 70–80 % confluency at fixation, corresponding to an intended target of ~120,000 cells per channel, although lower effective cell numbers were expected when attachment to glass was inefficient. The 96-well glass-bottom wells used in the second experiment were seeded at the equivalent areal density. Slides and plates were incubated under standard cell-culture conditions at 37 °C and 5% $CO_2$ after seeding. Evaporation was limited by sealing ibidi slides and 96-well glass-bottom plates with parafilm; surrounding wells of the 96-well plate were filled with PBS, and ibidi slides were placed in a 10 cm cell-culture dish containing a wet tissue. Because HCT116 cells attach loosely on this glass format and can detach during liquid changes, all subsequent reagent

exchanges were performed by slow side-of-channel pipetting rather than vacuum aspiration to minimize cell loss; this practical change was particularly important after the second-experiment +NT contamination event.

Induction was performed on day 2 (≈24 h after seeding in the standard schedule) by full medium replacement: each +dox channel/well received complete growth medium containing 100 ng/mL doxycycline and 1 µM Shield-1, and each matched −dox channel/well received complete medium without inducer. The 1 µM Shield-1 co-treatment was included to stabilize the destabilization-domain-tagged dCas9 (§2.4.4). After ~24 h of induction (day 3), cells were fixed with 4% paraformaldehyde in PBS for 10 min at room temperature; 100 µL was added per channel/well, removed, and re-added once at the start of fixation, and then washed three times with RNase-free PBS. From this point, all reagents were RNase-free and 0.2 U/µL Superase RNase inhibitor was included in fixation-to-hybridization working solutions that required RNase protection.

Cell membranes were labeled with 10 µg/mL Concanavalin A-Alexa488 in PBS supplemented with Superase (~100 µL per channel, 20 min at room temperature, protected from light) and washed three times with PBS. Post-fixation was performed with Bis(NHS)PEG5 in PBS, freshly prepared (5 mM in the first experiment and 1.5 mM in the second; 40 µL added, removed, then 60 µL re-added; 30 min at room temperature), followed by three PBS washes. Cells were permeabilized with 0.5% Triton X-100 in PBS (~100 µL, removed and re-added; 10 min at room temperature with rocking) and washed twice with PBS. The PFA-fixation and ConcA membrane-labeling steps were identical between the two experiments and across the ibidi and 96-well plate formats; the post-fixation Bis(NHS)PEG5 concentration was the only parameter that differed.

Pre-hybridization used 100 µL of hybridization buffer (H1FA50) per channel/well for 15 min at 37 °C. The library mix was prepared in H1FA50 supplemented with 2 mM VRC and the MYC and GAPDH probe libraries (D1 detecting GAPDH, D2 detecting MYC). Probe library concentration and incubation duration differed between the two experiments and were chosen jointly to maintain probe-to-target stoichiometry across the longer second-run incubation: the first experiment used 10 nM per target with overnight incubation, and the second experiment used 1 nM per target with a four-day incubation (Thursday afternoon to Monday morning). This design followed the protocol rationale that longer hybridization permits lower probe concentration while maintaining RNA-FISH signal and reducing nonspecific background and probe consumption. In both cases, library mix was added 40 µL → remove → 60 µL per channel/well to improve in-channel exchange, and the slide or plate was incubated at 37 °C in the same parafilm-sealed humidified-dish arrangement used during seeding. Post-hybridization washes were the same in both experiments: three rinses

with 50% formamide / 2× SSC, two stringency washes in 50% formamide / 2× SSC for 5 min at ~35 °C, three washes with 2× SSC + 0.2% Tween-20, and a final rinse in 2× SSC.

Imaging was performed on a Nikon CrestOptics X-Light V3 spinning-disk confocal microscope equipped with two Photometrics Kinetix back-illuminated sCMOS cameras for dual-camera fluorescence detection, using a 100× silicone-oil objective (NA 1.35) for the smRNA-FISH stacks. Each field of view comprised 41 optical sections acquired at 0.3 µm z-spacing, spanning approximately 12 µm in total. The three imaged channels corresponded to the RNA-FISH spot signal used for GAPDH/MYC detection (C0, displayed in yellow), the Concanavalin A-Alexa488 membrane label (C1), and the DAPI nuclear counterstain (C2). DAPI was applied as a 1:1000 dilution in 2× SSC + Tween-20 for nuclear segmentation. The MYC and GAPDH RNA-FISH signals were read out in two sequential rounds using DNA-imager oligonucleotides diluted to 20 nM working concentration in 2× SSC + Tween-20 from 50 µM stocks: D1 imager was applied first to detect GAPDH, incubated for ~4 min, and imaged together with DAPI; D1 was then washed out with several rinses of 2× SSC + Tween-20, and the D2 imager was applied to detect MYC, incubated for ~4 min, and imaged at the same fields of view where possible. Acquisition settings (exposure, laser power, gain, objective, and z-stack range) were held matched between −dox and +dox conditions within each experiment to avoid technical intensity bias. For the first experiment, each of the six ibidi channels was imaged as 10 fields of view, giving 60 stacks. The second experiment captured the equivalent ibidi panel (excluding the lost +NT channel) and the four wells of the 96-well glass-bottom plate, using the same per-condition FOV count.

The image-analysis workflow and exported quantitative outputs (per-cell and per-spot tables produced by cell-mask segmentation followed by MYC and GAPDH spot detection and assignment) were generated by Jonas Grini (PhD candidate, Beckwith laboratory), and the resulting tables were used for the analyses reported here. A targeted re-run of the same masking-and-spot-counting code, with localized parameter adjustments, was used to re-quantify a single field of view (FOV6, C2 = D +dox) that had originally failed automated processing; this rescue is summarized in §2.12.2 and documented in Appendix F.5, with its impact incorporated into the §3.4.1 sensitivity interpretation.

## 2.12 RNA-FISH image-derived spot-count analysis

The RNA-FISH image-analysis workflow (cell-mask segmentation followed by MYC and GAPDH spot detection and assignment) was implemented by Jonas Grini, PhD candidate in the Beckwith laboratory, and the exported per-cell and per-spot tables produced by that workflow are the input to the analyses described here. Both smRNA-FISH experiments are reported in this thesis: the first experiment (FACS-

derived population, D / B / NT panel) is summarized in §3.4.1, and the second experiment (H100 platform population, A / B panel on ibidi with D and a complete NT pair on the 96-well plate) is summarized in §3.4.2. Each condition contained 10 fields of view (FOVs) in both experiments. Probe D1 was treated as GAPDH and probe D2 as MYC throughout. The main per-cell output was the number of assigned GAPDH and MYC spots per segmented cell.

**Scope of the smRNA-FISH data.** One smRNA-FISH experiment was performed per population (FACS-derived in experiment 1, H100 in experiment 2), so the data are reported here as an orthogonal single-cell readout that complements bulk RT-qPCR rather than as a fully biologically replicated single-cell expression series. The smRNA-FISH endpoints defined below — per-cell MYC, per-cell MYC / GAPDH, and FOV-level medians — are interpreted at this level of replication, and the FOV-level exclusion criteria are declared and applied uniformly across all conditions before any fold change is computed.

### 2.12.1 Endpoint hierarchy and FOV-level QC

The smRNA-FISH analysis uses an explicit three-level endpoint hierarchy:

- **Primary biological endpoint:** per-cell MYC spot count. MYC is the gene whose perturbation is the biological question, and each segmented cell is the unit on which transcripts are counted.
- **Secondary robustness readout:** per-cell MYC / GAPDH ratio. Agreement between the per-cell MYC change and the per-cell MYC / GAPDH change between paired conditions supports that a MYC change is not driven by a global staining or imaging shift. GAPDH is used here as a technical robustness transcript, not as a formal housekeeping normalizer equivalent to the way reference genes are used in RT-qPCR; the per-cell MYC count, not the MYC / GAPDH ratio, is reported as the headline single-cell number throughout.
- **Supporting robustness analysis:** FOV-level medians (median MYC per FOV; median MYC / GAPDH per FOV). Cells within the same FOV share acquisition focus, illumination background, segmentation, and spot-assignment behavior, so the FOV is the natural technical grouping unit. Agreement between the single-cell and FOV-level summaries is used as a robustness check rather than as the primary endpoint.

GAPDH plays two technical roles in the analysis. At the per-cell level, strong GAPDH signal in a cell indicates that a low MYC value in the same cell reflects MYC biology rather than a generic staining or imaging failure. At the FOV level, a coordinated dip in per-cell GAPDH across a contiguous block of FOVs flags an acquisition-level technical artifact (as exploited for the C1 FOVs 0–6 exclusion in §3.4.2). Cells with GAPDH = 0 are excluded from the per-cell MYC / GAPDH ratio calculation but retained in the per-cell MYC count if MYC > 0. Non-targeting (NT) cells are reported

as a parallel control beside the guide arms in both the single-cell and FOV-level analyses; NT is not used as a divisive normalizer of the guide fold changes.

FOV-level quality control was performed before final fold-change calculation, using a set of formalized exclusion criteria declared in this section and applied uniformly across all conditions in both experiments. FOVs were excluded only when at least one of the criteria below was met; FOVs were never excluded on the basis of MYC values alone or because the resulting fold change was numerically inconvenient. The realized exclusion lists for the two experiments are summarized together with all rescue decisions in Appendix F (Table F.4).

**Formalized FOV-level exclusion criteria.**

1. **Reference-channel (GAPDH) failure:** weak or absent per-cell GAPDH signal across the FOV, identified by per-cell GAPDH being substantially lower than in the matched FOVs of the same condition or in same-slide control channels. Because GAPDH is the within-cell technical reference (§2.12 above), an FOV in which GAPDH detection has failed cannot support a per-cell MYC interpretation regardless of the MYC values it returns.
2. **MYC spot-to-cell assignment failure:** MYC spots detected by the spot-finder but not assigned to segmented cells (e.g. assignment rates below ~75 % in an FOV where neighbouring FOVs of the same condition assign >= 90 %), indicating that the segmentation–assignment step rather than the underlying spot detection has broken down.
3. **Segmentation / focus failure:** loss of cell-mask integrity (e.g. uniform diffuse Concanavalin A signal with no per-cell boundaries, as in the E3 NT+ failure) or z-stack focus problems severe enough that GAPDH cannot be evaluated.
4. **Coherent within-channel acquisition artifact:** a contiguous block of FOVs within a single channel/well in which both GAPDH and MYC per-cell signal drop together, while the same-slide control channels do not show the same coherent reduction. This criterion is grounded in the cross-channel evidence in GAPDH (a reference signal independent of the biological question) so that exclusion does not depend on MYC numbers alone.

FOVs that satisfied none of these criteria were retained, and the same criteria were applied to every condition and to every channel/well of both smRNA-FISH experiments. Where a failure mode was correctable (e.g. a channel-order mismatch in the B2 / B3 acquisitions of the second experiment, or the local-thresholding failure of D +dox FOV6 in the first experiment), the affected FOVs / wells were re-quantified by a targeted re-run of the same masking-and-spot-counting code rather than excluded; the rescue procedures and their before/after impact are documented in the subsections below and summarized in Appendix F (Table F.4).

### 2.12.2 First-experiment FOV6 sensitivity rescue

One QC-excluded FOV in the first experiment (D +dox, C2 FOV6) was re-quantified using a targeted re-run of the same masking-and-spot-counting code with the known FOV-level alignment shift applied and a fixed DoG intensity threshold. The §3.4.1 results report the QC-excluded version as the headline number, with the FOV6-rescued numbers shown as a sensitivity comparison; the direction of the guide-D effect is preserved under either treatment of FOV6, while the absolute MYC-only knockdown magnitude is sensitive to FOV6 inclusion. The full per-FOV rescue parameters and the side-by-side sensitivity numbers are tabulated in Appendix F.5 (Table F.4).

### 2.12.3 Second-experiment guide-D channel-order rescue

In the second smRNA-FISH experiment, the two guide-D wells on the 96-well plate (B2, B3) were acquired with a different `.nd2` channel order than the morning batch, so the standard pipeline initially detected bright DAPI structures as if they were RNA-FISH spots. An initial in-house corrected-channel rescue showed that the B2 / B3 acquisitions could be recovered by using the appropriate channel indices. Jonas Grini then independently re-processed the same acquisitions with the corrected channel order using the laboratory image-analysis workflow, and this corrected output is used as the primary guide-D analysis in §3.4.2. The in-house rescue is retained as a supporting sensitivity analysis. The two analyses agreed on direction and approximate magnitude despite different segmentation performance (Jonas corrected D+ / D− per-cell mean MYC FC 0.48; in-house rescue 0.52). Detection thresholds, per-pipeline cell counts, and the side-by-side fold-change table are given in Appendix F.4 (Table F.3).

### 2.12.4 Second-experiment NT and B-channel QC decisions

Two further condition-level QC decisions were applied in the second experiment. First, the recovered +dox NT well on the 96-well plate (E3) was not used as a matched +dox NT comparator because direct image inspection showed a per-well ConcA segmentation failure together with a genuine ~4× per-FOV MYC reduction in cells that were otherwise present and had healthy nuclei; NT is therefore reported in §3.4.2 as a parallel −dox baseline rather than as a +/− contrast. Second, within the ibidi B− channel (C1), FOVs 0–6 showed a coherent low-signal block in both the GAPDH QC channel and the MYC target channel that was not present in the matched +dox channel or in the parallel −dox A and NT channels on the same slide; these FOVs were therefore excluded as a within-channel acquisition artifact in the guide-B comparison, grounded on the cross-channel evidence in GAPDH rather than on the MYC numbers alone. The full direct-image evidence for the E3 ConcA failure (Figures F.2–F.4) and the per-well QC decision audit are documented in Appendix F.3 and F.5 (Table F.4).

## 2.13 Data organization, plotting, and software

Instrument outputs from RT-qPCR and ChIP-qPCR were exported from CFX Maestro as table-based files containing Cq values, amplification summaries, melt-curve information, endpoint fluorescence, and plate-view summaries. Data were organized into raw exports, cleaned summary tables, derived analysis tables, and plotting scripts. Python was used to process exported tables and generate derived summaries and figures for the March 27, March 31, April 1, April 19, April 20, April 21, April 30, May 1, and May 6 datasets.

Microscopy files were inspected using Fiji/ImageJ and Napari. Fiji/ImageJ was used for visual inspection and preparation of .lsm microscopy images, including mCherry transfection checks, anti-Cas9 immunofluorescence, and BFP-channel induction/background images. Napari was used to inspect and render .nd2 RNA-FISH image stacks. RNA-FISH quantitative outputs were organized as per-cell spot-count tables, per-FOV summaries, QC tables, and plotting scripts. The exported image-analysis tables were used to calculate per-cell MYC counts, per-cell MYC/GAPDH ratios, FOV-level medians, fold changes, and QC summaries.

Runs with limited replication, missing values, failed controls, weak melt support, or FOV-level imaging artifacts were summarized descriptively rather than by formal inferential statistics.

## 2.14 Use of artificial intelligence tools

Generative artificial intelligence tools were used in a limited support role during preparation of this thesis. Specifically, AI tools were used to assist with modification and troubleshooting of Python code used to generate figures, and to support troubleshooting and interpretation during RNA-FISH data analysis.

All code modifications, figure outputs, data-processing decisions, and scientific interpretations were reviewed by the author before inclusion in the thesis. AI tools were not used to generate experimental data, were not treated as scientific sources, and were not used as a substitute for primary literature, supervisor feedback, laboratory records, or direct inspection of the experimental data.

# 3 Results

Chapter 3 presents the experimental evidence in five steps. First, platform validation and guide construction established the experimental system (§3.1). Second, RT-qPCR identified guide- and population-dependent MYC-lowering patterns, with the strongest H100 support for guides A and D and FACS-derived support for guide B (§3.2). Third, ChIP-qPCR did not detect guide-specific CTCF loss at the mapped target assays (§3.3). Fourth, RNA-FISH provided orthogonal single-cell support for reduced MYC in selected guide conditions (§3.4). Finally, the integrated guide-level summary combines these readouts to distinguish expression-level support from the unresolved upstream occupancy mechanism (§3.5).

## 3.1 Platform generation and sgRNA validation

The inducible dCas9 platform was established in HCT116-based cells by plasmid delivery, drug selection, expansion, and fluorescence-based enrichment. The main platform-level outputs available for this thesis are summarized in Table 3.1.

**Table 3.1. Platform-level validation and enrichment outputs.**

| Check | Result recorded | Use in thesis |
|---|---|---|
| FACS enrichment | BD FACSAria II BFP sort of the H100 platform population (violet 405 nm laser, DAPI 450/40 channel for BFP): BFP-positive gate represented 0.23% of singlet-gated events for the H100 sample versus 0.22% for the wild-type HCT116 control on the same gate; 3291 BFP-positive events were nevertheless collected into 1 mL medium and re-expanded | Establishment of the FACS-derived BFP-enriched H100 subpopulation as a strongly bottlenecked subpopulation selected from a low-frequency BFP-positive tail (interpreted in §4.3) |
| dCas9 induction check | March 31 qPCR plate: selected plus samples showed higher detectable dCas9 signal than matched minus samples | Supporting induction check |
| Anti-Cas9 IF | Microscopy-based platform check: detectable Cas9-associated signal was observed in cells | Qualitative evidence of platform expression |
| Parallel populations | Project records: the H100 platform population and the FACS-derived BFP-enriched H100 subpopulation were maintained separately after sorting | Defines the two HCT116-derived populations used for downstream RT-qPCR |

Flow cytometry detected only a very small BFP-positive fraction in the H100 platform population, close to the wild-type HCT116 background gate (0.23% versus 0.22% on the same DAPI 450/40 BFP gate; Table 3.1). Nevertheless, BFP-positive events were sorted from this population, yielding 3291 collected events. The resulting FACS-

derived population should therefore be interpreted as a strongly bottlenecked BFP-enriched subpopulation selected from a very low-frequency BFP-positive tail of the H100 starting material, rather than as evidence that the bulk H100 population was broadly BFP-positive. This distinction is used throughout the RT-qPCR results because the March 27, April 21, and May 1 experiments were performed in the H100 platform population, whereas the March 31, April 1, and April 19 experiments were performed in the FACS-derived BFP-enriched H100 subpopulation. As described in §2.2, these two HCT116-derived populations should not be treated as interchangeable biological replicates; the practical consequence of the low-frequency BFP gate for choosing which population to take forward is discussed in §4.3.

## 3.2 RT-qPCR identifies guide-associated MYC reductions

The functional experiments used guide A, guide B, guide D, and a non-targeting control. Guides A and B targeted the promoter-proximal MYC CTCF binding site approximately 2 kb upstream of the MYC promoter. Guide D targeted a distal OSE/CCAT1-associated CTCF site approximately 521 kb upstream of MYC. This distal site was included because previous work in HCT116 cells linked an OSE-associated CTCF site to WNT-dependent MYC gating, MYC mRNA export, nuclear-pore-associated positioning, and colon cancer cell growth (Chachoua et al., 2022). NT served as the non-targeting comparator for induction- or platform-associated effects.

The RT-qPCR datasets used in Chapter 3 are summarized in Table 3.2. Fold change is used as the primary expression readout because it is easier to read directly than dCq values: values below 1 indicate lower MYC in the plus condition relative to the matched minus condition.

**Table 3.2. RT-qPCR run overview.** "H100" denotes the H100 platform population and "FACS-derived" denotes the FACS-derived BFP-enriched H100 subpopulation, as defined in §2.2.

| Run/date | Population and design | Main QC status and use |
|---|---|---|
| March 27, 2026 | H100; A, B, D, NT; fixed-volume / reconstructed RNA input | YWHAZ-normalized MYC; weak MYC melt support |
| March 31, 2026 | FACS-derived; A, B, D, NT; fixed-volume loading | YWHAZ/B2M-normalized MYC; input confound and weak controls |
| April 1, 2026 | FACS-derived; B only; 8 ng equal-mass loading | Technically cleaner guide B rerun |
| April 19, 2026 | FACS-derived; A, B, D, NT; 8 ng equal-mass loading | Improved MYC melt support |
| April 21, 2026 | H100; A, B, D, NT; 20 ng equal-mass loading | Raw and normalized MYC; no called MYC melt peaks |
| May 1, 2026 | H100 DNase rerun; A, B, D, NT; 20 ng equal-mass loading; fresh NZYRT and primers | Recovered MYC Cq range and melt support; clean MYC NRT |

### 3.2.1 RT-qPCR run overview and QC weighting

The March 27 H100 run was the first four-guide expression screen. Figure 3.1 shows YWHAZ-normalized MYC fold change for A, B, D, and NT.

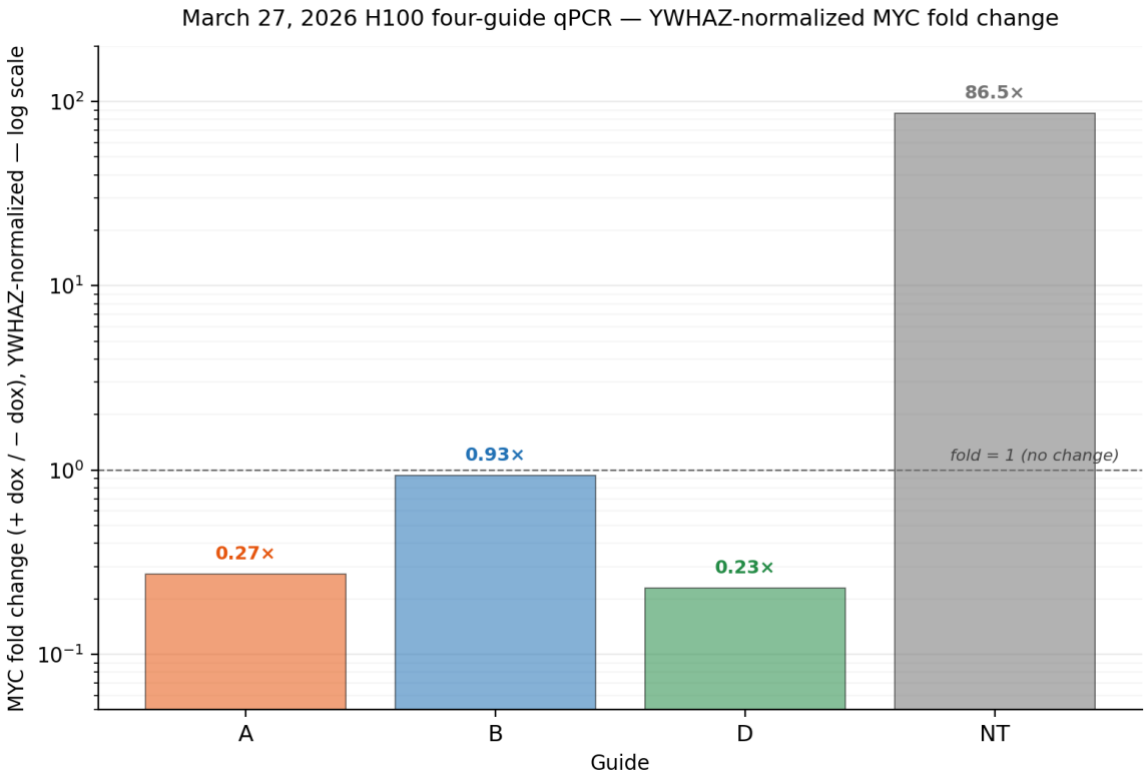


**Figure 3.1.** YWHAZ-normalized MYC fold change from the March 27, 2026 four-guide H100 qPCR run. Fold change was calculated as +dox / −dox after YWHAZ normalization (+dox samples were co-treated with Shield-1; the comparison is induced versus uninduced within the same guide arm). Bars show guide-level fold change on a log y-axis; the dashed line marks fold = 1 (no induction-associated change). Values below 1 indicate lower MYC after induction. The log scale prevents the NT outlier (~87×) from compressing the guide A, B, and D bars near zero.

In Figure 3.1, guides A and D showed lower normalized MYC in the plus condition, whereas guide B was closer to neutral. NT did not behave as a stable no-change control, driven by an extraction failure in the +NT sample that collapsed the reference-gene signal under fixed-volume loading. Because this run had weak MYC melt support and limited replication structure (Table 3.3), it was used as an exploratory guide-ranking result rather than as validation.

The March 31 plate tested the same guide set in the FACS-derived BFP-enriched H100 subpopulation (§2.2) and added a larger plate structure, B2M as an additional reference gene, NTC/NRT controls, and a small number of dCas9 wells. Figure 3.2 shows the YWHAZ-normalized fold-change summary for the main MYC readout.

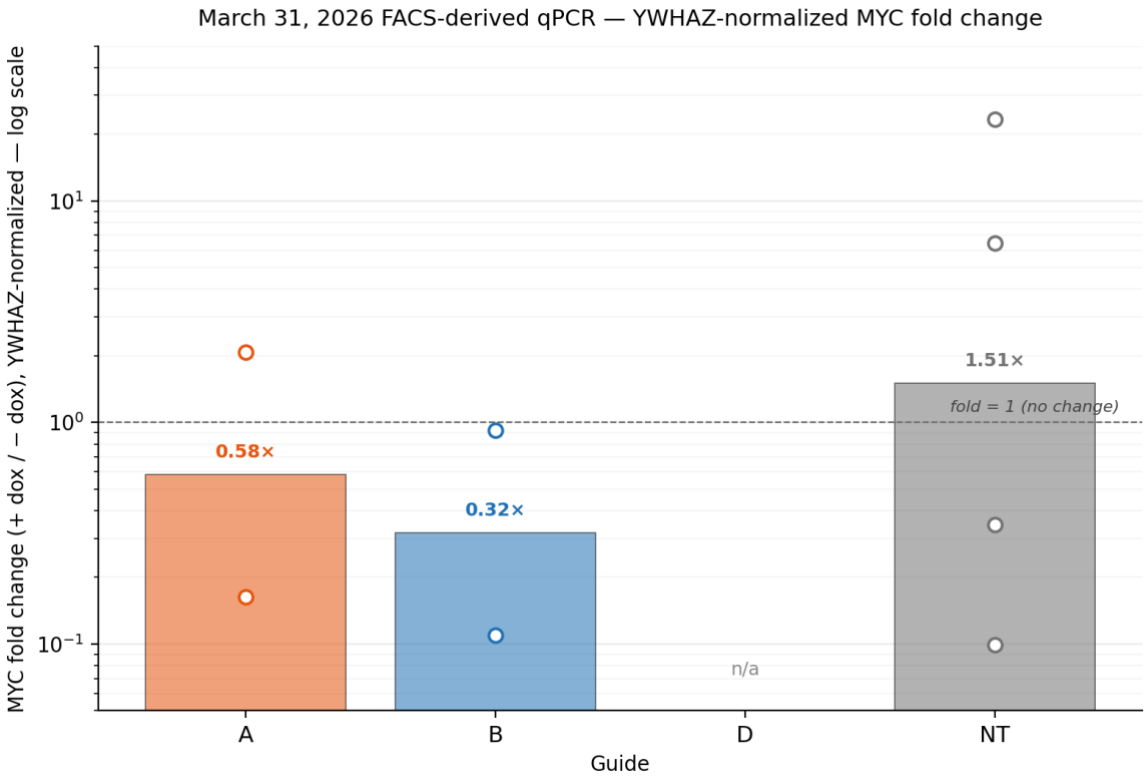


**Figure 3.2.** YWHAZ-normalized MYC fold change from the March 31, 2026 FACS-derived qPCR plate. Fold change was calculated as +dox / −dox after YWHAZ normalization (+dox samples were co-treated with Shield-1; the comparison is induced versus uninduced within the same guide arm). Bars show guide-level geometric means on a log y-axis with biological-replicate fold changes overlaid as colored circles; the dashed line marks fold = 1 (no induction-associated change). Values below 1 indicate lower MYC after induction. Guide D is shown as "n/a" because one paired sample did not yield a usable Cq.

Figure 3.2 shifted attention toward guide B because guide B showed lower normalized MYC than its matched minus condition. Guides A and D were not similarly consistent on this plate. The NT comparisons were mixed, including an outlier-driven shift, and therefore did not provide a clean baseline for biological interpretation. The plate also had important QC problems: fixed-volume RNA loading produced unequal RNA mass across samples, NTC/NRT behavior was weak, and MYC melt support was poor (Table 3.3). The result was therefore informative for guide prioritization but not sufficient for validation.

The April 1 run was a focused guide B rerun in the FACS-derived population using leftover RNA from the March 31 series. It used equal-mass loading at 8 ng RNA per well and included the paired B1 and B2 comparisons. Rather than presenting the April 1 result as a standalone two-replicate figure, Figure 3.3 places the April 1 equal-mass replicates (orange squares) into the broader context of guide B behavior across all six RT-qPCR runs in this thesis.

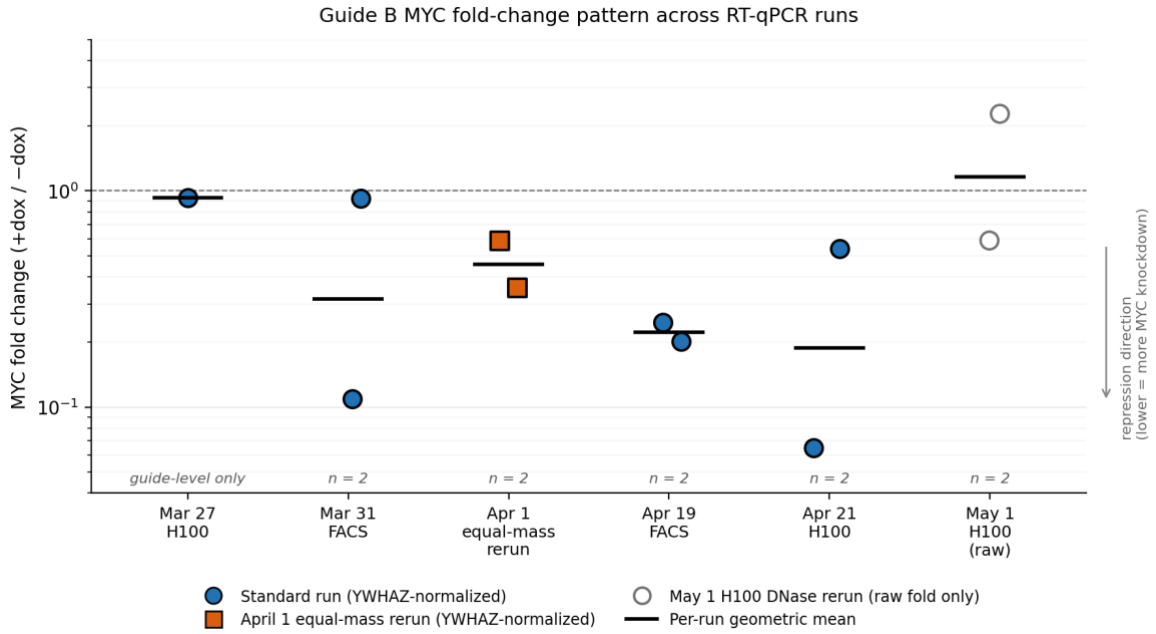


**Figure 3.3.** Guide B MYC fold change (+dox / −dox) across the six RT-qPCR runs of this thesis, shown on a log scale. Each dot represents one biological replicate (B1 or B2), and short horizontal ticks show the per-run geometric mean. Filled blue circles show YWHAZ-normalized values from standard runs. Filled orange squares show the April 1 equal-mass rerun on leftover March 31 RNA, also YWHAZ-normalized. Open gray circles show the May 1 H100 DNase rerun raw MYC readout; May 1 is handled separately because NT reference-gene shifts made normalized fold changes non-specific (§3.2.3). On May 1 both B1 and B2 were inhibitor-affected (§3.2.3), so the May 1 points are shown for traceability but are not used in the cross-run guide-B interpretation. The dashed line at fold = 1 indicates no change; lower values indicate lower MYC in the +dox condition.

In Figure 3.3, both April 1 equal-mass replicates were below 1 after YWHAZ normalization (B1 = 0.36, B2 = 0.59), consistent with the direction seen in the March 31, April 19, and April 21 runs. The B1 decrease was numerically larger, but weaker analytically because raw MYC did not move in the same direction, indicating that the normalized decrease depended substantially on reference-gene movement. B2 was more consistent because normalized MYC and raw MYC moved in the same general direction. Although the April 1 rerun improved RNA-input control for guide B, MYC amplicon-window melt support remained weak when re-scored against the consistent 88.5–90.5 °C window (1/8 formal MYC sample wells; Table 3.3). The run therefore served primarily as a technical check of the guide B fold-change pattern in leftover March 31 RNA, rather than as strong amplicon-validated evidence from a new biological series. Across the cross-run trajectory, guide B values clustered below the no-change line in five of six runs and showed wide replicate spread in every run with at least two replicates, reflecting a consistent direction-of-effect signal that no single run resolved into a tight reproducible knockdown — a pattern interpreted in §4.

MYC melt-curve support differed strongly across the qPCR series. Because CFX Maestro auto-calls can include peaks outside the expected MYC amplicon temperature range, cross-run melt support was re-scored from the exported melt-peak files using a single consistent definition: a called melt peak in an unknown MYC sample well with melt temperature in the [88.5, 90.5] °C MYC amplicon window. The 88.5-90.5 °C window was chosen because the cleanest run in the series (April 19 FACS-derived) produced a tight cluster of MYC peaks at 89.0-89.5 °C, and a 1 °C tolerance accommodates modest run-to-run shifts while still excluding the ~79-80 °C primer-dimer/non-specific peaks that dominated several other plates. Table 3.3 and Figure 3.4 summarize the resulting MYC amplicon-window support across the six RT-qPCR runs.

**Table 3.3. Cross-run MYC amplicon-window melt support.** Support was scored as a called MYC peak within 88.5–90.5 °C in unknown MYC sample wells. May 1 was scored by manual derivative-curve review because CFX auto-call returned no peaks. Full re-scoring rules and rationale are given in the paragraph above this table.

| Run | MYC-window melt support | QC implication |
|---|---|---|
| March 27 H100 | 3/16 unknown MYC wells (18.8%) | Weak MYC-specific support |
| March 31 FACS-derived | 4/40 unknown MYC wells (10.0%) | Weak MYC-specific support |
| April 1 FACS guide B | 1/8 formal MYC sample wells (12.5%) | Weak MYC-specific support despite equal-mass loading |
| April 19 FACS-derived | 37/40 unknown MYC wells (92.5%) | Strong MYC-specific support; first technically strong MYC qPCR run |
| April 21 H100 | 2/32 unknown MYC wells (6.3%) | Weak MYC-specific support; mostly non-MYC-like peaks (~79-80 °C) |
| May 1 H100 DNase rerun | 27/32 unknown MYC wells (84.4%) at 89.5 °C | Strong MYC-specific support recovered after DNase treatment and fresh NZYRT |

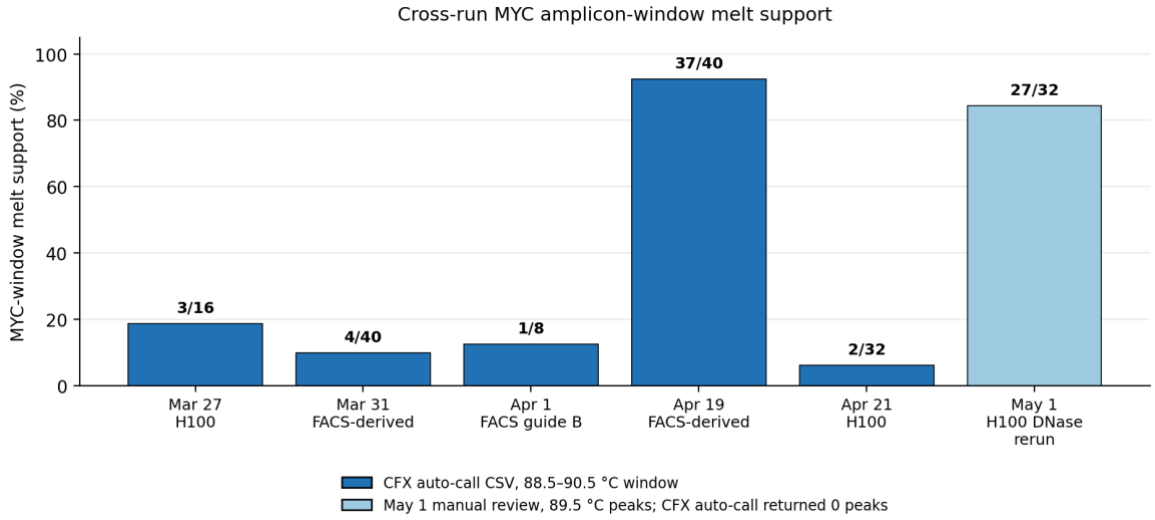


**Figure 3.4.** Cross-run MYC amplicon-window melt support. Bars show the percentage of unique unknown MYC sample wells with at least one called peak in the 88.5–90.5 °C MYC amplicon window, scored from exported CFX Maestro auto-call melt-peak files. Labels above bars show the number of wells within this window over the total number of unknown MYC sample wells inspected. Peaks outside this window were not counted as MYC-specific support, even if CFX Maestro called a peak. May 1 (lighter bar) was scored from manual derivative-curve review of 89.5 °C peaks because CFX auto-call returned no peaks for any well on that plate.

Table 3.3 and Figure 3.4 sharpen the cross-run picture: the early runs, including the April 1 equal-mass rerun, all had limited MYC amplicon-window support and therefore cannot carry magnitude-validating weight on their own. April 19 FACS-derived was the first early-series run with strong MYC-specific melt support and therefore receives more technical weight than the earlier March 31 FACS-derived run, even though the biological interpretation remained complicated. April 21 H100 again lacked MYC amplicon-window support and is treated as directional rather than validating despite equalized RNA input. May 1 recovered strong MYC-specific support when the H100 RNA was rerun with fresh NZYRT and DNase-treated RNA.

Additional April 19 and April 21 QC observations are summarized in Table 3.4.

**Table 3.4. Additional April 19 and April 21 RT-qPCR QC observations.**

| QC feature | April 19 FACS-derived | April 21 H100 | Note |
|---|---|---|---|
| RNA input per well | 8 ng | 20 ng | Later Cq not due to lower RNA input |
| MYC amplicon-window melt support (88.5-90.5 °C) | 37/40 wells | 2/32 wells | April 19 validates; April 21 directional only |
| MYC Cq behavior | earlier than April 21 | ~10 cycles later | Run-specific technical limitation |
| NRT behavior | later per ng input | ~1–2 cycles earlier per ng input | Higher relative non-RT signal on April 21 |
| YWHAZ NRT proximity | close to sample Cq | close to sample Cq | YWHAZ-normalized interpretation limited |

Table 3.4 adds two technical details that affect interpretation of the April 21 H100 run. First, MYC Cq values were approximately 10 cycles later on April 21 than on April 19 despite higher RNA input per well. Second, per-ng-input NRT values were earlier on April 21, consistent with greater relative non-RT signal. Together with the absence of called MYC melt peaks, these observations mean that April 21 is useful for directional guide ranking but not for confident fold-change magnitude.

### 3.2.2 FACS-derived RT-qPCR: guide-B MYC reduction with parallel NT shift

The April 19 qPCR run was performed in the FACS-derived population using equalized RNA input and a broader guide layout. Compared with March 31, the run had much stronger MYC melt support (Table 3.3). Figure 3.5 shows the YWHAZ-normalized fold-change pattern.

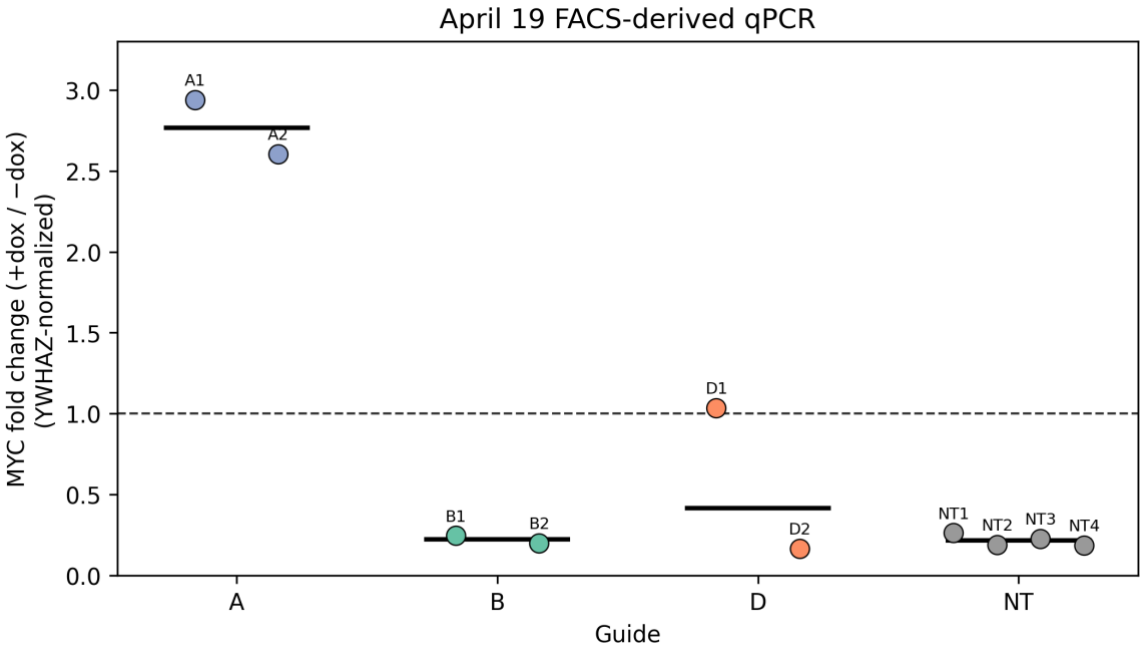


**Figure 3.5.** YWHAZ-normalized MYC fold change from the April 19, 2026 FACS-derived qPCR run. Each point shows the +dox/−dox fold change for one matched biological pair, and horizontal black lines show the guide-level geometric mean across pairs. The dashed line marks no induction-associated change (+dox samples were co-treated with Shield-1; the comparison is induced versus uninduced within the same guide arm).

In Figure 3.5, guide B showed lower normalized MYC in both B1 and B2, with guide-level fold change of approximately 0.22. However, NT showed a similar shift, with NT pairs clustering between approximately 0.19 and 0.26. D was mixed, with one pair near neutral and one lower, and A moved in the opposite direction with fold changes above 1. The April 19 run therefore improved technical confidence in the qPCR assay but weakened the guide-specific interpretation of B because the non-targeting control shifted similarly.

### 3.2.3 H100 RT-qPCR supports guide-A and guide-D2 MYC decreases after assay recovery

The April 21 H100 run repeated the four-guide comparison in the H100 platform population with equalized 20 ng RNA input. This made raw MYC comparisons more interpretable than in earlier fixed-volume runs. Figure 3.6 shows the YWHAZ-normalized +dox/−dox MYC fold change per guide with biological-replicate values overlaid; raw and B2M-normalized fold changes are reported as sensitivity checks in the prose below.

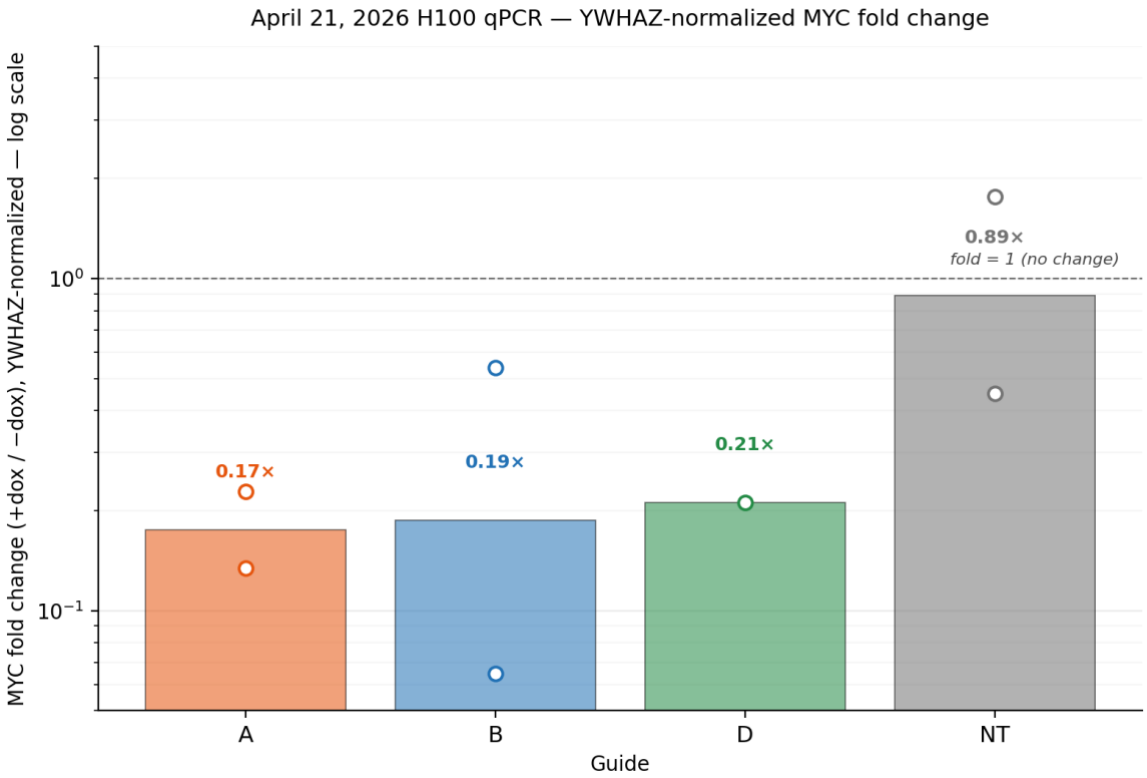


**Figure 3.6.** YWHAZ-normalized MYC fold change from the April 21, 2026 H100 qPCR run. Bars show guide-level geometric means of the +dox/−dox per-pair fold change on a log y-axis, with biological-replicate fold changes overlaid as open circles (two per guide except guide D, where only D1 is plotted because the matched D2 MYC wells did not produce usable Cq values; see Table 3.4). The dashed line marks fold = 1 (no induction-associated change); +dox samples were co-treated with Shield-1, and the comparison is induced versus uninduced within the same guide arm. Values below 1 indicate lower MYC after induction.

Figure 3.6 identifies guide A as the clearest H100 MYC-lowering pattern in this run, with a YWHAZ-normalized geometric-mean fold change of approximately 0.17× and consistent direction across A1 and A2. Sensitivity checks in the other normalizations agree: the raw-MYC fold change for guide A was approximately 0.12× and the B2M-normalized value was approximately 0.09×. Guide B also showed lower YWHAZ-normalized MYC (geometric mean approximately 0.19×) but with much larger replicate spread: B1 fell below 0.1× while B2 sat above 0.5×, reflecting severe duplicate spread in the −B1 minus MYC wells. Guide D was not cleanly supported on this run because only D1 was usable; D1 sits near the guide-D bar (~0.21× YWHAZ-normalized), but the raw MYC change for D was small compared with the normalized change. The NT control gave a YWHAZ-normalized geometric mean close to 1.0 (~0.89×), with one replicate (NT1) above 1 and one (NT2) below — i.e. NT did not show a clear downward shift in this normalization as it did in the raw and B2M-normalized summaries (raw geometric mean ~0.47×, B2M-normalized geometric mean ~0.55×). The main technical limitation was the complete absence of called

MYC melt peaks in the unknown MYC wells (Table 3.3), together with the additional cross-run QC constraints summarized in Table 3.4.

The H100 RNA used in this run was prepared on April 3 from cultures grown in 24-well plates. Prep-stage Countess and NanoDrop observations are summarized in Table 3.5. These observations indicate high viability at harvest, but also show that the samples were dense by the harvest-day cell-count estimate and that two minus-condition samples had low 260/230 ratios consistent with extraction-buffer carryover. Section 4.4 discusses how these prep-stage observations relate to the late MYC Cq and absent MYC melt peaks on this run.

**Table 3.5. April 3 H100 RNA-prep observations relevant to the April 21 qPCR run.**

| Feature | Observation | Interpretation |
|---|---|---|
| Viability | 95–100% across 16 samples | No evidence of widespread cell death at harvest |
| Countess concentration | 0.35–1.71 million cells/mL | Equivalent to approximately 0.35–1.71 million cells per well, based on the ~1 mL harvest volume |
| Density estimate | Several samples exceeded a practical near-confluence benchmark for HCT116 in 24-well format | Based on Countess values and approximate harvest volume; interpreted as dense harvest-state context rather than a precise confluence calculation |
| NanoDrop concentration | 10.7–126.9 ng/µL | Wide RNA-yield range; lowest readings are approximate |
| 260/230 hotspot | -B1 = 0.10 and -B2 = 0.39 | Localized carryover risk in two minus-condition samples |

The May 1 H100 rerun recovered MYC-specific melt support and showed raw MYC decreases for guide A and the D2 guide-D replicate. Because NT and reference-gene values shifted in the same direction after normalization, normalized fold changes are reported as diagnostics rather than as standalone guide-specific effect sizes; raw MYC is the clearest directional readout for this run. The May 1 RT-qPCR run was a targeted rerun of the April 21 H100 design with three controlled changes: the same RNA samples as April 21 were treated with TURBO DNase before use, a previously unopened NZYRT mix aliquot was used for reverse transcription, and the MYC, B2M, and YWHAZ primer working stocks were freshly diluted from concentrated stocks. RNA mass per well was held at 20 ng to keep the cross-run comparison interpretable. Four additional wells were included as an internal control for the NZYRT change: aliquots of the same April 21 RNA, without DNase treatment, were diluted to the same working concentration and run alongside the DNase-treated samples (referred to here as the “OLD” wells; +A1, +A2, +B1, +B2 only). This design

separates the contributions of NZYRT freshness and DNase treatment to any change in MYC Cq.

The results showed a substantial recovery of MYC signal compared with April 21. Across the 32 unknown MYC sample wells, 27/32 (84.4%) had called melt peaks at 89.5 °C, with peak heights of approximately 350–700 (Table 3.3), comparable to the April 19 FACS-derived run (92.5% MYC amplicon-window support; Table 3.3). The five remaining sample wells without called peaks at the auto-detection threshold (-B1, +B2, and one -D1 replicate) corresponded to the same samples flagged for extraction-buffer carryover in Table 3.5; manual inspection of the raw melt curves confirmed that these wells contained subthreshold 89.5 °C peaks rather than absent product. MYC NTC peaks appeared at approximately 79 °C, consistent with primer-dimer rather than MYC amplicon. MYC NRT for the +B2 control sample was undetermined, indicating effective removal of gDNA-derived signal in the MYC channel after DNase treatment. YWHAZ NRT shifted from approximately Cq 22 on April 21 to Cq 36 on May 1, also consistent with effective gDNA removal.

Sample MYC Cq values fell into the 24–30 range, approximately 10 cycles earlier than the April 21 run despite identical RNA input mass and otherwise comparable plate setup. The OLD-wells comparison attributed most of this April 21-to-May 1 MYC Cq recovery to fresh NZYRT activity, with DNase treatment providing the expected separate effect of removing gDNA-derived signal from the cDNA-specific readout; the per-sample April 21 vs. May 1 OLD-well Cq table and supporting reasoning are reported in Appendix C.3 (Table C.4).

Inhibitor carryover from the April 3 RNA prep persisted into the May 1 rerun. Four samples (-B1, -B2, -D1, +B2) were flagged as inhibitor-affected by the combined 260/230 ≤ 0.5 + multi-target Cq suppression rule (Table 3.6), and the May 1 +/– contrasts for guide B (both B1 and B2) and for guide D1 are therefore not interpretable as cleanly as the contrasts for A1, A2, D2, NT1, and NT2. The full per-sample 260/230 and Cq detail is in Appendix C.3.

**Table 3.6. May 1 inhibitor/carryover flags.** Samples were flagged when NanoDrop purity and/or multi-target Cq behavior indicated residual extraction-buffer carryover.

| Sample | Post-DNase 260/230 | qPCR behavior | Status |
|---|---|---|---|
| -B1 | 0.10 | MYC and B2M both late | Inhibitor-affected |
| -B2 | 0.23 | MYC late; poor purity | Inhibitor-affected |
| -D1 | 0.40 | MYC ~30 and B2M ~26 | Inhibitor-affected |
| +B2 | 1.08 | MYC ~28.3, B2M ~27.0, YWHAZ ~24.9; MYC melt below auto-call threshold | Inhibitor-affected by Cq pattern |

The non-targeting control behavior on the May 1 plate again limited guide-specific interpretation of normalized fold changes. Reference-gene Cq values were unexpectedly earlier in the +NT samples than in the matched -NT samples for B2M (-NT1 at 23.79 vs. +NT1 at 22.54; -NT2 at 22.64 vs. +NT2 at 21.85). YWHAZ was run as a single well per sample on this plate, and the -NT2 YWHAZ well was non-interpretable (Cq 30.63). As a result, NT normalization was not a stable guide-specific denominator: the NT pairs themselves gave strong apparent reductions after reference normalization (B2M-normalized FC ~0.17 for both NT pairs; YWHAZ-normalized FC ~0.105 for NT1 and ~0.0003 for NT2), even though the raw MYC decrease in NT was more modest (0.40 for NT1 and 0.30 for NT2). NT was therefore used as a control-behavior warning rather than as a reliable denominator for guide-specific normalization.

Because the May 1 run used equal-mass RNA input, DNase-treated RNA, fresh NZYRT, freshly diluted primers, and recovered MYC melt support, raw MYC Cq values were the clearest directional readout for this run. Among non-flagged guide pairs, A1, A2, and D2 showed lower raw MYC after induction (A1 0.23, A2 0.13, D2 0.10). These raw decreases were larger than the NT raw shift (NT geometric mean ~0.35), but not by enough to make May 1 a clean NT-adjusted guide-specific result on its own. Reference-normalized values for A1, A2, and D2 also fell below 1 within each guide pair (YWHAZ-normalized: 0.42, 0.26, 0.32; B2M-normalized: 0.54, 0.61, 0.76), but the normalized NT controls shifted in the same direction and therefore weaken guide-specific interpretation rather than strengthening it. The May 1 run is therefore best interpreted as a technically stronger H100 rerun that supports a raw-MYC decrease for A and D2, while the normalized fold changes remain diagnostic and non-specific because of NT reference-gene behavior. The B1, B2, and D1 +/− contrasts were not interpretable because inhibitor carryover affected one or both paired samples; the matching B2 numerical decrease and the B1/D1 apparent increases all sit on top of suppressed baselines and are not used in interpretation. Guide B contrasts on the May 1 H100 plate were therefore uninterpretable for both B1 and B2.

**Table 3.7. May 1 H100 DNase rerun fold-change summary across RT-qPCR readouts.** Raw MYC fold change is the clearest directional readout for this run because the NT controls shifted after reference normalization. YWHAZ- and B2M-normalized values are shown as normalization diagnostics, not as standalone guide-specific effect sizes. Flagged pairs are listed for traceability but their numerical values are not emphasized because inhibitor carryover suppressed one or both paired samples.

| Pair | QC status | Raw MYC FC | YWHAZ-normalized FC | B2M-normalized FC | Interpretation |
|---|---|---|---|---|---|
| A1 | Called 89.5 °C peaks | 0.23 | 0.42 | 0.54 | Raw decrease; normalized values not NT-specific |
| A2 | Called 89.5 °C peaks | 0.13 | 0.26 | 0.61 | Raw decrease; normalized values not NT-specific |
| D2 | Called 89.5 °C peaks | 0.10 | 0.32 | 0.76 | Raw decrease, single usable D pair; normalized values not NT-specific |
| B1 | Inhibitor-affected -B1 | not emphasized | not emphasized | not emphasized | Not interpretable |
| B2 | Inhibitor-affected -B2 and +B2 | not emphasized | not emphasized | not emphasized | Not interpretable |
| D1 | Inhibitor-affected -D1 | not emphasized | not emphasized | not emphasized | Not interpretable |
| NT1 | Reference-gene shift | 0.40 | 0.105 | 0.169 | Control-behavior warning |
| NT2 | Reference-gene shift; single-well YWHAZ failure | 0.30 | 0.0003 | 0.172 | Control-behavior warning |

Figure 3.7 shows the per-pair May 1 fold changes across the three RT-qPCR readouts, with raw MYC emphasized as the most interpretable directional readout and the normalized values shown as reference-gene diagnostics. The raw-only per-pair view, including the inhibitor-affected B and D1 pairs and the NT controls, is reproduced as Figure C.1 in Appendix C for traceability.

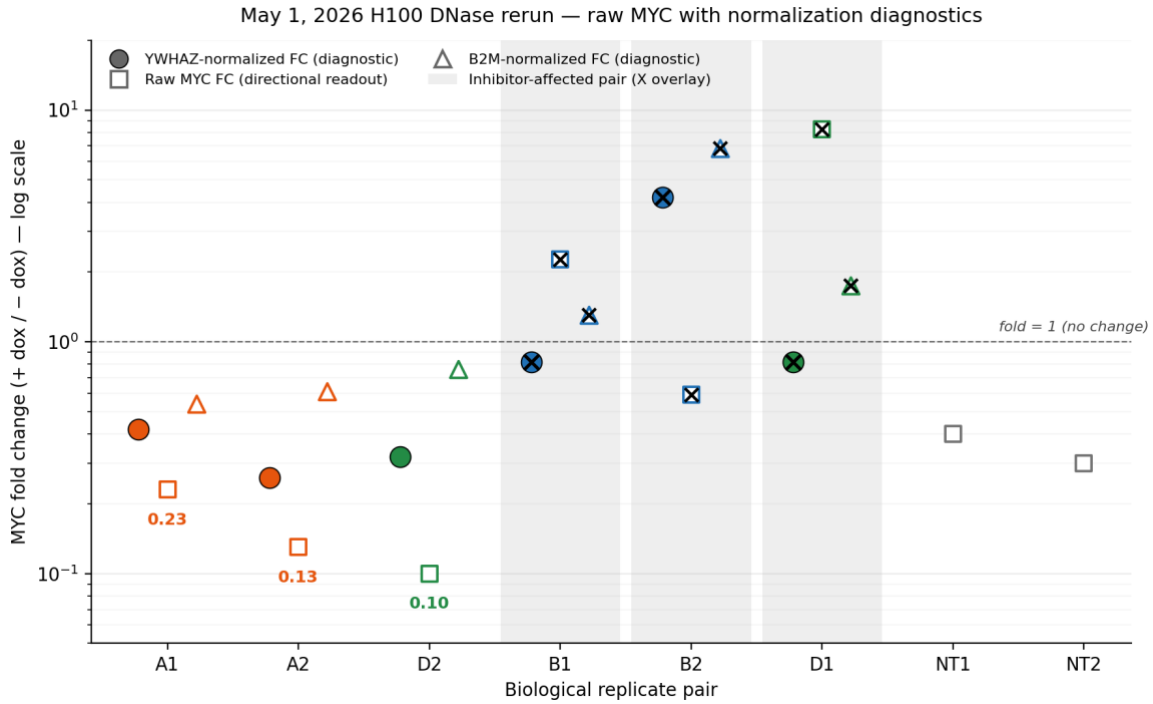


**Figure 3.7.** May 1, 2026 H100 DNase rerun MYC fold change across RT-qPCR readouts. For each biological replicate pair, fold-change values are plotted on a shared log y-axis: raw MYC (open square; clearest directional readout for this run), YWHAZ-normalized MYC (filled circle), and B2M-normalized MYC (open triangle). The dashed line marks fold = 1 (no induction-associated change). Pairs shown on a gray background and overlaid with an X were inhibitor-affected by the combined 260/230 + multi-target-Cq criterion (B1, B2, D1; Table 3.6) and are shown for traceability only. NT1 and NT2 are plotted with raw MYC alone because reference-gene shifts on this plate made the normalized NT values non-interpretable as guide-specific controls (§3.2.3). For the three clean guide pairs, raw MYC decreased in A1, A2, and D2, but the normalized NT controls also shifted downward; May 1 therefore supports a raw-MYC decrease while weakening normalized guide-specific claims.

## 3.3 ChIP-qPCR did not detect guide-specific CTCF loss

ChIP-qPCR was developed as an occupancy-oriented assay to support later testing of CTCF binding at targeted MYC-locus sites. The series consisted of three runs (Appendix D, Table D.1): the April 20 IP-optimization plate, the April 30 B/NT2 follow-up, and the May 6 A/D/NT3 follow-up. Each guide-versus-control follow-up represents a single biological IP per condition read out in technical triplicate qPCR wells; biological replicate IPs were not performed within this thesis, and the resulting limits on what these single-replicate runs can resolve are quantified at the end of this section and in Appendix D.6. Fragmentation optimization identified S5, corresponding to 5 Bioruptor Pico cycles, combined with 2 µL MNase as the preferred working condition. The 2 µL MNase + S5 lane was selected because it gave the clearest nucleosomal ladder, with bands at approximately 160, 320, and 480 bp, together with a useful fragment distribution across the broader 200–1000 bp ChIP-compatible range. Figure 3.8 shows the gel used for this optimization.

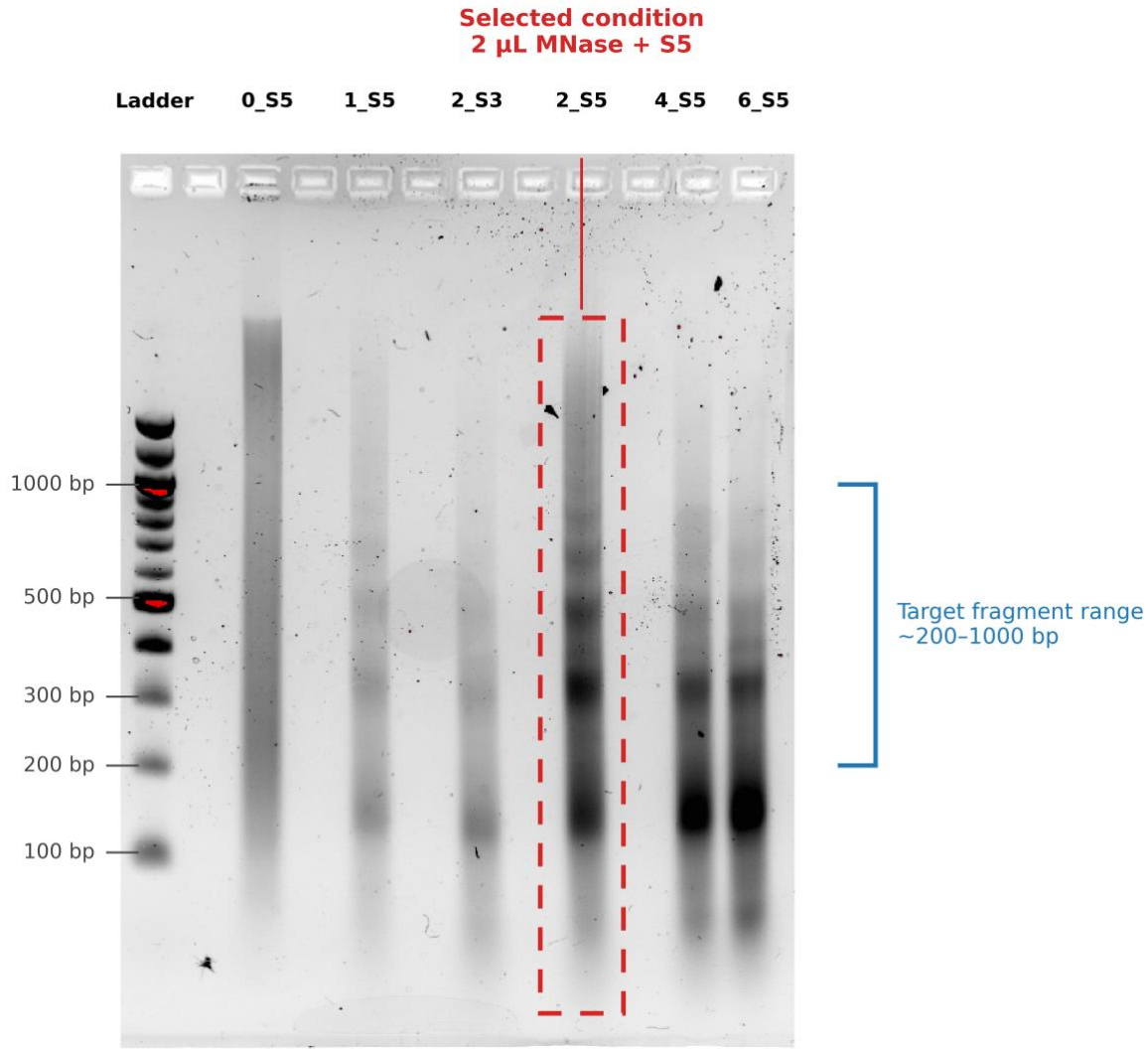


**Figure 3.8.** Annotated agarose gel summary of the ChIP fragmentation optimization. Crosslinked HCT116-derived chromatin was digested with MNase and subjected to Bioruptor Pico sonication. Lane labels from left to right: ladder, 0 µL MNase + S5 sonication, 1 µL MNase + S5, 2 µL MNase + S3, 2 µL MNase + S5, 4 µL MNase + S5, and 6 µL MNase + S5 (S3 = 3 Bioruptor Pico cycles, S5 = 5 cycles, 30 s ON / 30 s OFF). The red dashed box marks 2 µL MNase + S5, and the blue bracket marks the approximate 200–1000 bp target fragment range.

The April 20 ChIP-qPCR IP test was then used to evaluate whether the assay could generate usable enrichment patterns. The plate used anti-CTCF antibody for the three CTCF-site assays (`mycP_CTCF`, `OSE_CTCF`, `negC_CTCF`) and anti-Pol II antibody for the `GAPDH` positive-control assay only; matched IgG and NTC wells were included for every assay. Figure 3.9 shows fold enrichment of IP over IgG for assays with usable enrichment values, and Table 3.8 reports the underlying mean Cq values together with a compact QC interpretation per assay.

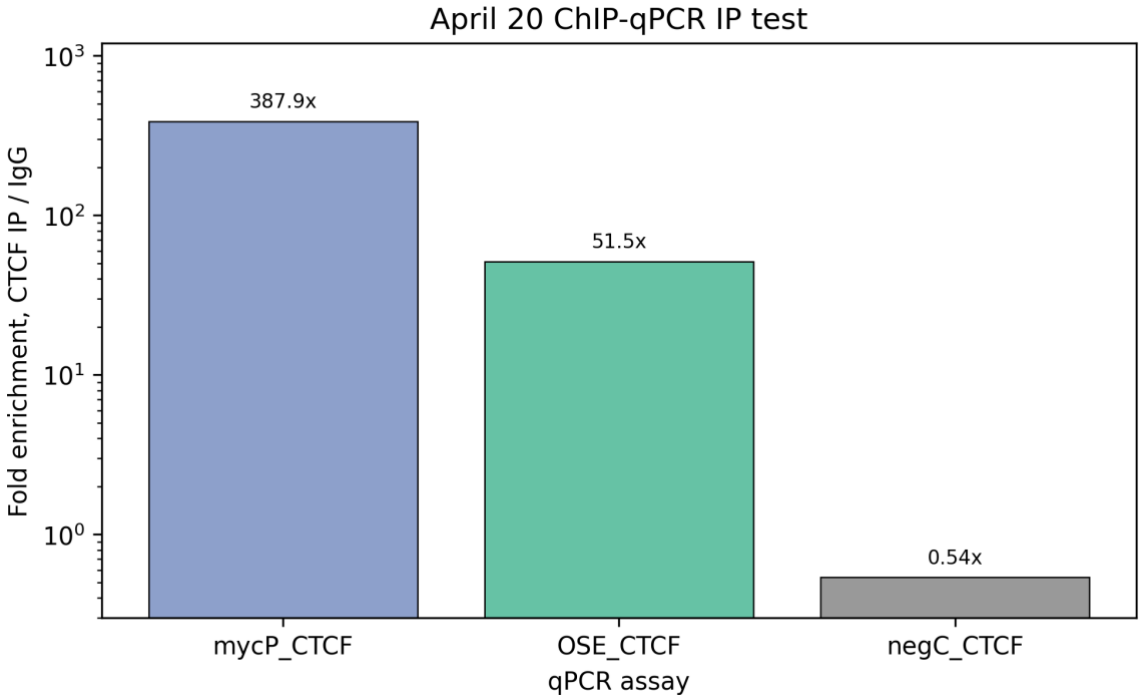


**Figure 3.9. April 20 ChIP-qPCR IP-optimization test.** Bars show CTCF IP/IgG fold enrichment for the CTCF-site assays with usable enrichment estimates. The y-axis is logarithmic. GAPDH/Pol II was not plotted because the positive-control IP did not yield a usable enrichment estimate.

The April 20 ChIP-qPCR optimization run showed strong enrichment for the `mycP_CTCF` assay in Figure 3.9 and Table 3.8, with clear CTCF IP over IgG signal and the strongest Cq/NTC behavior among the tested assays, although the CFX export did not return automatic melt peak calls for these wells. The `mycP_CTCF` primer pair maps to the promoter-proximal MYC CTCF site (chr8:127,734,021–127,734,151; 131 bp; §2.10.4), so this April 20 result is consistent with strong promoter-proximal CTCF enrichment. However, this run remains an assay-development result rather than a guide-induced occupancy test. The `OSE_CTCF` primer pair mapped cleanly to the distal guide D/OSE region (chr8:127,215,027–127,215,169), and the `negC_CTCF` primer pair mapped to the published negative-control region (chr2:5,791,569–5,791,703). The `OSE_CTCF` result was directionally positive but less secure because of the input outlier, missing IP replicate, and positive NTC behavior, while `GAPDH` and `negC_CTCF` did not function as useful controls in this run. The `GAPDH` failure is specifically a failure of the anti-Pol II positive-control IP, not of the CTCF IPs run on the same plate: the `mycP_CTCF` and `OSE_CTCF` assays used a different antibody (anti-CTCF) and showed clean enrichment over IgG, indicating that the chromatin preparation, IgG-blocked beads, qPCR setup, and CTCF IP were working in parallel on the same chromatin lysate. The Pol II positive-control failure therefore limits what can be claimed about overall IP-pipeline robustness using GAPDH as a reference but does not invalidate the CTCF IP results on the same plate. The April 20 run therefore

supported assay-development readiness, with the strongest positive evidence coming from the mapped promoter-proximal mycP_CTCF assay.

The OSE input outlier noted in the Table 3.8 caption is the B02 well (Cq 37.88 versus 23.18 in B01 and 22.85 in B03); excluding B02 brings the input mean from 27.97 to 23.02 cycles and reduces the SD from 8.59 to ~0.24, matching the tighter pattern seen in other assays. Excluding B02 does not change the direction of the OSE enrichment but it does shift the absolute %-input estimate.

**Table 3.8. Underlying mean Cq values and QC interpretation for the April 20 ChIP-qPCR optimization run.** Mean across technical triplicates; values for OSE_CTCF input exclude the B02 outlier well (Cq 37.88 versus 23.18 in B01 and 22.85 in B03). NaN indicates no amplification within 40 cycles. The IP target was anti-CTCF for the three CTCF-site assays and anti-Pol II for the GAPDH positive-control assay only.

| Assay | IP target | Input (Cq) | IP (Cq) | IgG (Cq) | NTC (Cq) | Interpretation |
|---|---|---|---|---|---|---|
| mycP_CTCF | anti-CTCF | 23.36 | 25.03 | 33.63 | NaN (clean) | Clear CTCF enrichment; clean NTC |
| OSE_CTCF | anti-CTCF | 23.02 | 27.21 | 32.90 | 34.43 | Directional enrichment; input outlier and positive NTC |
| GAPDH | anti-Pol II | 30.84 | 38.45 (1/3 wells amplified) | NaN | 37.25 | Pol II positive control failed |
| negC_CTCF | anti-CTCF | 28.73 | 30.26 | 29.36 | 27.95 (NTC earlier than IP) | Negative-region assay failed |

A subset of inputs was also amplified at 1:10 dilution on the same plate to verify the dilution strategy used downstream for percent-input calculation (Table 3.9). Observed Cq shifts were close to but somewhat smaller than the expected log2(10) ≈ 3.32 cycles for a 10-fold dilution, with the cleanest agreement for mycP_CTCF.

**Table 3.9. Comparison of undiluted vs 1:10-diluted input Cq values for three assays in the April 20 run.** Expected delta Cq for a 10-fold dilution is log2(10) ≈ 3.32 cycles.

| Assay | Undiluted input Cq | Diluted input Cq | Delta Cq (diluted - undiluted) |
|---|---|---|---|
| mycP_CTCF | 23.36 | 26.26 | 2.90 |
| OSE_CTCF (excl. B02) | 23.02 | 25.53 | 2.51 |
| GAPDH | 30.84 | 32.16 | 1.32 |

A follow-up four-condition ChIP-qPCR was initiated on April 28 and read out by qPCR on April 30. This run tested B- / B+ / NT2- / NT2+ with anti-CTCF and IgG IPs per condition, using `mycP_CTCF` as the target assay and `negC_CTCF` as the negative-region assay. NanoDrop yields after IP cleanup ranged from 31.8 to 88.4 ng/µL across the 12 ChIP DNA samples, but A260/A230 ratios were uniformly low (~0.6-0.9), suggesting cleanup-buffer carryover and meaning that NanoDrop concentrations should be interpreted cautiously. Table 3.10 summarizes the qPCR result; the physical plate layout is shown in Appendix D (Figure D.2), the underlying per-condition mean Cq values for input, CTCF IP, IgG IP, and NTC wells are tabulated in Appendix D (Table D.2), and a compact summary of all three ChIP-qPCR run designs is in Table D.1.

**Table 3.10. April 30 B/NT2 ChIP-qPCR percent input at `mycP_CTCF`.** Percent input uses the 1% qPCR-input correction (see §2.10). NT2+ excludes the C04 outlier (mean of C05/C06).

| Condition | CTCF % input | IgG % input | CTCF / IgG | QC / interpretation |
|---|---|---|---|---|
| B- | 5.91% | 3.55% | 1.67x | High IgG background |
| B+ | 5.66% | 1.24% | 4.57x | Similar CTCF % input to B- |
| NT2- | 5.65% | 0.12% | 48.24x | Very low IgG background |
| NT2+ | 4.94% | 0.83% | 5.91x | Slightly lower than NT2-, not guide-B-specific |

The `mycP_CTCF` assay produced internally consistent qPCR behavior in the April 30 run: all sample wells had called melt peaks at 88.0-88.5 °C, the six `mycP_CTCF` NTC wells were undetected, and most technical triplicates were tight. By percent-input normalization, CTCF signal at `mycP_CTCF` was similar across all four conditions, ranging from 4.94% to 5.91% input. The main B comparison did not show reduced occupancy after induction: B+ was 5.66% input compared with 5.91% input in B-, corresponding to a B+ / B- ratio of approximately 0.96x. B+ was also not lower than induced NT2 by percent input. This run is therefore interpretable as a direct promoter-proximal occupancy-oriented test for guide B. However, it remains a single technically limited ChIP-qPCR run, not a definitive absence-of-effect experiment.

The run remained limited by control behavior. IgG background varied strongly between conditions, making fold-over-IgG less stable than percent input as the primary readout, and the `negC_CTCF` negative-region assay again failed specificity expectations. The detailed curve review and per-well Cq distributions are treated as assay-QC material in Appendix D rather than as part of the main Results narrative. The April 30 result therefore does not support guide-B-specific CTCF depletion at the promoter-proximal MYC CTCF site, but it also remains a technically limited single ChIP-qPCR run rather than a definitive absence-of-effect experiment.

A second follow-up ChIP-qPCR experiment was read out on May 6 using an expanded A/D/NT3 design. This experiment included matched input, CTCF IP, and IgG IP material for A-, A+, D-, D+, NT3-, and NT3+, and qPCR was run separately for the promoter-proximal `mycP_CTCF` assay and the distal `OSE_CTCF` assay. The main purpose was to test whether guides A or D produced measurable CTCF occupancy loss at their corresponding target regions. Table 3.11 and Figure 3.10 summarize the percent-input results; the physical plate layouts are shown in Appendix D (Figures D.3, D.4), and the underlying per-condition mean Cq values for both assays are tabulated in Appendix D (Table D.3).

**Table 3.11. May 6 A/D/NT3 ChIP-qPCR percent-input summary.** Percent input uses the 1% qPCR-input correction (see §2.10). Values are descriptive summaries from the matched ChIP-qPCR run; A is target-relevant at `mycP_CTCF`, and D is target-relevant at `OSE_CTCF`.

| Assay | Condition | CTCF % input | IgG % input | CTCF / IgG |
|---|---|---|---|---|
| `mycP_CTCF` | A- | 2.69% | 0.14% | 18.74x |
| `mycP_CTCF` | A+ | 4.98% | 0.23% | 21.23x |
| `mycP_CTCF` | D- | 3.55% | 0.07% | 53.58x |
| `mycP_CTCF` | D+ | 6.45% | 0.26% | 24.68x |
| `mycP_CTCF` | NT3- | 4.92% | 0.14% | 35.16x |
| `mycP_CTCF` | NT3+ | 7.16% | 0.17% | 42.37x |
| `OSE_CTCF` | A- | 1.19% | 0.16% | 7.61x |
| `OSE_CTCF` | A+ | 1.08% | 0.16% | 6.59x |
| `OSE_CTCF` | D- | 1.29% | 0.07% | 18.30x |
| `OSE_CTCF` | D+ | 2.07% | 0.29% | 7.05x |
| `OSE_CTCF` | NT3- | 1.34% | 0.10% | 13.80x |
| `OSE_CTCF` | NT3+ | 2.14% | 0.20% | 10.84x |

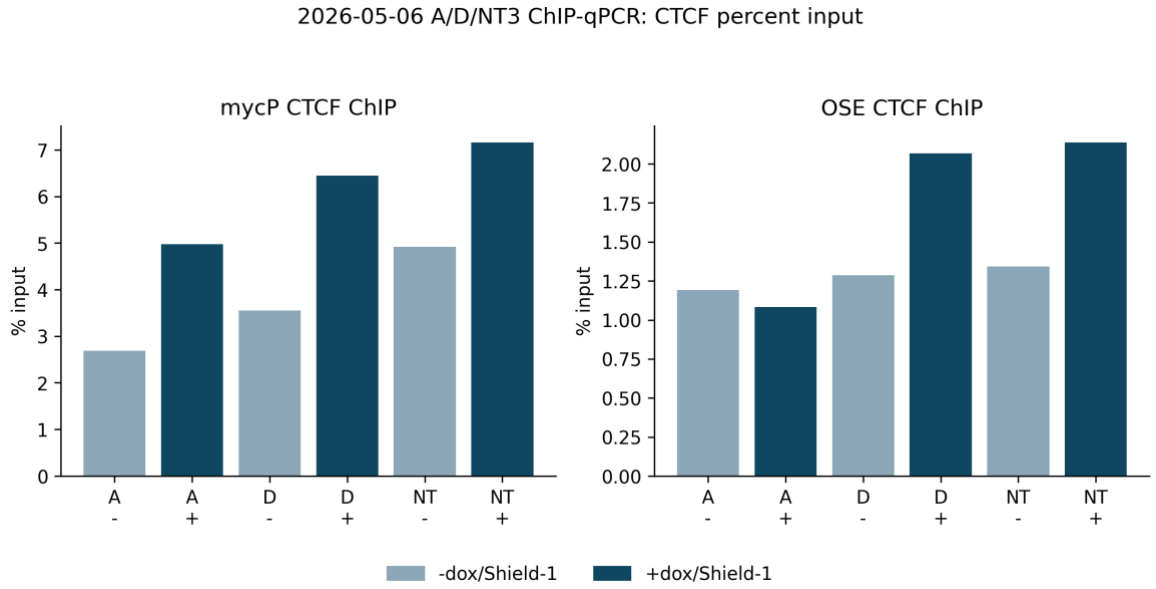


**Figure 3.10.** May 6 A/D/NT3 ChIP-qPCR CTCF percent input at `mycP_CTCF` and `OSE_CTCF`. Bars show percent input after the 1% input correction for matched minus and plus conditions.

The clearest locus-specific conclusion came from the mapped distal `OSE_CTCF` assay. Guide D did not reduce CTCF percent input at OSE after induction: D+ was 2.07% input compared with 1.29% input in D-, corresponding to a D+ / D- ratio of approximately 1.61x. The NT3 control shifted in almost the same direction at the same assay, with NT3+ at 2.14% input compared with 1.34% input in NT3- (approximately 1.59x). After normalizing the D plus/minus ratio to the NT3 plus/minus ratio, the D-specific ratio was approximately 1.01x. This result does not support guide-D-specific CTCF depletion at the distal OSE/CCAT1-associated CTCF site in this run.

The promoter-proximal `mycP_CTCF` readout also did not show occupancy loss for guide A: A+ was higher than A- by percent input (4.98% versus 2.69%). The May 6 `mycP_CTCF` NTC wells produced weak expected-temperature melt features, with two near the assay-specific threshold and one slightly above it. The May 6 promoter result is therefore less clean than the April 30 promoter readout and the May 6 OSE readout, but it still does not support guide-A-associated CTCF depletion.

The supporting assay-QC checks are reported in Appendix D: the May 6 `OSE_CTCF` assay had cleaner no-template behavior than the promoter-proximal assay, the Universal chemistry was more reliable than the NZY side block for specificity, and selected May 6 qPCR products migrated in the expected 100-200 bp range. These checks support cautious use of the May 6 occupancy readout, but they do not change the guide-level conclusion.

Figure 3.11 summarizes the direct CTCF ChIP-qPCR occupancy tests performed after assay optimization. Across the April 30 and May 6 follow-up runs, none of the guide-targeted comparisons showed guide-specific CTCF depletion under the tested conditions.

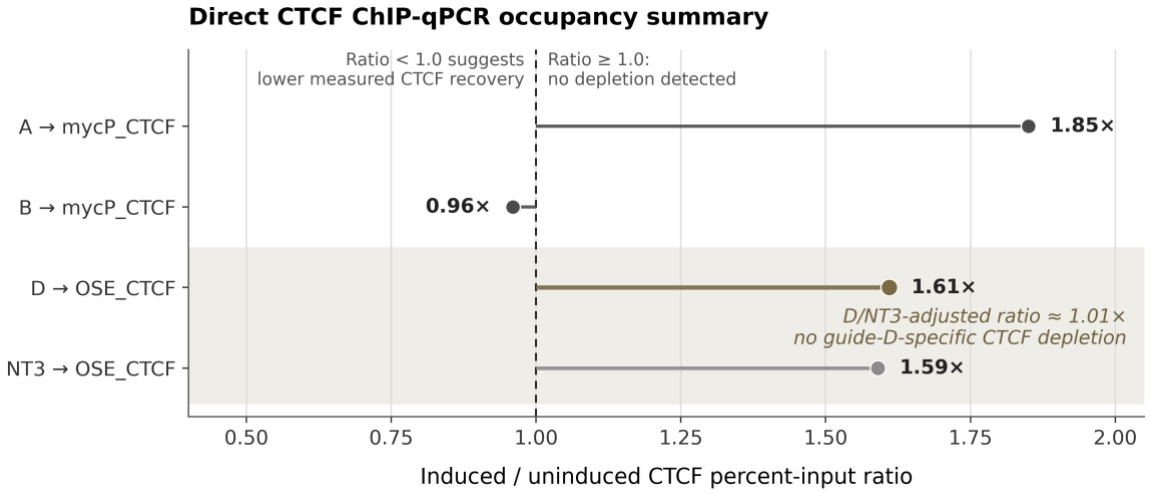


**Figure 3.11.** Summary of direct CTCF ChIP-qPCR occupancy tests after assay optimization. Ratios show induced (+dox/Shield-1) CTCF percent input divided by matched uninduced values. A ratio below 1 would indicate reduced CTCF recovery after induction, whereas ratios near or above 1 do not support depletion. Guide B did not show reduced CTCF recovery at the mapped promoter-proximal `mycP_CTCF` assay, guide A did not show depletion at the same assay in the May 6 run, and guide D shifted similarly to the NT3 control at the distal `OSE_CTCF` assay. The NT-adjusted guide-D ratio was approximately 1.01x, supporting no guide-D-specific CTCF depletion under the tested conditions.

Taken together, the ChIP-qPCR series developed usable workflow conditions and produced direct occupancy-oriented measurements, but it did not validate guide-specific CTCF depletion. The April 30 guide-B test did not show reduced percent input at the mapped promoter-proximal assay, the May 6 guide-A test did not show reduced percent input at the same assay, and the May 6 guide-D test did not show reduced percent input at the mapped OSE assay. The May 6 gel adds evidence that the qPCR products were in the expected size range. The expression effects observed by RT-qPCR and RNA-FISH therefore require further mechanistic validation rather than being confirmed consequences of measured CTCF displacement.

Two run-spanning observations bound how these negative results should be interpreted. First, the −dox baseline `mycP_CTCF` percent input varied by more than two-fold between independent chromatin preparations across the matched −dox conditions (B− 5.91% on April 30 versus A− 2.69%, D− 3.55%, and NT3− 4.92% on May 6). In addition, an induction-associated upshift was observed at `OSE_CTCF` for both D and NT3 on May 6 (D+/D− ≈ 1.61× versus NT3+/NT3− ≈ 1.59×; NT-adjusted D ratio ≈ 1.01×). The matched −/+ input mean Cq values in Appendix D (Table D.3) shifted by ≈ 0.4–0.6 cycles between −dox and +dox conditions at `OSE_CTCF`, which is

sufficient to explain the joint upshift without invoking guide-specific biology. The control structure therefore behaves consistently with an input-Cq/chromatin-batch-level shift between matched conditions rather than a guide-specific change. Second, when these between-condition baseline differences are considered together with single-replicate IPs measured in technical triplicate, changes smaller than approximately two-fold in percent input are not separable from technical variation at the present replication level. The ChIP-qPCR follow-ups therefore did not detect guide-specific CTCF loss: CTCF recovery was similar or higher after induction in the tested guide-target comparisons. These results do not support strong bulk CTCF eviction at the mapped target assays under the tested conditions, but they do not exclude smaller, partial, transient, or cell-heterogeneous occupancy changes.

## 3.4 RNA-FISH supports reduced per-cell MYC in selected guide conditions

### 3.4.1 FACS-derived RNA-FISH supported reduced per-cell MYC for guides B and D

The first RNA-FISH experiment supported reduced per-cell MYC after induction for guides B and D in the FACS-derived population (per-cell mean MYC FC 0.51 for B and 0.42 for D), while the QC-filtered NT control did not show a comparable decrease. Endpoint hierarchy, FOV-level QC, and the supporting MYC/GAPDH robustness readout are documented below; the detailed FOV exclusion and rescue audit lives in Appendix F.5 (Table F.4).

RNA-FISH was used as an orthogonal single-cell readout of MYC RNA abundance in the FACS-derived population. The experiment included three sgRNA conditions: guide D, guide B, and the non-targeting control guide NT, each analyzed under matched uninduced (−dox) and induced (+dox/Shield-1) conditions. Probe D1 was GAPDH (co-detected as a technical QC transcript; see §2.12) and probe D2 was MYC. Each condition contained 10 FOVs. The headline single-cell metric is the per-cell MYC spot count; FOV-level median MYC summaries are reported as a supporting robustness analysis (cells within the same FOV share image quality, segmentation, background, and spot-assignment properties), and per-cell MYC/GAPDH is reported as a secondary robustness readout rather than a normalized biological readout (§2.12).

Representative RNA-FISH image data are shown in Figure 3.12 to illustrate the image structure underlying the spot-count analysis. The example is a +B field of view displayed in Napari as a three-dimensional rendering across all 41 acquired z-planes, with MYC RNA-FISH spots shown in yellow, the cell-membrane marker in green, and DAPI-stained nuclei in blue. The image is shown for visualization only; quantitative interpretation was based on the exported per-cell and per-spot measurements after FOV-level quality control.

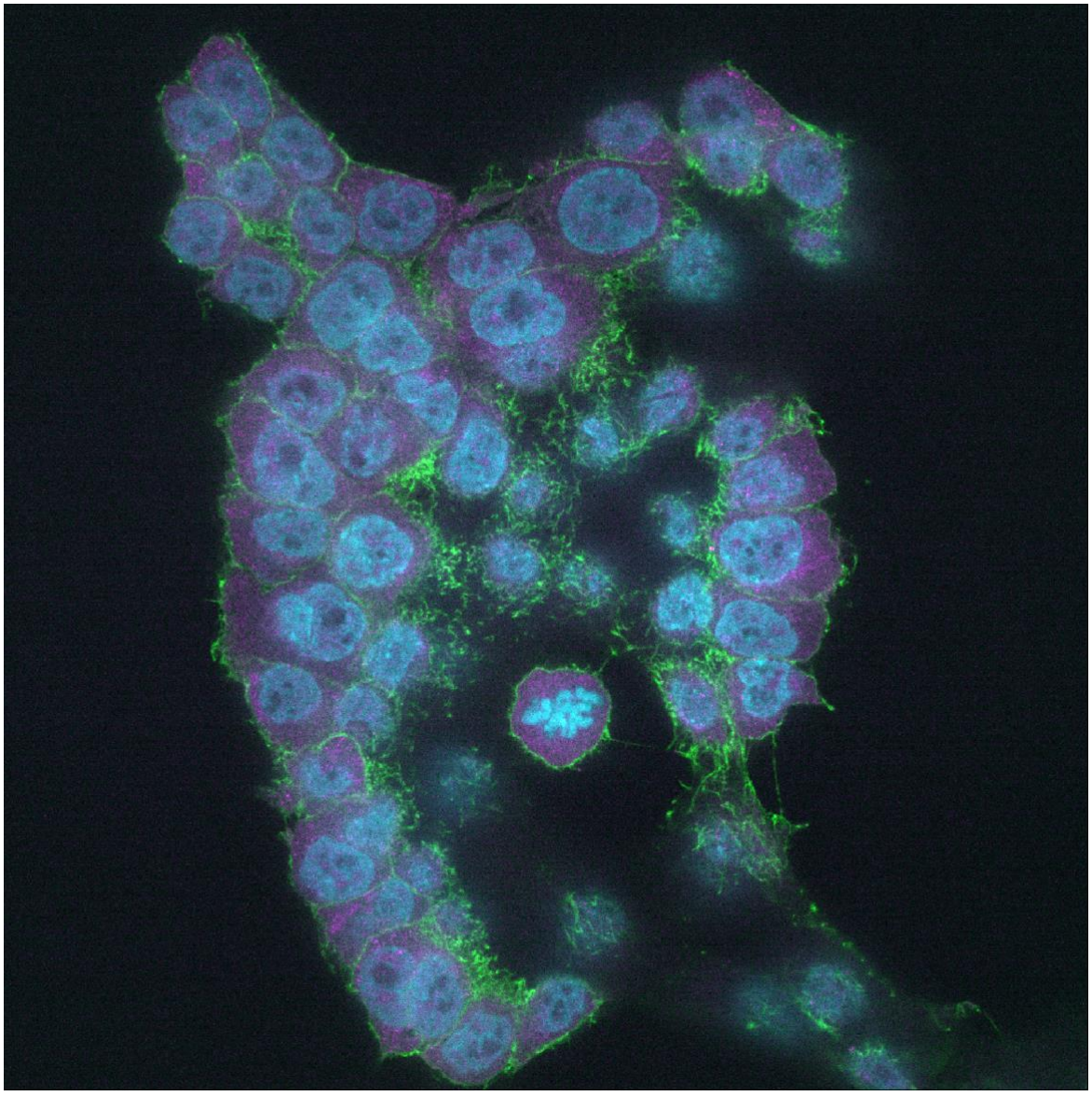

**Figure 3.12.** Representative RNA-FISH image stack from the +B condition. Three-dimensional Napari rendering of one +B field of view across all 41 acquired z-planes. MYC RNA-FISH spots are shown in yellow, the cell-membrane marker in green, and DAPI-stained nuclei in blue. Image contrast was adjusted for visualization; quantitative analysis was performed from exported per-cell and per-spot measurements rather than from visual inspection of the rendered image.

Before quantification, the formalized FOV-level exclusion criteria declared in §2.12 were applied uniformly to all six conditions. The main text therefore reports the biological single-cell output, while the FOV-level exclusion list, rescue checks, and aggregated decision summary are kept in Appendix F.5 (Table F.4). The primary single-cell analysis compared per-cell MYC spot counts between matched −dox and +dox conditions; per-cell MYC/GAPDH ratios are retained as a secondary robustness readout, and the FOV-level median analysis is reported as a supporting robustness analysis.

The single-cell readout supports the headline finding that guides B and D both showed reduced MYC after induction, whereas NT did not show a comparable decrease. Across all segmented cells in the included FOVs, the per-cell mean MYC spot count fell from 45.9 (D −dox, n = 838) to 19.5 (D +dox, n = 755) for guide D — a single-cell mean fold change of 0.42 — and from 39.4 (B −dox, n = 914) to 20.1 (B +dox, n = 957) for guide B (single-cell mean fold change 0.51). For NT, the per-cell mean MYC count moved in the opposite direction, from 20.5 (NT −dox, n = 654) to 27.2 (NT +dox, n = 672), giving a single-cell mean fold change of 1.33. Per-cell median MYC counts told the same story: D 30.5 → 10 (FC 0.33), B 26 → 10 (FC 0.39), NT 8 → 14 (FC 1.75). The per-cell MYC/GAPDH ratio (§2.12) shifted in the same direction as per-cell MYC alone for both targeting guides — D 0.188 → 0.074 (FC 0.39), B 0.168 → 0.078 (FC 0.46), NT 0.110 → 0.129 (FC 1.18) — supporting that the per-cell MYC reduction is not driven by a global staining or imaging shift in the induced conditions. Single-cell summary statistics per condition are listed in Table 3.12.

**Table 3.12. Single-cell RNA-FISH summary by condition (per-cell MYC is the headline biological readout; per-cell MYC/GAPDH is a secondary robustness readout, §2.12) and FOV-level summary (supporting robustness analysis).** Single-cell statistics are computed across all segmented cells in the included FOVs after the QC exclusions summarized in Appendix F.5; n is the number of segmented cells per condition. Per-cell MYC/GAPDH ratio excludes cells with GAPDH = 0. FOV-level fold changes were calculated from the median of included FOV-level medians as the +dox value divided by the matched −dox value within each arm; the FOV-level MYC/GAPDH 95 % confidence interval was estimated by bootstrap resampling of included FOVs. NT is shown as a parallel control beside the guide arms rather than used to divisively normalize the guide fold changes.

| Guide | n cells (−dox / +dox) | Per-cell mean MYC FC | Per-cell median MYC FC | Per-cell median ratio FC | FOV-level median MYC FC | FOV-level median ratio FC (95 % CI) |
|---|---|---|---|---|---|---|
| D | 838 / 755 | 0.42 | 0.33 | 0.39 | 0.32 | 0.46 (0.29–0.57) |
| B | 914 / 957 | 0.51 | 0.39 | 0.46 | 0.37 | 0.44 (0.40–0.63) |
| NT | 654 / 672 | 1.33 | 1.75 | 1.18 | 1.45 | 1.10 (0.65–2.06) |

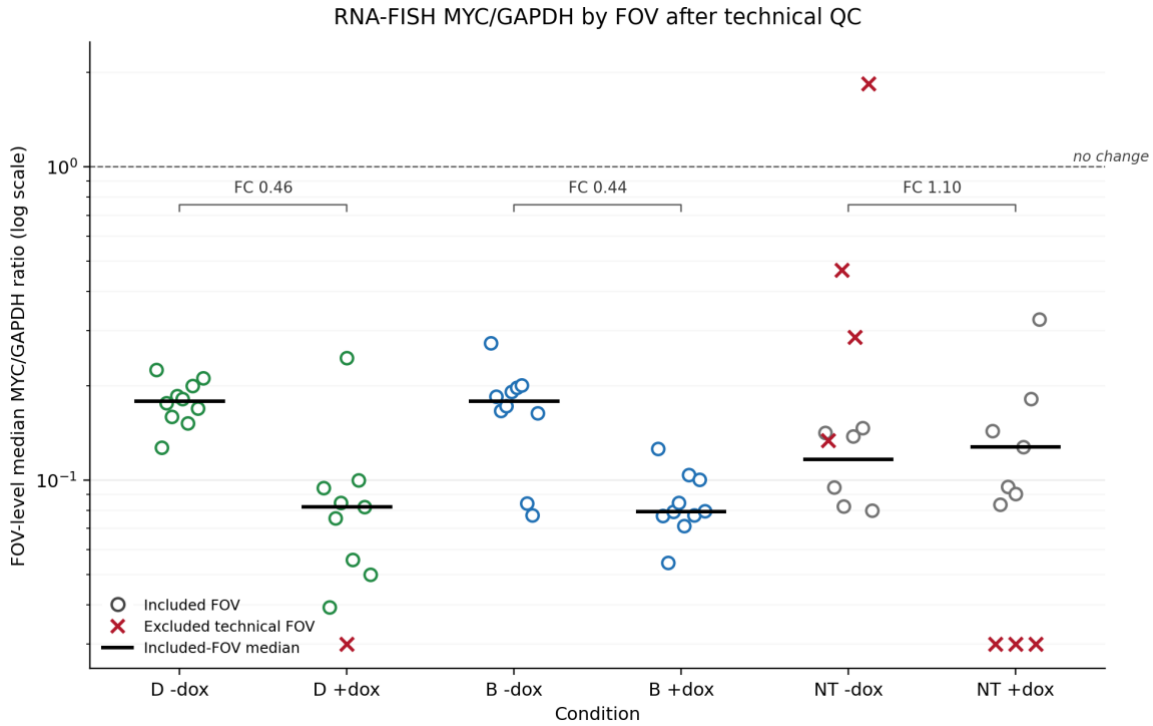


**Figure 3.13.** RNA-FISH FOV-level median MYC/GAPDH ratios after technical QC. Each circle represents one included FOV, red X markers show excluded technical FOVs, and black horizontal lines show the included-FOV median for each condition. Bracket labels report fold changes calculated as the +dox included-FOV median divided by the matched −dox included-FOV median. Excluded FOVs with zero MYC/GAPDH ratios are shown at the lower plotting limit because the y-axis is log-scaled. The FOV-level analysis shown here gave the same direction of effect as the primary single-cell summaries in Table 3.12 (guides B and D reduced after induction, NT not).

The FOV-level supporting analysis agrees with the single-cell direction (Table 3.12). The FOV-level median MYC-only fold changes were 0.32 (D) and 0.37 (B), with NT at 1.45; the FOV-level median MYC/GAPDH fold changes were 0.46 (D, 95 % bootstrap CI 0.29–0.57) and 0.44 (B, 95 % CI 0.40–0.63), with NT at 1.10 (95 % CI 0.65–2.06). The B and D MYC/GAPDH bootstrap intervals lie entirely below 1.0 while the NT interval spans 1.0, supporting directional separation between targeting guides and non-targeting control under FOV-resampled uncertainty. NT is shown beside B and D as a parallel control rather than used as a divisive normalizer of the guide fold changes, because the included NT −dox MYC/GAPDH baseline was lower than the guide-arm baselines (~0.110 vs ~0.180) so that an NT-divided ratio would compound this baseline mismatch with the within-guide signal.

The RNA-FISH result therefore supports an induction-associated reduction in per-cell MYC for both guide B and guide D at single-cell resolution. The per-cell MYC/GAPDH ratio shifts in the same direction as per-cell MYC alone, supporting that the per-cell MYC reduction is not driven by a global staining or imaging shift, but the headline finding is the per-cell MYC reduction itself rather than a normalized ratio.

This result strengthens the expression-readout side of the thesis because the NT control does not show a similar per-cell MYC reduction after FOV-level QC. At the same time, it remains supportive rather than definitive: the analysis depends on technical FOV exclusion, guide A was not included in this RNA-FISH experiment, and RNA-FISH does not directly test whether CTCF occupancy was displaced at the targeted sites.

### 3.4.2 H100 RNA-FISH supports reduced per-cell MYC for guides A and D

The second RNA-FISH experiment supported reduced per-cell MYC after induction for guide A (per-cell mean MYC FC 0.64) and for rescued guide D (per-cell mean MYC FC 0.48 from Jonas Grini's corrected re-processing as the primary analysis, with the earlier in-house rescue giving FC 0.52 as a supporting sensitivity analysis) in the H100 platform population. Guide B is treated as conditional because its contrast depends on excluding the C1 FOVs 0–6 low-signal block. The matched +dox NT comparator could not be recovered (E3 well failure), so NT is reported as a parallel −dox baseline rather than as a +/− contrast.

A second RNA-FISH experiment was performed in the H100 platform population (§2.2; in contrast to the FACS-derived BFP-enriched H100 subpopulation used in the first experiment). The second experiment introduced guide A — which was not in the first experiment — and used a longer (four-day) primary hybridization at a lower probe concentration (1 nM per target). Guide A, guide B, and the −dox NT control were prepared on a fresh six-channel ibidi µ-slide; guide D and a complete −dox/+dox NT pair were prepared in matched wells of a 96-well glass-bottom plate to recover the +dox NT condition that was lost from C6 of the previously opened ibidi slide because of contamination (§2.11; Appendix F.2). The probe-detection assignment was the same as in the first experiment (D1 = GAPDH, D2 = MYC), and the same Jonas-pipeline single-cell tables were used as the input.

Three QC issues affected the second experiment and were handled under the formalized criteria declared in §2.12: guide-D required corrected channel assignment for the B2/B3 plate-well acquisitions, the recovered +dox NT well (E3) failed the segmentation/focus criterion, and a coherent low-signal FOV block was excluded from the guide-B minus channel. The main text uses the post-QC biological contrasts, while detailed procedures, before/after numbers, rescue logic, and cross-validation are reported in Appendix F (Tables F.3-F.5).

The second-experiment headline is the guide-A single-cell MYC reduction in the H100 platform population, supported visually by the ibidi-slide FOV-level MYC/GAPDH summary in Figure 3.14. The guide-D contrast was recovered from the separate 96-well plate acquisition after channel-order correction and is summarized separately in Appendix F.4. Guide A showed reduced per-cell MYC after induction, with the A+ channel (n = 662 cells across 10 FOVs) giving a per-cell mean MYC fold

change of 0.64 relative to the matched A− channel (n = 478 cells across 10 FOVs). Guide D was interpretable after correction of a channel-order mismatch in the B2 / B3 plate-well acquisitions (§2.12). Jonas Grini's corrected re-processing of the same acquisitions is used as the primary guide-D analysis and gave a per-cell mean MYC fold change of 0.48. The earlier in-house corrected-channel rescue gave a similar fold change of 0.52 and is retained as a supporting sensitivity analysis (in-house B3, D+: n = 1,463 cells across 10 FOVs; B2, D−: n = 759 cells across 6 FOVs with ≥ 30 segmented cells; an initial May 14 Jonas export revealed a B3 D1/D2 assignment issue that was corrected on May 15 — see Appendix F.4). Per-cell GAPDH, the co-detected technical-QC transcript (§2.12), stayed essentially constant in both contrasts (guide A: mean 222 → 222; guide D in-house: mean 105.2 → 102.2), supporting that the per-cell MYC reductions reflect MYC biology rather than a generic staining or imaging difference. Guide B showed a weaker per-cell mean MYC reduction in the same direction (FC 0.70), but this comparison depended on exclusion of a coherent within-channel low-signal block in the B− channel (C1 FOVs 0–6; §2.12) and is therefore treated as conditional. The matched H100 +dox NT condition could not be recovered as a clean single-cell comparator because of the E3 well failure (Appendix F.2; F.3); NT− is reported alongside as a parallel −dox baseline rather than as a +/− contrast. The ibidi A/B/NT− single-cell summary is in Appendix F.6 (Table F.5). The rescued guide-D plate-well analysis is summarized separately in Appendix F.4 (Table F.3), and the failed E3 +dox NT comparator is documented in Appendix F.3 and audited in Appendix F.5 (Table F.4).

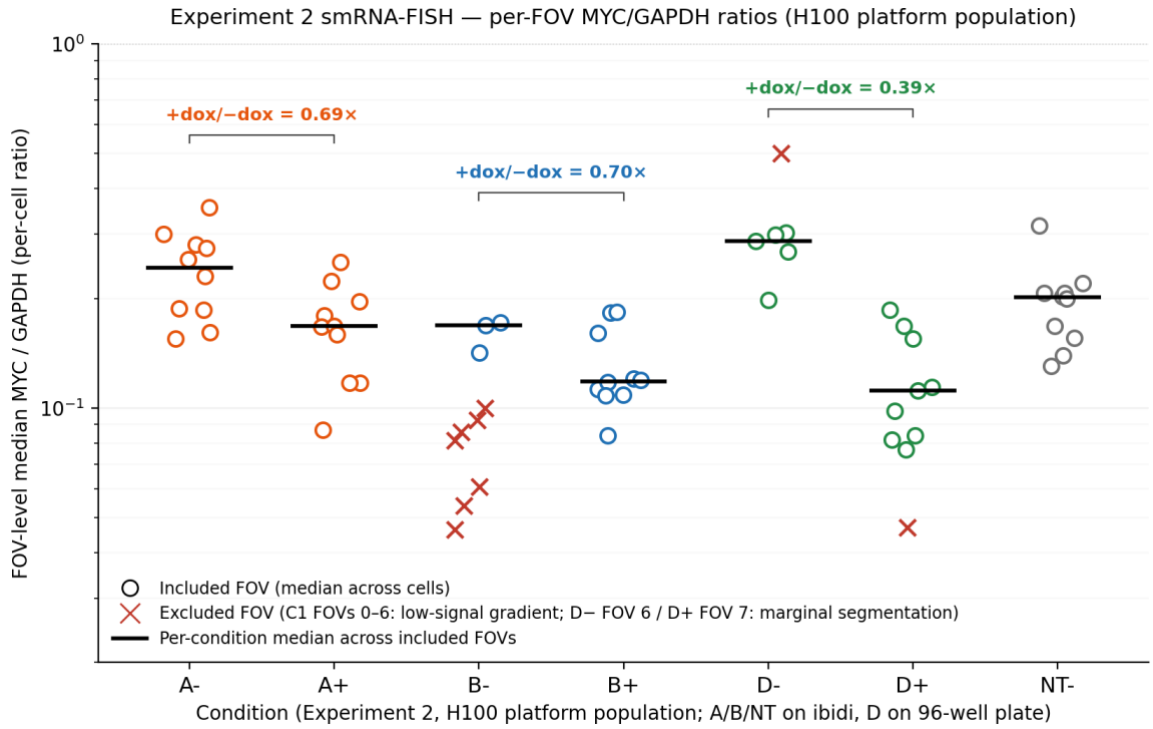


**Figure 3.14. Experiment 2 RNA-FISH per-FOV MYC/GAPDH ratios for ibidi-slide H100 conditions.** Each circle represents one field of view (FOV), plotted as the median per-cell MYC/GAPDH ratio among cells with GAPDH > 0. Horizontal black bars show the median across included FOVs for each condition. Red X markers indicate excluded B− FOVs from C1 FOVs 0–6, which were removed as a within-channel technical artifact because both GAPDH and MYC were coherently reduced relative to the retained C1 FOVs 7–9 (§2.12). Bracket labels report +dox/−dox fold changes calculated from included FOV-level medians. NT− is shown as a parallel −dox baseline only because the matched +dox NT condition was not recovered as a usable single-cell comparator (Appendix F.2–F.3). Guide-D plate-well rescue results are not plotted here and are summarized separately in Appendix F.4.

The second RNA-FISH experiment therefore supports a per-cell MYC reduction after induction for guide A and rescued guide D in the H100 platform population, with guide B conditional on the C1 FOVs 0–6 within-channel exclusion and the matched +dox NT comparator not recovered. The guide-A direction is consistent with the H100 RT-qPCR April 21 and May 1 results for guide A (§3.2.3), and the guide-D direction is consistent with the first-experiment guide-D readout in the FACS-derived population (§3.4.1). The detailed QC and rescue logic, the per-condition single-cell tables, and the in-house / Jonas Grini cross-validation are documented in Appendix F.

## 3.5 Integrated guide-level summary

Because no single assay fully resolved guide function, the main biological interpretation comes from integrating guide-level evidence across bulk expression, single-cell expression, and occupancy readouts.

Read in isolation, the six-run RT-qPCR series resolves into a small set of melt-supported, technically interpretable contrasts. The early March 27, March 31, and April 1 runs are treated as directional guide-prioritization results because MYC amplicon-window melt support was weak. April 19 was the clearest FACS-derived qPCR run and supported lower guide-B MYC, but NT shifted in the same direction. April 21 was directional H100 support, and the May 1 DNase rerun was the strongest H100 RT-qPCR recovery run: among clean guide pairs, raw MYC decreased for A1, A2, and D2, while reference-normalized values remained non-specific because NT also shifted after normalization.

Across the expression readouts, inducible dCas9 targeting was associated with reduced MYC expression in several guide/context combinations. This effect was clearest in the RNA-FISH readouts, with RT-qPCR providing supporting but more technically variable bulk evidence. However, the ChIP-qPCR follow-ups did not validate guide-specific CTCF depletion, leaving the upstream mechanism unresolved. Table 3.13 summarizes the guide-level interpretation across runs in compact form; per-run numbers and the QC and rescue audit trail are in §3.2–§3.4 and Appendices C, D, and F.

**Table 3.13. Compact cross-run guide summary.**

| Guide | Expression evidence | ChIP-qPCR evidence | Main limitation | Current interpretation |
|---|---|---|---|---|
| A | H100 RT-qPCR (April 21, May 1) and H100 RNA-FISH support reduced MYC | No guide-specific CTCF loss detected at mycP_CTCF | FACS-derived qPCR moved opposite; H100 RNA-FISH lacked +dox NT comparator | H100 MYC-lowering pattern, not occupancy-validated |
| B | FACS-derived RT-qPCR and RNA-FISH support reduced MYC | April 30 ChIP-qPCR did not validate guide-B occupancy loss | May 1 H100 B pairs inhibited; H100 RNA-FISH B result conditional | Expression-supported mainly in the FACS-derived context, not occupancy-validated |
| D | H100 May 1 D2 RT-qPCR and RNA-FISH in both populations (two independent pipelines) support reduced MYC | No guide-specific CTCF loss detected at OSE_CTCF | D1 inhibited; H100 RNA-FISH required channel-order rescue and lacked +dox NT comparator | Most consistent cross-readout MYC-lowering pattern, not occupancy-validated |
| NT | Used as non-targeting comparator across runs | Not applicable | Plus-associated shifts and RNA-FISH QC issues | Useful but imperfect baseline |

The main integrated result is that guide A and guide D are the strongest H100 MYC-lowering candidates. Guide A is supported by H100 RT-qPCR in both April 21 and May 1 and by the second RNA-FISH experiment. Guide D is supported by the May 1 D2 H100 RT-qPCR contrast and by RNA-FISH in both HCT116-derived populations, including independent re-processing of the rescued H100 guide-D acquisition. Guide B remains expression-supported mainly in the FACS-derived context and is less secure in H100 because the May 1 B pairs were inhibitor-affected and the second RNA-FISH guide-B contrast depends on exclusion of a low-signal FOV block. Across all three guides, ChIP-qPCR did not validate guide-specific CTCF depletion at the mapped target assays, so the expression effects remain guide-associated MYC reductions rather than confirmed consequences of measured CTCF displacement.

# 4 Discussion

## 4.1 Main findings

This thesis tested whether inducible CRISPR/dCas9 targeting of CTCF-associated regulatory sites reduces MYC expression in HCT116-derived cells, and whether these expression effects are accompanied by detectable changes in CTCF occupancy.

Returning to the four aims set out in §1.9: the inducible dCas9-only platform was established (Aim 1), MYC expression was quantified by bulk RT-qPCR and single-cell RNA-FISH and showed guide-associated reductions in selected contexts (Aim 3), and CTCF ChIP-qPCR at the promoter-proximal and distal target assays was performed but did not detect guide-specific CTCF loss (Aim 2). The integrative aim (Aim 4) is therefore answered interpretively rather than mechanistically: the expression-level effects are consistent with site-specific perturbation, but the upstream occupancy step remains unresolved and requires direct dCas9 target-engagement testing before the proposed CTCF-displacement mechanism can be accepted or rejected.

Four main findings emerged. First, a stable inducible dCas9 platform with degron-controlled basal expression (FKBP12-DD plus Shield-1; §2.3.1) was established and taken far enough to support guide-based perturbation experiments in both the H100 platform population and a later FACS-derived BFP-enriched H100 subpopulation (§4.3).

Second, two RNA-FISH experiments provided the strongest orthogonal expression-level evidence for reduced per-cell MYC in both HCT116-derived populations. The first experiment (FACS-derived population) showed reduced per-cell MYC for guides B and D after induction (B per-cell mean MYC FC 0.51; D per-cell mean MYC FC 0.42), while the NT control did not show a comparable decrease (§3.4.1). The second experiment (H100 platform population) introduced guide A and showed reduced per-cell MYC (per-cell mean MYC FC 0.64) and, after a channel-order rescue described in §2.12, also showed reduced per-cell MYC for guide D (per-cell mean MYC FC 0.52, independently corroborated at 0.48 by Jonas Grini's independent re-processing pipeline applied to the same B2 / B3 acquisitions; §2.12). The MYC/GAPDH robustness readout supports the per-cell MYC direction in every case where it is computable (MYC/GAPDH FCs in the 0.39–0.69 range, depending on guide and experiment) and is reported as a confirmatory check rather than as the headline metric. The same-slide NT− condition served as a parallel −dox baseline consistent with the A− baseline; the matched +dox NT comparator was not recovered in the second experiment, so NT is reported as a parallel −dox baseline rather than as a +/−

contrast (§3.4.2). The FOV-level supporting analyses agreed with the single-cell direction in both experiments.

Third, RT-qPCR supported MYC-lowering patterns for selected guide/condition contrasts, but these patterns differed across the two HCT116-derived populations and across runs, and recurring NT shifts limited guide-specific interpretation (§4.2). Fourth, the ChIP-qPCR workflow reached assay-development readiness and was extended to direct B/NT2 and A/D/NT3 follow-up tests, but these did not validate guide-specific CTCF depletion. The `mycP_CTCF` assay maps to the promoter-proximal guide A/B target site, and the published `OSE_CTCF` assay maps to the distal guide D/OSE region; neither assay showed guide-specific occupancy loss in the follow-up ChIP-qPCR tests (§4.5). The thesis therefore supports expression-level perturbation, not a resolved CTCF-displacement mechanism.

These findings should be interpreted in the context of the original biological aim: to test whether inducible, site-specific dCas9 positioning could perturb CTCF-associated regulatory logic at the MYC locus without permanently editing the underlying DNA sequence. Previous work positioned the promoter-proximal MYC CTCF site as a shared enhancer-docking element used by multiple cancer-associated enhancer landscapes (Schuijers et al., 2018), while distal CCAT1/OSE-linked architecture has been connected to long-range MYC regulation and WNT-dependent gating in colorectal cancer cells (Xiang et al., 2014; Chachoua et al., 2022). Acute CTCF depletion studies further support the premise that CTCF can affect MYC output through enhancer-promoter looping (Hyle et al., 2019), and a recent preprint extends the distal-site model toward MYC expression plasticity (Gao et al., 2026). Against this background, the observed reductions in MYC output are biologically plausible as guide-associated perturbation effects, but they cannot yet be assigned confidently to CTCF eviction because direct ChIP-qPCR did not detect guide-specific loss of CTCF occupancy under the tested conditions.

The expression evidence is best read as a cross-experiment pattern rather than as a simple ranking of individual guides. Guide-associated MYC reductions were observed in both bulk RT-qPCR and single-cell RNA-FISH, but the clearest signals depended on population context and readout: guide A was most consistent in the later H100 RT-qPCR experiments, guide B was strongest in the FACS-derived expression series and RNA-FISH, and guide D had support from both the distal-site RT-qPCR contrast and RNA-FISH. This pattern supports the broader conclusion that inducible dCas9 targeting can be linked to MYC output changes, while also showing that the apparent guide hierarchy is context-sensitive.

The central unresolved issue is mechanistic. The April 30 and May 6 ChIP-qPCR follow-ups added occupancy-oriented measurements for guides B, A, and D, but did not show guide-specific CTCF depletion. The thesis therefore supports expression-

level perturbation and assay-development progress, but not definitive validation of CTCF displacement at MYC.

## 4.2 Guide-specific interpretation

Guides A and B were designed to interrogate the promoter-proximal CTCF docking model described by Schuijers et al. (2018). In that model, reduced MYC expression after perturbation would be more consistent with loss of a productive enhancer-docking function than with loss of a simple insulating boundary, which might instead be expected to increase enhancer access. Guide D tested a different regulatory hypothesis, based on distal OSE/CCAT1-associated CTCF function and WNT-dependent MYC gating in HCT116 cells (Chachoua et al., 2022), with the broader distal-site interpretation also supported by the MYC-expression-plasticity model proposed by Gao et al. (2026). The RNA-FISH support for reduced MYC across guides A (second experiment, H100), B (first experiment, FACS-derived; and conditionally in the second experiment, H100), and D (first experiment FACS-derived; second experiment H100 after channel-order rescue, §2.12) is therefore notable because it points toward both the promoter-proximal docking model (A and B) and the distal OSE/CCAT1 model (D), with both guide-A and guide-D H100 single-cell signals especially relevant because they appear in the same population as the H100 RT-qPCR April 21 / May 1 results. The current data remain insufficient to distinguish direct CTCF-dependent effects from guide-, population-, or assay-dependent effects.

Motif geometry is therefore not a minor design detail. CTCF-mediated looping depends on motif orientation and local anchor context (de Wit et al., 2015), while CTCF perturbation by guide-based epigenome editing is strongest when guide placement precisely overlaps the cognate motif (Tarjan et al., 2019; Moore et al., 2025). If a guide lands adjacent to the functional CTCF contact surface rather than directly across it, dCas9 could still interfere with nearby regulatory geometry without producing a large bulk CTCF ChIP-qPCR decrease. This is one reason why the current data should be interpreted as guide-associated MYC expression evidence rather than as validated CTCF displacement.

Guide A provides the clearest promoter-proximal H100 expression signal, and is now the only guide in this thesis supported by both bulk RT-qPCR and single-cell RNA-FISH within the same HCT116-derived population. Its RT-qPCR interpretation improved after the May 1 rerun because MYC amplification and melt support recovered under the improved workflow, and both A1 and A2 moved in the same raw-MYC direction. The second RNA-FISH experiment, performed in the H100 platform population, added an orthogonal single-cell expression readout for guide A: per-cell mean MYC fold change 0.64, per-cell median MYC/GAPDH fold change 0.69, FOV-level median MYC/GAPDH fold change 0.69, with a same-slide NT− parallel

–dox control consistent with the A– baseline (§3.4.2). However, guide A remains an unvalidated promoter-proximal perturbation effect because NT movement persisted on the May 1 RT-qPCR plate, the matched +dox NT RNA-FISH comparator could not be recovered in the second experiment (Appendix F.2; §3.4.2), and the May 6 promoter-proximal ChIP-qPCR readout did not show guide-specific occupancy loss.

Guide B is best interpreted as a FACS-derived expression signal rather than as a fully validated H100 effect. The early qPCR evidence pointed toward B2, and the RNA-FISH single-cell analysis supported reduced per-cell MYC after induction in the FACS-derived population (per-cell mean MYC FC 0.51, median 0.39). Per-cell GAPDH (the co-detected technical QC transcript used for per-cell and FOV-level technical QC, §2.12) supported equivalent staining and segmentation across the matched conditions, and the per-cell MYC/GAPDH ratio (a secondary robustness readout, not the headline endpoint) shifted in the same direction (FOV-level FC ~0.44), so the per-cell MYC reduction is not driven by a global staining shift. The H100 guide-B contrasts remain weak because the May 1 B samples showed inhibitor-like multi-target Cq suppression, the second-experiment guide-B RNA-FISH result depends on excluding C1 FOVs 0–6 as a within-channel low-signal artifact, and the April 30 ChIP-qPCR follow-up did not show guide-B-specific CTCF depletion at the promoter-proximal assay.

Guide D is the strongest distal-site expression candidate because reduced MYC was observed across both HCT116-derived populations and independently reproduced after corrected channel assignment, but the lack of OSE_CTCF depletion prevents assigning the effect to confirmed CTCF displacement. Its biological rationale is distinct from A/B because it targets an OSE/CCAT1-associated CTCF site linked to WNT-dependent MYC gating, and the observed MYC-lowering pattern is consistent with that regulatory model. The May 1 H100 D2 RT-qPCR contrast showed a raw MYC decrease (FC 0.10), although normalized values are treated as diagnostics because the May 1 NT controls also shifted after reference normalization. The first RNA-FISH experiment supported reduced per-cell MYC for guide D in the FACS-derived population (per-cell mean MYC FC 0.42; the FOV6 sensitivity check preserves the direction either way, §3.4.1), and the second RNA-FISH experiment corroborated guide D in the H100 platform population after the channel-order rescue described in §2.12 (per-cell mean MYC FC 0.52, independently corroborated at 0.48 by Jonas Grini's re-processing pipeline). The MYC/GAPDH robustness readout supports the per-cell MYC direction in every case where it can be computed and is reported as a confirmatory check rather than as the headline metric. Direction and magnitude of the guide-D per-cell MYC reduction are therefore reproduced across two HCT116-derived populations, three single-cell measurements, and two independent

processing pipelines, alongside the raw-MYC direction in the May 1 H100 RT-qPCR result.

Within the H100 platform population specifically, both bulk RT-qPCR and single-cell RNA-FISH point to reduced MYC for guide A and guide D, with each readout favoring a different guide on different criteria. In RT-qPCR (May 1), guide A is the cleaner promoter-proximal raw-MYC signal because both A1 and A2 decreased after induction (FC 0.23 and 0.13), whereas only D2 was usable for guide D in that run (D1 was inhibitor-affected; §3.2.3), and the single D2 pair gave the largest per-pair raw MYC reduction across the H100 series (FC 0.10). At single-cell resolution in the second RNA-FISH experiment (also H100), guide D gave the larger per-cell mean MYC fold change (~50 % per-cell MYC reduction) versus guide A's ~36 % reduction. The combined picture in H100 is therefore: guide A as the replicate-consistent raw RT-qPCR direction, and guide D as the larger-magnitude single-cell RNA-FISH effect, with both guides reducing MYC directionally across two technically and biologically independent measurement modalities.

The evidence remains mechanistically incomplete: NT instability persists in qPCR, the matched +dox NT RNA-FISH comparator could not be recovered in the second experiment, the second-experiment B2 (D−) acquisition had DAPI-image-quality limitations that left only 5 well-segmented FOVs in the in-house rescue (Jonas Grini's independent re-processing pipeline reaches all 10 FOVs and confirms the same direction), and the May 6 `OSE_CTCF` ChIP-qPCR follow-up did not validate distal CTCF displacement.

The NT control became a central limitation rather than a simple negative baseline. Plus-associated movement appeared repeatedly in NT comparisons, especially in the later qPCR series; on the May 1 H100 plate this shift was reference-gene-driven rather than MYC-driven, which is why raw MYC is treated as the clearest directional readout for that run and the YWHAZ- and B2M-normalized values are reported as diagnostics rather than divisive comparisons against NT (full per-sample detail in §3.2.3). The remaining sources of NT instability across the series — induction-related transcriptional effects, platform-context drift, RNA-prep variability, and reagent-batch effects — cannot be separated with the present data, but the May 1 evidence makes reference-gene-side instability the most concretely supported component.

## 4.3 H100 and the FACS-derived population

As defined in §2.2, the FACS-derived population is a BFP-enriched subpopulation of H100 obtained by sorting and re-expansion, not an independently derived cell line. Bottlenecking and re-expansion can shift population composition, transgene copy-number distribution, dCas9/BFP expression level, stress history, and baseline MYC regulation. Differences between H100 and the FACS-derived subpopulation should

therefore be interpreted as context/population effects within the same HCT116-derived platform background, not as effects of independent cell-line origin.

This distinction matters because the apparent guide-associated expression patterns differed between the two populations. Guide B was most prominent in the FACS-derived series, whereas guide A became most prominent in the later H100 runs. The simplest interpretation is not that one population gives the true answer and the other does not. Rather, the current data show that the observed qPCR effects are population-context-sensitive and require side-by-side testing of H100 and the FACS-derived subpopulation under matched conditions before a biological difference can be claimed.

Choosing which population to take forward has therefore not been straightforward, in part because the FACS sort was less successful as a broad enrichment than initially hoped. As reported in §3.1, the BFP-positive gate represented only 0.23% of singlet-gated events in the H100 sample, essentially indistinguishable from the wild-type HCT116 background of 0.22% on the same gate. In other words, the bulk H100 starting material did not show clear BFP enrichment over wild type, and the 3291 collected events came from a very low-frequency high-BFP tail rather than from a broadly BFP-positive population. This has two practical consequences. First, the FACS-derived population is best read as a strongly bottlenecked subpopulation: it is more uniform with respect to the BFP-positive gate it was selected on, but it carries the population-composition shifts that bottlenecking and re-expansion typically produce, and it is no longer demographically representative of the parent H100 population. Second, retaining H100 as a parallel readout was therefore the safer choice for the H100-context experiments (April 21 and May 1), even though the FACS-derived subpopulation produced cleaner per-well behavior on some early plates. Neither population can be promoted to the single “platform of record” on the basis of the present data: H100 is broader and not BFP-enriched, and the FACS-derived subpopulation is BFP-enriched but bottlenecked from a low-frequency gate. The follow-up plan in §4.6 is therefore framed around side-by-side testing of both populations under matched conditions, rather than committing to one of them prematurely.

## 4.4 Technical limitations and methodological lessons

The technical lessons are part of the interpretation, not just troubleshooting. The qPCR evidence is limited by reference-gene behavior, melt-curve support, RNA input and preparation quality, control behavior, imaging QC, and limited replication. The decision to use YWHAZ + B2M rather than the conventional GAPDH default was based on the Hu et al. (2023) colorectal-cancer-cell-line screen, which identified YWHAZ + B2M as the optimal two-gene reference panel for HCT116 by geNorm, NormFinder, and BestKeeper, and which showed that GAPDH/ACTB were less stable

across the panel. Within this panel, YWHAZ was generally more usable than B2M in the present data, but May 1 showed why reference genes still had to be audited per run: B2M produced the diagnostic +dox NT plus-shift, and YWHAZ was under-replicated on that plate. The RT-qPCR interpretation in this thesis therefore used YWHAZ-normalized MYC fold change as the preferred normalized expression readout where NT behavior was acceptable, while raw MYC and B2M-normalized values served as diagnostics. On May 1 specifically, raw MYC became the clearest directional readout because equal-mass loading, DNase treatment, fresh NZYRT, and recovered melt support made raw MYC interpretable while reference normalization became non-specific. The most reliable qPCR evidence came from contrasts where raw MYC reduction, normalized MYC reduction, melt support, sample-level QC, and NT behavior were concordant. This interpretation is consistent with the MIQE emphasis on primer validation, transparent controls, reference-gene behavior, and melt-curve support in qPCR experiments (Bustin et al., 2009).

Reverse-transcription performance was the dominant run-level qPCR variable. The May 1 OLD-well control showed that April 21 RNA could produce MYC Cq values about 10 cycles earlier when rerun with fresh NZYRT, supporting RT activity as the main contributor to the April 21 weak-MYC behavior rather than template amount alone. DNase treatment improved cDNA-specific interpretation and removed problematic NRT signal, but it did not by itself explain the recovery. Future qPCR runs should therefore use fresh single-use reverse-transcriptase aliquots, DNase-treated RNA, equal-mass loading, and a standardized freeze-thaw policy.

Sample-level inhibition also constrained guide interpretation. Very low 260/230 ratios correctly flagged some problematic samples, but the May 1 +B2 sample showed that a borderline NanoDrop profile can still produce an inhibitor-like multi-target Cq signature. The multi-target Cq matrix was therefore a more sensitive detector of borderline inhibition than NanoDrop ratios alone. This is why affected guide-B and guide-D sample pairs were treated cautiously even when the numerical MYC fold change looked large.

RNA-FISH partly addresses the qPCR control problem because the QC-filtered NT conditions did not decrease in the first experiment, whereas B and D did. However, several FOVs in the first experiment showed channel-specific detection or spot-assignment failures, and excluded FOVs were concentrated in NT. The second RNA-FISH experiment in the H100 platform population added an independent guide-A single-cell readout but lost its +dox NT comparator entirely (Appendix F.2; §3.4.2), so NT could only be reported as a parallel −dox baseline rather than as a +/− contrast in that experiment. The same QC criteria were applied across conditions in both experiments, but the asymmetric failure pattern (NT losses concentrated in NT FOVs of the first experiment, and in the +dox NT well of the second experiment) means that

RNA-FISH should be treated as supportive single-cell evidence rather than as a final quantitative validation endpoint.

Single-guide interpretation also has a CRISPR-specific caveat. Recent CRISPRi work shows that seed-sequence effects can produce off-target transcriptional activity (Rohatgi et al., 2024), and dCas9 binding itself can act as a transcriptional roadblock depending on genomic placement and orientation (Zukher et al., 2023). These papers do not invalidate the observed guide-associated MYC reductions, but they reinforce why the thesis treats concordance across independent guides, matched controls, and orthogonal readouts as more persuasive than any single guide contrast alone.

Finally, the project was not structured for formal inferential statistics across all runs. Several datasets were exploratory, technically constrained, or uneven in replication. Descriptive fold-change summaries are therefore more appropriate than underpowered hypothesis tests, and fold change was emphasized because it communicates direction and approximate magnitude more directly than dCq.

## 4.5 ChIP-qPCR implications

The ChIP-qPCR work strengthens the thesis as an assay-development project but does not provide definitive guide-specific CTCF displacement evidence. Fragmentation optimization identified 2 µL MNase + S5 as a workable preparation condition, and April 20 supported strong CTCF enrichment at the mapped promoter-proximal `mycP_CTCF` assay. UCSC In-Silico PCR mapped the `mycP_CTCF` and `OSE_CTCF` assays to their intended target regions (§2.10.4, Table 2.7).

The technical interpretation of a negative or flat ChIP-qPCR result should also be held to chromatin-assay standards rather than read as a simple absence result. ENCODE-style ChIP guidelines emphasize replication, antibody validation, background controls, and quantitative QC before strong conclusions are drawn from occupancy data (Landt et al., 2012), and antibody validation is application-specific rather than transferable across all assay formats (Uhlen et al., 2016). In the present work, the CTCF ChIP-qPCR assays reached useful assay-development status, but the single-run follow-ups and control limitations mean that non-detection of guide-specific depletion remains mechanistically inconclusive.

The follow-up occupancy tests did not show guide-specific CTCF depletion. April 30 showed effectively flat `mycP_CTCF` percent input after guide B induction (B+ / B- ≈ 0.96x), and May 6 showed no reduction for guide A at `mycP_CTCF`. At the distal `OSE_CTCF` assay, guide D and NT3 shifted almost identically after induction, giving an NT-adjusted D ratio close to 1.0. The May 6 gel supported expected-size qPCR products, but this remains a size check rather than sequence validation.

These negative occupancy-oriented results should not be over-read as proof that the guides have no functional effect. The ChIP-qPCR runs were single follow-ups with control limitations: April 30 had variable IgG background, May 6 mycP_CTCF had weak NTC melt features, and negC_CTCF failed under the current cycling conditions. Quantitatively, the run-spanning baseline analysis in §3.3 places the practical limit of detection of these single-replicate runs at roughly a two-fold percent-input reduction at the mapped target assays: the negative occupancy result therefore rules out a strong (>=2×) bulk CTCF eviction at mycP_CTCF for guides A/B and at 0SE_CTCF for guide D under the tested conditions, but does not rule out smaller, partial, or cell-heterogeneous occupancy changes.

The lack of bulk-detectable CTCF loss by ChIP-qPCR should therefore be read as an important boundary on the mechanistic interpretation rather than simply as a failed perturbation experiment. CRISPRd was introduced as a way to reversibly disrupt specific transcription factor-DNA interactions using Cas9/dCas9 occupancy (Shariati et al., 2019), but this strategy depends on whether the guide-positioned protein can effectively compete with the endogenous factor at a given locus. For CTCF-bound sites, Tarjan et al. (2019) showed that CTCF displacement is possible, particularly when epigenome editors are precisely targeted to the cognate motif, but also that the magnitude and stability of displacement depend on targeting and effector context. More recent multi-locus CRISPRi work using motif-directed truncated guides further illustrates that CTCF-associated regulatory elements can be interrogated by guide-based perturbation, while also emphasizing that guide design and chromatin context shape functional output (Moore et al., 2025). The present ChIP-qPCR result therefore supports a cautious interpretation: the inducible platform can be linked to guide-associated MYC expression changes, but the upstream occupancy step has not yet been validated at the targeted MYC sites.

The May 6 Universal/NZY side comparison adds a separate methodological caution. Using April 30 -NT DNA, NZY shifted the same input and CTCF IP material earlier and produced much stronger melt peaks than the Universal PCR/SYBR setup, while preserving a similar expected-temperature product peak. However, the matched NZY NTC also amplified strongly at the expected melt temperature, whereas the Universal NTC remained undetected. This raises the possibility that master-mix chemistry can influence borderline NTC/NRT behavior in this project, but it does not prove that NZY chemistry is inherently unreliable because the April 30 NZY mycP_CTCF NTCs were clean. The side comparison is therefore useful as a chemistry/QC check, not as an independent specificity or occupancy result.

More importantly, May 1 RT-qPCR and RNA-FISH support MYC mRNA reduction for some guide/condition combinations even though CTCF percent input was not reduced. The combination of reduced MYC expression and unchanged or increased

CTCF recovery after induction could reflect functional interference without bulk-detectable CTCF eviction, but direct dCas9 target-engagement testing is required before this interpretation can be distinguished from incomplete guide landing, cell-state effects, or indirect guide-associated effects. Under the functional-interference reading, dCas9 binding at the guide target site would perturb local regulatory function — cofactor recruitment, productive enhancer–promoter contact, or the effective output of the CTCF-anchored loop — without fully evicting resident CTCF from the motif, and CTCF could remain detectable by bulk ChIP-qPCR even if productive regulatory engagement is altered. This reading is consistent with the literature framing in §1.7.2: when tested without an effector domain, dCas9 alone has been shown to reduce CTCF occupancy at some CTCF motifs, but less strongly than dCas9-KRAB at the same sites (Tarjan et al., 2019). The alternative possibilities — incomplete or heterogeneous dCas9 recruitment in the bulk population, ChIP-qPCR sensitivity below modest occupancy shifts, or guide-, cell-state-, or induction-associated effects not captured by the current occupancy readout — remain equally consistent with the data and cannot be excluded without target-engagement evidence. In the present work, the combination of reduced MYC expression and no detected guide-specific decrease in bulk CTCF occupancy therefore supports expression-level perturbation, while leaving the upstream mechanism unresolved. The decisive next experiment is direct dCas9 ChIP-qPCR at the guide target sites rather than another CTCF ChIP-qPCR alone: if dCas9 is enriched at the A, B, or D target sites under induction while CTCF percent input remains unchanged, this would support target engagement without full eviction; if dCas9 is not enriched, the observed expression effects would need to be explained indirectly.

## 4.6 Future work: from repeat experiments to system validation

Future work should not be framed as a list of experiments to repeat, but as a staged validation of the inducible dCas9 system as a whole. The present data show that the platform is usable and that guide-associated MYC reductions can be observed in some readouts, but they do not yet resolve which experimental layer is limiting interpretation: the HCT116-derived cell populations themselves, the inducible dCas9 platform, guide recruitment to the intended target sites, CTCF occupancy measurement, or downstream MYC expression readout. The next phase should therefore move from simple replication of individual contrasts toward a tiered platform-validation ladder, in which each level confirms what the level above it depends on. Table 4.1 summarizes this four-layer framework, and the paragraphs below expand on the controls and readouts that would make each layer interpretable.

**Table 4.1. Four-layer validation framework for the next phase of work.** Each layer addresses a distinct uncertainty that the present data cannot resolve and that constrains the interpretation of all layers below it.

| Layer | Question | Validation work |
|---|---|---|
| Cell population | Are the H100 platform population and the FACS-derived BFP-enriched subpopulation comparable enough to be treated as the same experimental context? | Identity / mycoplasma, BFP and dCas9 distribution, induction response, growth behavior, baseline MYC under matched conditions. |
| Platform | Is the inducible dCas9 system genuinely off/on controlled? | dCas9 expression, nuclear localization, basal leakiness, and drug-only effects under matched −/+ dox/Shield-1. |
| Target engagement | Does dCas9 bind the intended guide target sites? | dCas9 ChIP-qPCR at the A, B, and D motifs before any further interpretation of CTCF occupancy changes. |
| Assay controls | Do the readouts have positive and negative controls strong enough to make a difference detectable? | Strengthened control structure across RT-qPCR, ChIP-qPCR, and RNA-FISH (Tables 4.2 and 4.3). |

### Layer 1 — cell population validation

The current work used two related but non-identical HCT116-derived populations: the broader H100 platform population and a FACS-derived BFP-enriched subpopulation. Because the FACS-derived population was selected from a very low-frequency BFP-positive tail (§3.1) and then re-expanded, it may differ from the parental H100 population in transgene expression, copy-number distribution, growth history, and baseline MYC regulation. Future work should therefore first establish whether these populations behave similarly under matched culture and induction conditions before guide-specific differences between them are interpreted as biological. Practical validation steps include STR profiling and mycoplasma testing to confirm cell identity and culture health; flow cytometry for BFP and anti-Cas9 immunofluorescence or western blotting before each experiment to quantify the platform-positive fraction and confirm dCas9 expression and nuclear localization; Cas9 RT-qPCR or a matched protein readout under −/+ induction to test the induction contrast; a doubling-time / confluency check to control for MYC changes caused by cell state rather than by guide targeting; and a side-by-side baseline-MYC measurement in H100 and the FACS-derived subpopulation under matched seeding density, passage number, and induction timing.

### Layer 2 — platform validation

The second level should confirm that the inducible dCas9 platform itself is off/on controlled, not just present. This means measuring dCas9 expression and nuclear localization under matched −/+ dox and Shield-1, characterizing basal (uninduced) dCas9 protein and any background activity from leaky expression, and including a drug-only condition (doxycycline plus Shield-1 in wild-type HCT116 without the dCas9 cassette) to test whether the inducer molecules themselves contribute to the recurring +dox-associated shifts seen on NT samples (§3.2.3, §4.4). Without this layer it is not possible to separate platform-induction effects from guide-targeting effects in any downstream readout.

### Layer 3 — target-engagement validation

The most direct missing mechanistic test is dCas9 ChIP-qPCR at the guide A, B, and D target sites, ideally using a validated anti-Cas9 antibody or an engineered epitope tag if available. This is the experiment that separates four mechanistic possibilities currently conflated by the present data: failed guide landing, dCas9 landing without CTCF eviction, CTCF eviction without detectable contact change, and transcriptional effects driven by dCas9 occupancy or guide off-target behavior rather than the intended CTCF mechanism. If dCas9 is enriched at the intended sites while CTCF percent input remains unchanged, the data would support a model in which dCas9 perturbs regulatory function without complete bulk-detectable CTCF eviction (§4.5). If dCas9 is not enriched, the observed MYC changes would need to be explained by indirect, population-level, or technical effects. CTCF ChIP-qPCR should be revisited only after this target-engagement step, and only with the strengthened control structure described below.

### Layer 4 — assay-control validation

The non-targeting (NT) guide remains a necessary control, but the present qPCR series shows that NT cannot be treated as a passive no-change baseline because reference-gene Cq movement on the +dox NT samples inflates reference-normalized contrasts (§3.2.3, §4.4). The next phase should therefore broaden the negative-control set and add positive controls at each assay layer, so that a non-effect is interpretable rather than ambiguous. Table 4.2 lists negative controls that would isolate the specific source of a flat result, and Table 4.3 lists positive controls that would establish that each assay can detect a real effect when one is present.

**Table 4.2. Negative controls beyond NT for the next phase.**

| Negative control | What it controls for |
|---|---|
| Wild-type HCT116 + doxycycline + Shield-1 | Drug effects independent of the dCas9 platform |
| dCas9 platform without sgRNA | dCas9 induction effects independent of guide targeting |
| Non-targeting sgRNA (current NT) | Guide / vector / selection background |
| Safe-harbor or irrelevant-locus sgRNA | dCas9 binding at DNA without MYC-locus targeting |
| IgG ChIP | Non-specific immunoprecipitation |
| Validated negative genomic ChIP-qPCR region | Local enrichment specificity (replaces the failed negC_CTCF, §3.3) |
| NTC / NRT in every RT-qPCR plate | qPCR contamination and gDNA contribution |
| No-primary RNA-FISH or scrambled-probe channel | Imaging-pipeline background |

**Table 4.3. Positive controls beyond the current set.**

| Positive control | What it proves |
|---|---|
| anti-Pol II ChIP at the GAPDH promoter | ChIP workflow can recover a known active-chromatin signal |
| CTCF ChIP at a robust CTCF site unrelated to MYC | CTCF antibody and IP conditions work at a positive locus |
| dCas9 ChIP-qPCR at the guide target site | The guide actually recruits dCas9 (Layer 3 above) |
| dCas9-KRAB or CRISPRi control guide at a repression-positive promoter | The system can produce a detectable transcriptional effect when full repression is expected |
| MYC-responsive condition (e.g. serum or WNT-related stimulation, where appropriate) | RT-qPCR / RNA-FISH MYC readout can detect a real biological change |
| RNA-FISH housekeeping target (e.g. GAPDH probe set used here) | Single-cell imaging and spot-detection pipeline works on a high-abundance reference |

### Downstream readouts once Layers 1–3 are established

If Layers 1–3 confirm that the populations are comparable, the platform is off/on controlled, and dCas9 is recruited to the intended sites, the next phase can test whether site-specific perturbation changes chromatin architecture or enhancer-promoter communication. Prior work links CTCF and cohesin-mediated loop organization to local insulation and regulatory contact structure (Rao et al., 2014; Sanborn et al., 2015; Fudenberg et al., 2016; Nora et al., 2017), and MYC-specific studies show that CTCF perturbation can affect MYC regulation through enhancer-

promoter looping (Hyle et al., 2019). Targeted 3C/4C, Capture-C, or HiChIP would therefore connect the present expression and ChIP-qPCR readouts to the chromatin-contact mechanisms that motivated the guide design (Mumbach et al., 2016; Downes et al., 2022). For occupancy validation, CUT&RUN or CUT&Tag could provide lower-background alternatives to repeating ChIP-qPCR alone, especially if input material or signal-to-background remains limiting (Skene & Henikoff, 2017; Kaya-Okur et al., 2019). For the single-cell expression arm, a future RNA-FISH session should include guide A, guide B, guide D, and a complete −/+dox NT pair within the same imaging session, with channel order, laser power, exposure, and gain locked and verified per well, predefined FOV-level QC criteria, and representative image review of segmentation and spot assignment before fold-change interpretation. The most useful within-platform repeat would be performed in the H100 platform population so that the existing guide-A and guide-D H100 single-cell signals can be tested for reproducibility against a same-population +dox NT control (§3.4.2; Appendix F.2).

Framed this way, the next phase tests whether the observed guide-associated MYC reductions persist after platform, population, and control validation, rather than repeating the same contrasts in the same configuration. The decisive layer is target engagement (Layer 3): until dCas9 ChIP-qPCR has been performed at the A, B, and D sites, the present data cannot distinguish a most-consistent guide-associated expression-level effect from a system-level artifact, and the upstream regulatory mechanism remains under-constrained.

# 5 Conclusion

This thesis shows that inducible CRISPR/dCas9 targeting of selected CTCF-associated regulatory sites at the MYC locus is associated with reduced MYC expression in HCT116-derived colorectal cancer cells. The effect was most clearly supported by single-cell RNA-FISH and was also observed by bulk RT-qPCR in selected guide-specific and population-specific contexts. Together, these results support expression-level perturbation of MYC by inducible, effector-free dCas9 targeting, while also showing that the strength and reproducibility of the effect depend on guide identity, cell population context, and assay quality.

The work established a reusable inducible dCas9-only platform for testing regulatory-site function without permanently editing the underlying DNA sequence. Guides A and B targeted a promoter-proximal CTCF-associated docking site near MYC, while guide D targeted a distal OSE/CCAT1-associated CTCF site within the broader 8q24 regulatory landscape. Across the experimental series, guide A and guide D provided the clearest H100 MYC-lowering evidence, whereas guide B was supported mainly in the FACS-derived BFP-enriched population. RNA-FISH provided the strongest orthogonal support, showing reduced per-cell MYC for guides B and D in the FACS-derived population and for guide A and rescued guide D in H100. RT-qPCR supported the same overall direction in selected contexts, but normalized effect sizes required cautious interpretation because of NT-control behavior, reference-gene shifts, and run-level reverse-transcription variability.

Despite the expression-level effects, CTCF ChIP-qPCR did not detect guide-specific CTCF loss at the mapped promoter-proximal `mycP_CTCF` or distal `OSE_CTCF` assays. The ChIP-qPCR series reached interpretable assay-development status, but the direct B/NT2 and A/D/NT3 follow-up runs did not show clear guide-specific depletion of CTCF under the tested conditions. These data therefore rule out strong bulk CTCF eviction at the assayed target regions, but they do not exclude smaller, partial, transient, or cell-heterogeneous occupancy changes. The central mechanistic conclusion is therefore that MYC expression was reduced in guide-associated patterns, but the originally hypothesized steric CTCF-displacement mechanism was not validated.

The most important next step is direct dCas9 ChIP-qPCR at the guide A, B, and D target sites. This experiment would determine whether the guides successfully recruit dCas9 to their intended genomic positions and would separate failed guide landing from dCas9 landing without detectable CTCF eviction. Once target engagement is confirmed, CTCF ChIP-qPCR should be repeated with biological replicates, improved negative-region controls, and sufficient sensitivity to detect smaller occupancy changes. Complementary methods such as CUT&RUN,

CUT&Tag, 3C/4C, Capture-C, or HiChIP would then be useful for testing whether dCas9 targeting alters local CTCF occupancy or MYC-associated enhancer–promoter contacts.

Overall, this thesis is best viewed as a platform- and assay-development study with a supported expression-level result. It establishes an inducible, reversible, effector-free dCas9 framework for perturbing CTCF-associated regulatory sites, identifies guide-associated reductions in MYC expression across bulk and single-cell readouts, and defines the technical constraints that currently limit mechanistic interpretation. The work therefore fulfils the platform-development and expression-testing aims set out in §1.9, while leaving the upstream occupancy mechanism as the key unresolved aim for future validation. It provides a strong starting point for dissecting CTCF-associated regulatory logic at the MYC locus.

## References


Bell, A. C., & Felsenfeld, G. (2000). Methylation of a CTCF-dependent boundary controls imprinted expression of the Igf2 gene. *Nature, 405*(6785), 482–485. https://doi.org/10.1038/35013100

Bustin, S. A., Benes, V., Garson, J. A., Hellemans, J., Huggett, J., Kubista, M., Mueller, R., Nolan, T., Pfaffl, M. W., Shipley, G. L., Vandesompele, J., & Wittwer, C. T. (2009). The MIQE guidelines: Minimum information for publication of quantitative real-time PCR experiments. *Clinical Chemistry, 55*(4), 611–622. https://doi.org/10.1373/clinchem.2008.112797

Chachoua, I., Tzelepis, I., Dai, H., Lim, J. P., Lewandowska-Ronnegren, A., Beccaria Casagrande, F., Wu, S., Vestlund, J., Mallet de Lima, C. D., Bhartiya, D., Scholz, B. A., Martino, M., Mehmood, R., & Göndör, A. (2022). Canonical WNT signaling-dependent gating of MYC requires a noncanonical CTCF function at a distal binding site. *Nature Communications, 13*(1), 204. https://doi.org/10.1038/s41467-021-27868-3

Dang, C. V. (2012). MYC on the path to cancer. *Cell, 149*(1), 22–35. https://doi.org/10.1016/j.cell.2012.03.003

Dekker, J., & Mirny, L. (2016). The 3D genome as moderator of chromosomal communication. *Cell, 164*(6), 1110–1121. https://doi.org/10.1016/j.cell.2016.02.007

Dixon, J. R., Selvaraj, S., Yue, F., Kim, A., Li, Y., Shen, Y., Hu, M., Liu, J. S., & Ren, B. (2012). Topological domains in mammalian genomes identified by analysis of chromatin interactions. *Nature, 485*(7398), 376–380. https://doi.org/10.1038/nature11082

Downes, D. J., Smith, A. L., Karpinska, M. A., Velychko, T., Rue-Albrecht, K., Sims, D., Milne, T. A., Davies, J. O. J., Oudelaar, A. M., & Hughes, J. R. (2022). Capture-C: A modular and flexible approach for high-resolution chromosome conformation capture. *Nature Protocols, 17*, 445–475. https://doi.org/10.1038/s41596-021-00651-w

Femino, A. M., Fay, F. S., Fogarty, K., & Singer, R. H. (1998). Visualization of single RNA transcripts in situ. *Science, 280*(5363), 585–590. https://doi.org/10.1126/science.280.5363.585

Flavahan, W. A., Drier, Y., Liau, B. B., Gillespie, S. M., Venteicher, A. S., Stemmer-Rachamimov, A. O., Suvà, M. L., & Bernstein, B. E. (2016). Insulator dysfunction and oncogene activation in IDH mutant gliomas. *Nature, 529*(7584), 110–114. https://doi.org/10.1038/nature16490

Fudenberg, G., Imakaev, M., Lu, C., Goloborodko, A., Abdennur, N., & Mirny, L. A. (2016). Formation of chromosomal domains by loop extrusion. *Cell Reports, 15*(9), 2038–2049. https://doi.org/10.1016/j.celrep.2016.04.085

Gao, C., Martino, M., Chaurasiya, A., et al. (2026). *A distal CTCF-binding site drives MYC expression plasticity in a negative feed-forward loop* [Preprint]. bioRxiv. https://doi.org/10.64898/2026.01.28.702300

Gilbert, L. A., Larson, M. H., Morsut, L., Liu, Z., Brar, G. A., Torres, S. E., Stern-Ginossar, N., Brandman, O., Whitehead, E. H., Doudna, J. A., Lim, W. A., Weissman, J. S., & Qi, L. S. (2013). CRISPR-mediated modular RNA-guided regulation of transcription in eukaryotes. *Cell, 154*(2), 442–451. https://doi.org/10.1016/j.cell.2013.06.044

Hnisz, D., Abraham, B. J., Lee, T. I., Lau, A., Saint-André, V., Sigova, A. A., Hoke, H. A., & Young, R. A. (2013). Super-enhancers in the control of cell identity and disease. *Cell, 155*(4), 934–947. https://doi.org/10.1016/j.cell.2013.09.053

Hu, Y., Liu, L., Jiang, Q., Fang, W., Chen, Y., Hong, Y., & Zhai, X. (2023). Screening and validation of the optimal panel of reference genes in colonic epithelium and relative cancer cell lines. *Scientific Reports, 13*, 17472. https://doi.org/10.1038/s41598-023-45174-4

Hyle, J., Zhang, Y., Wright, S., Xu, B., Shao, Y., Easton, J., Tian, L., Feng, R., Xu, P., & Li, C. (2019). Acute depletion of CTCF directly affects MYC regulation through loss of enhancer–promoter looping. *Nucleic Acids Research, 47*(13), 6699–6713. https://doi.org/10.1093/nar/gkz462

Kaya-Okur, H. S., Wu, S. J., Codomo, C. A., Pledger, E. S., Bryson, T. D., Henikoff, J. G., Ahmad, K., & Henikoff, S. (2019). CUT&Tag for efficient epigenomic profiling of small samples and single cells. *Nature Communications, 10*, 1930. https://doi.org/10.1038/s41467-019-09982-5

Landt, S. G., Marinov, G. K., Kundaje, A., Kheradpour, P., Pauli, F., Batzoglou, S., Bernstein, B. E., Bickel, P., Brown, J. B., Cayting, P., Chen, Y., DeSalvo, G., Epstein, C., Fisher-Aylor, K. I., Euskirchen, G., Gerstein, M., Gertz, J., Hartemink, A. J., Hoffman, M. M., Iyer, V. R., Jung, Y. L., Karmakar, S., Kellis, M., Kharchenko, P. V., Li, Q., Liu, T., Liu, X. S., Ma, L., Milosavljevic, A., Myers, R. M., Park, P. J., Pazin, M. J., Perry, M. D., Raha, D., Reddy, T. E., Rozowsky, J., Shoresh, N., Sidow, A., Slattery, M., Stamatoyannopoulos, J. A., Tolstorukov, M. Y., White, K. P., Xi, S., Farnham, P. J., Lieb, J. D., Wold, B. J., & Snyder, M. (2012). ChIP-seq guidelines and practices of the ENCODE and modENCODE consortia. *Genome Research, 22*(9), 1813–1831. https://doi.org/10.1101/gr.136184.111

Mohr, S. E., Hu, Y., Ewen-Campen, B., Housden, B. E., Viswanatha, R., & Perrimon, N. (2016). CRISPR guide RNA design for research applications. *The FEBS Journal, 283*(17), 3232–3238. https://doi.org/10.1111/febs.13777

Moore, M. M., Wekhande, S., Issner, R., Collins, A., Cruz, A. J., Liu, Y. V., Javed, N., Casaní-Galdón, S., Buenrostro, J. D., Epstein, C. B., Mattei, E., Doench, J. G., Bernstein, B. E., Shoresh, N., & Najm, F. J. (2025). Multi-locus CRISPRi targeting with a single truncated guide RNA. *Nature Communications, 16*, 1357. https://doi.org/10.1038/s41467-025-56144-x

Mueller, F., Senecal, A., Tantale, K., Marie-Nelly, H., Ly, N., Collin, O., Basyuk, E., Bertrand, E., Darzacq, X., & Zimmer, C. (2013). FISH-quant: Automatic counting of transcripts in 3D FISH images. *Nature Methods, 10*(4), 277–278. https://doi.org/10.1038/nmeth.2406

Mumbach, M. R., Rubin, A. J., Flynn, R. A., Dai, C., Khavari, P. A., Greenleaf, W. J., & Chang, H. Y. (2016). HiChIP: Efficient and sensitive analysis of protein-directed genome architecture. *Nature Methods, 13*(11), 919–922. https://doi.org/10.1038/nmeth.3999

Nora, E. P., Goloborodko, A., Valton, A.-L., Gibcus, J. H., Uebersohn, A., Abdennur, N., Dekker, J., Mirny, L. A., & Bruneau, B. G. (2017). Targeted degradation of CTCF decouples local insulation of chromosome domains from genomic compartmentalization. *Cell, 169*(5), 930–944.e22. https://doi.org/10.1016/j.cell.2017.05.004

Qi, L. S., Larson, M. H., Gilbert, L. A., Doudna, J. A., Weissman, J. S., Arkin, A. P., & Lim, W. A. (2013). Repurposing CRISPR as an RNA-guided platform for sequence-specific control of gene expression. *Cell, 152*(5), 1173–1183. https://doi.org/10.1016/j.cell.2013.02.022

Raj, A., van den Bogaard, P., Rifkin, S. A., van Oudenaarden, A., & Tyagi, S. (2008). Imaging individual mRNA molecules using multiple singly labeled probes. *Nature Methods, 5*(10), 877–879. https://doi.org/10.1038/nmeth.1253

Rao, S. S. P., Huntley, M. H., Durand, N. C., Stamenova, E. K., Bochkov, I. D., Robinson, J. T., Sanborn, A. L., Machol, I., Omer, A. D., Lander, E. S., & Aiden, E. L. (2014). A 3D map of the human genome at kilobase resolution reveals principles of chromatin looping. *Cell, 159*(7), 1665–1680. https://doi.org/10.1016/j.cell.2014.11.021

Rohatgi, N., Fortin, J.-P., Lau, T., Ying, Y., Zhang, Y., Lee, B. L., Costa, M. R., Reja, R., & Kampmann, M. (2024). Seed sequences mediate off-target activity in the CRISPR-interference system. *Cell Genomics, 4*(12), 100693. https://doi.org/10.1016/j.xgen.2024.100693

Sanborn, A. L., Rao, S. S. P., Huang, S.-C., Durand, N. C., Huntley, M. H., Jewett, A. I., Bochkov, I. D., Chinnappan, D., Cutkosky, A., Li, J., Geeting, K. P., Gnirke, A., Melnikov, A., McKenna, D., Stamenova, E. K., Lander, E. S., & Aiden, E. L. (2015). Chromatin extrusion explains key features of loop and domain formation in wild-type and engineered genomes. *Proceedings of the National Academy of Sciences of the United States of America, 112*(47), E6456–E6465. https://doi.org/10.1073/pnas.1518552112

Schuijers, J., Manteiga, J. C., Weintraub, A. S., Day, D. S., Zamudio, A. V., Hnisz, D., Lee, T. I., & Young, R. A. (2018). Transcriptional dysregulation of MYC reveals common enhancer-docking mechanism. *Cell Reports, 23*(2), 349–360. https://doi.org/10.1016/j.celrep.2018.03.056

Shariati, S. A. M., Dominguez, A., Xie, S., Wernig, M., Qi, L. S., & Skotheim, J. M. (2019). Reversible disruption of specific transcription factor–DNA interactions using CRISPR/Cas9. *Molecular Cell, 74*(3), 622–633.e4. https://doi.org/10.1016/j.molcel.2019.04.011

Skene, P. J., & Henikoff, S. (2017). An efficient targeted nuclease strategy for high-resolution mapping of DNA binding sites. *eLife, 6*, e21856. https://doi.org/10.7554/eLife.21856

Srinivasan, R., Sun, T., Sandles, A., Wu, D., Wang, L., Patel, H., Pabalate, R., Bader, M., Heidersbach, A., Ho, C., Xie, S., Ng, A., & Haley, B. (2026). Chemically-inducible CRISPR/Cas9 circuits for ultra-high dynamic range gene perturbation. *Nature Communications, 17*, 504. https://doi.org/10.1038/s41467-025-67201-w

Tarjan, D. R., Flavahan, W. A., & Bernstein, B. E. (2019). Epigenome editing strategies for the functional annotation of CTCF insulators. *Nature Communications, 10*, 4258. https://doi.org/10.1038/s41467-019-12166-w

Uhlen, M., Bandrowski, A., Carr, S., Edwards, A., Ellenberg, J., Lundberg, E., Rimm, D. L., Rodriguez, H., Hiltke, T., Snyder, M., & Yamamoto, T. (2016). A proposal for validation of antibodies. *Nature Methods, 13*(10), 823–827. https://doi.org/10.1038/nmeth.3995

Whyte, W. A., Orlando, D. A., Hnisz, D., Abraham, B. J., Lin, C. Y., Kagey, M. H., Rahl, P. B., Lee, T. I., & Young, R. A. (2013). Master transcription factors and mediator establish super-enhancers at key cell identity genes. *Cell, 153*(2), 307–319. https://doi.org/10.1016/j.cell.2013.03.035

Xiang, J.-F., Yin, Q.-F., Chen, T., Zhang, Y., Zhang, X.-O., Wu, Z., Zhang, S., Wang, H.-B., Ge, J., Lu, X., Yang, L., & Chen, L.-L. (2014). Human colorectal cancer-specific CCAT1-L lncRNA regulates long-range chromatin interactions at the MYC locus. *Cell Research, 24*(5), 513–531. https://doi.org/10.1038/cr.2014.35

Zukher, I., Dujardin, G., Sousa-Luís, R., & Proudfoot, N. J. (2023). Elongation roadblocks mediated by dCas9 across human genes modulate transcription and nascent RNA processing. *Nature Structural & Molecular Biology, 30*, 1536–1548. https://doi.org/10.1038/s41594-023-01090-9

de Wit, E., Vos, E. S. M., Holwerda, S. J. B., Valdes-Quezada, C., Verstegen, M. J. A. M., Teunissen, H., Splinter, E., Wijchers, P. J., Krijger, P. H. L., & de Laat, W. (2015). CTCF binding polarity determines chromatin looping. *Molecular Cell, 60*(4), 676–684. https://doi.org/10.1016/j.molcel.2015.09.023

# Appendix A. RNA prep characterization

This appendix consolidates the per-sample RNA prep characterization data referenced in Chapters 2–5. Three RNA preparations were used for the main RT-qPCR runs in this thesis: the April 3, 2026 H100 prep (used for the April 21 and May 1 runs), the April 5, 2026 FACS-derived prep (used for the April 19 run), and the May 1, 2026 post-DNase NanoDrop re-measurement of the April 3 H100 prep. Cell counts and viabilities were measured on a Countess 3 prior to RNA extraction. RNA concentration and 260/280 and 260/230 purity ratios were measured by NanoDrop using the RNA-40 setting.

Per-sample NanoDrop records also exist for the earlier March 27 H100 and March 31 FACS-derived exploratory RT-qPCR runs (project documentation), but these are not tabulated here because both runs are treated as exploratory/directional with weak MYC amplicon-window melt support (§3.2.1, Table 3.3) and do not carry the main quantitative interpretation in Chapter 3.

## A.1 April 3 H100 prep (used for April 21 RT-qPCR)

Cells were grown in 24-well plates and harvested into approximately 1 mL of suspension. Countess viabilities were uniformly high (95–100%, median 99%). Cell concentrations of 0.35 to 1.71 million cells/mL correspond to approximately 350,000 to 1.71 million cells per well. Using approximately 300,000 HCT116 cells per well in a 24-well plate as a practical near-confluence reference, the Countess values suggest that every sample was at or above confluence and that most were approximately 2–5× over this benchmark.

**Table A.1. April 3 H100 prep — Countess and NanoDrop results.**

| Sample | Cells (mill/mL) | Viability | RNA (ng/µL) | 260/280 | 260/230 |
|---|---|---|---|---|---|
| -D1 | 0.94 | 99% | 14.4 | 2.11 | 1.68 |
| +D1 | 0.84 | 99% | 126.9 | 2.10 | 1.90 |
| -D2 | 1.71 | 99% | 117.1 | 2.12 | 1.80 |
| +D2 | 0.42 | 99% | 67.9 | 2.14 | 1.68 |
| -B1 | 0.58 | 99% | 21.8 | 2.30 | 0.10 |
| +B1 | 0.38 | 100% | 73.8 | 2.12 | 1.47 |
| -B2 | 0.88 | 98% | 10.7 | 2.29 | 0.39 |
| +B2 | 0.35 | 95% | 62.9 | 2.04 | 1.60 |
| -A1 | 1.17 | 98% | 56.3 | 2.09 | 1.52 |
| +A1 | 0.72 | 99% | 111.1 | 2.11 | 1.44 |
| -A2 | 1.09 | 99% | 69.7 | 2.09 | 1.03 |
| +A2 | 0.52 | 99% | 40.7 | 2.12 | 1.19 |
| -NT1 | 1.05 | 99% | 86.0 | 2.11 | 1.82 |
| +NT1 | 1.32 | 100% | 88.3 | 2.09 | 1.46 |
| -NT2 | 0.92 | 99% | 67.2 | 2.04 | 1.91 |
| +NT2 | 0.75 | 99% | 118.9 | 2.10 | 1.80 |

Two -dox samples (-B1 and -B2) had 260/230 ratios below 0.5 (0.10 and 0.39 respectively), indicating extraction-buffer carryover localized to these two samples rather than distributed across the prep. A subsequent re-measurement of these samples after DNase treatment (Table A.4) showed that the carryover persisted, and on the May 1 RT-qPCR plate the affected samples produced suppressed Cq values across multiple targets (§3.2.3).

## A.2 April 5 FACS-derived prep (used for April 19 RT-qPCR)

Cells were grown in 24-well plates and harvested into approximately 1 mL of suspension. Countess viabilities were 95–100%. The cell concentration range was wider than for the April 3 H100 prep, with one extreme high reading (+B1 at 7.4 mill/mL) and several low readings near or below 0.1 mill/mL. NanoDrop concentrations were used for the equal-mass loading on the April 19 plate (8 ng RNA per well) and are reported in Table A.3.

**Table A.2. April 5 FACS-derived prep — Countess results.**

| Sample | Cells (mill/mL) | Viability |
|---|---|---|
| -D1 | 0.084 | 88% |
| +D1 | 0.72 | 99% |
| -D2 | 0.11 | 86% |
| +D2 | 0.42 | 98% |
| -B1 | 0.82 | 100% |
| +B1 | 7.4 | 99% |
| -B2 | 1.1 | 100% |
| +B2 | 1.5 | 99% |
| -A1 | 2.48 | 97% |
| +A1 | 0.6 | 100% |
| -A2 | 0.45 | 96% |
| +A2 | 0.65 | 99% |
| -NT1 | 0.59 | 99% |
| +NT1 | 0.72 | 96% |
| -NT2 | 0.7 | 95% |
| +NT2 | 0.81 | 97% |
| -NT3 | 1.98 | 98% |
| +NT3 | 1.71 | 99% |
| -NT4 | 2.49 | 99% |
| +NT4 | 1.77 | 99% |

The per-pair direction was variable: in some pairs (D1, D2, B1) +dox had substantially more cells than -dox, while in others (A1) -dox had more cells than +dox. The +B1 reading of 7.4 mill/mL was an extreme outlier relative to the rest of the prep and was reported as recorded.

**Table A.3. April 5 FACS-derived prep — NanoDrop results.** Per-sample ng/µL, A260/280, and A260/230 measured immediately after the April 5 prep. Concentrations were used to load equal RNA mass (8 ng/well) on the April 19 FACS-derived RT-qPCR plate (§3.2.2, Appendix C.1).

| Sample | ng/µL | A260/280 | A260/230 |
|---|---|---|---|
| -D1 | 25.4 | 1.60 | 0.44 |
| +D1 | 38.9 | 1.90 | 0.91 |
| -D2 | 4.6 | 1.08 | 0.23 |
| +D2 | 22.0 | 1.93 | 1.16 |
| -B1 | 44.4 | 2.01 | 1.35 |
| +B1 | 23.7 | 1.91 | 1.16 |
| -B2 | 47.3 | 1.97 | 1.07 |
| +B2 | 36.9 | 1.97 | 1.60 |
| -A1 | 12.6 | 1.82 | 0.51 |
| +A1 | 16.1 | 1.81 | 0.85 |
| -A2 | 26.8 | 1.94 | 1.16 |
| +A2 | 15.8 | 1.86 | 0.86 |
| -NT1 | 11.7 | 1.98 | 0.26 |
| +NT1 | 36.4 | 2.00 | 1.39 |
| -NT2 | 30.0 | 2.01 | 1.06 |
| +NT2 | 48.8 | 2.09 | 0.60 |
| -NT3 | 32.5 | 2.07 | 1.07 |
| +NT3 | 24.1 | 1.96 | 1.20 |
| -NT4 | 16.6 | 2.10 | 0.95 |
| +NT4 | 49.0 | 2.01 | 1.30 |

Four samples (-D1 = 0.44, -D2 = 0.23, -A1 = 0.51 borderline, -NT1 = 0.26) had 260/230 ratios at or below the ~0.5 threshold later used as one component of the inhibitor-flag rule for the H100 prep (§3.2.3). -D2 additionally had a low 260/280 (1.08) and the lowest concentration in the prep (4.6 ng/µL). The April 5 prep did not enter the inhibitor-flagging exercise — that rule was developed for the April 3 H100 prep used on April 21 / May 1 — but these per-sample observations are reported here for completeness alongside the Countess data in Table A.2.

## A.3 May 1 post-DNase NanoDrop re-measurement of the April 3 H100 prep

Before the May 1 RT-qPCR rerun, the April 3 H100 RNA samples were treated with TURBO DNase (TURBO DNA-free workflow), inactivated, centrifuged, and transferred to fresh tubes. NanoDrop concentrations and purity ratios were re-measured to support 10 ng/µL working-stock dilution and to verify that the DNase treatment had not introduced excessive degradation. The post-DNase concentrations, not the April 3 values, were used for preparing the equal-mass loading on the May 1 plate.

**Table A.4. May 1 post-DNase NanoDrop results for the April 3 H100 prep.**

| Sample | Conc. (ng/µL) | 260/280 | 260/230 |
|---|---|---|---|
| -A1 | 46.2 | 1.75 | 0.90 |
| +A1 | 89.8 | 1.94 | 1.73 |
| -A2 | 103.9 | 1.92 | 1.41 |
| +A2 | 91.5 | 1.93 | 0.96 |
| -B1 | 20.6 | 1.42 | 0.10 |
| +B1 | 63.2 | 1.85 | 1.00 |
| -B2 | 12.7 | 1.12 | 0.23 |
| +B2 | 52.5 | 1.77 | 1.08 |
| -D1 | 63.5 | 1.33 | 0.40 |
| +D1 | 104.3 | 1.97 | 1.35 |
| -D2 | 95.6 | 1.95 | 1.33 |
| +D2 | 56.0 | 1.88 | 1.15 |
| -NT1 | 69.4 | 1.90 | 1.28 |
| +NT1 | 69.9 | 1.89 | 1.00 |
| -NT2 | 94.4 | 1.93 | 1.39 |
| +NT2 | 95.1 | 1.89 | 1.27 |

Table A.5 compares the April 3 pre-DNase NanoDrop values with the May 1 post-DNase re-measurement. The comparison is included because the May 1 RT-qPCR interpretation used both NanoDrop purity and multi-target Cq behavior to identify inhibitor-affected samples.

**Table A.5. April 3 versus May 1 post-DNase NanoDrop comparison for the H100 RNA samples.**

| Sample | Apr 3 conc. (ng/µL) | Post-DNase conc. (ng/µL) | Apr 3 260/230 | Post-DNase 260/230 | QC note |
|---|---|---|---|---|---|
| -A1 | 56.3 | 46.2 | 1.52 | 0.90 | Lower post-DNase purity, but not flagged by May 1 Cq pattern |
| +A1 | 111.1 | 89.8 | 1.44 | 1.73 | Acceptable |
| -A2 | 69.7 | 103.9 | 1.03 | 1.41 | Acceptable |
| +A2 | 40.7 | 91.5 | 1.19 | 0.96 | Lower post-DNase purity, but not flagged by May 1 Cq pattern |
| -B1 | 21.8 | 20.6 | 0.10 | 0.10 | Persistent carryover; inhibitor-affected on May 1 |
| +B1 | 73.8 | 63.2 | 1.47 | 1.00 | Borderline post-DNase purity, but not flagged by May 1 Cq pattern |
| -B2 | 10.7 | 12.7 | 0.39 | 0.23 | Persistent/worsened carryover; inhibitor-affected on May 1 |
| +B2 | 62.9 | 52.5 | 1.60 | 1.08 | Not extreme by NanoDrop, but inhibitor-affected by May 1 Cq pattern |
| -D1 | 14.4 | 63.5 | 1.68 | 0.40 | New post-DNase carryover signal; inhibitor-affected on May 1 |
| +D1 | 126.9 | 104.3 | 1.90 | 1.35 | Acceptable |
| -D2 | 117.1 | 95.6 | 1.80 | 1.33 | Acceptable |
| +D2 | 67.9 | 56.0 | 1.68 | 1.15 | Acceptable |

| Sample | Apr 3 conc. (ng/µL) | Post-DNase conc. (ng/µL) | Apr 3 260/230 | Post-DNase 260/230 | QC note |
|---|---|---|---|---|---|
| -NT1 | 86.0 | 69.4 | 1.82 | 1.28 | Acceptable |
| +NT1 | 88.3 | 69.9 | 1.46 | 1.00 | Borderline post-DNase purity, but not flagged by May 1 Cq pattern |
| -NT2 | 67.2 | 94.4 | 1.91 | 1.39 | Acceptable |
| +NT2 | 118.9 | 95.1 | 1.80 | 1.27 | Acceptable |

Compared with the April 3 pre-DNase values, the post-DNase 260/280 and 260/230 ratios were generally lower, consistent with carryover from the DNase inactivation reagent or from residual salts after centrifugation. The -B1 and -B2 260/230 values remained low after DNase treatment, indicating that the original carryover from extraction had not been removed by the DNase workflow. -D1 also developed a low post-DNase 260/230 of 0.40, and +B2 was later flagged by its multi-target Cq pattern despite a less extreme 260/230 value of 1.08. These four samples were the inhibitor-affected wells identified on the May 1 RT-qPCR plate by simultaneous Cq suppression across MYC, B2M, and YWHAZ (§3.2.3).

Together, these RNA-preparation, Countess, and NanoDrop records define the sample-quality context used to interpret the RT-qPCR runs in Chapter 3.

# Appendix B. RT-qPCR plate layouts

This appendix shows the layouts of the three main 96-well RT-qPCR plates referenced in Chapter 3: the April 19 FACS-derived plate (§3.2.2), the April 21 H100 plate (§3.2.3), and the May 1 H100 DNase rerun (§3.2.3). The three earlier exploratory plates (March 27 H100, March 31 FACS-derived, April 1 guide-B equal-mass rerun) are listed in the six-run summary (Table 2.6, §2.9) but are intentionally excluded from this appendix because their MYC melt-window support was weak (<= 18.8 % of unknown MYC wells; Table 3.3) and they are treated as directional guide-prioritization runs rather than as magnitude-validating contrasts (§3.5); their raw plate-setup records are kept alongside the run folders in the project documentation. The same selection applies to Appendix C, which consolidates per-sample Cq values only for the three quantitative runs. Each plate is shown as a colored 8×12 plate-map figure followed by a compact sample-design table summarizing what was tested. Sample identifiers follow the convention used throughout the thesis: a leading minus or plus sign denotes the doxycycline/Shield-1 induction status (− dox or + dox); the next character (A, B, D, or NT) is the guide identity; the final digit indicates the biological replicate within that guide. In the plate-map figures, cell color encodes guide identity (orange = A, blue = B, green = D, gray = NT) with saturation encoding induction state (− dox pale, + dox saturated); control wells use distinct colors (NTC red, NRT salmon, Cas9 induction-check purple, OLD = April 21 RNA pale yellow). Cell text is the target abbreviation (M = MYC, Y = YWHAZ, B = B2M, C9 = Cas9) on the top line and the sample identity with induction sign on the bottom line.

## B.1 April 19, 2026 FACS-derived plate

RNA input: 8 ng per well. Targets: MYC and YWHAZ. Four-guide design (A, B, D, NT) with NT replicated four times (NT1, NT2, NT3, NT4) to give greater statistical weight to the non-targeting baseline.

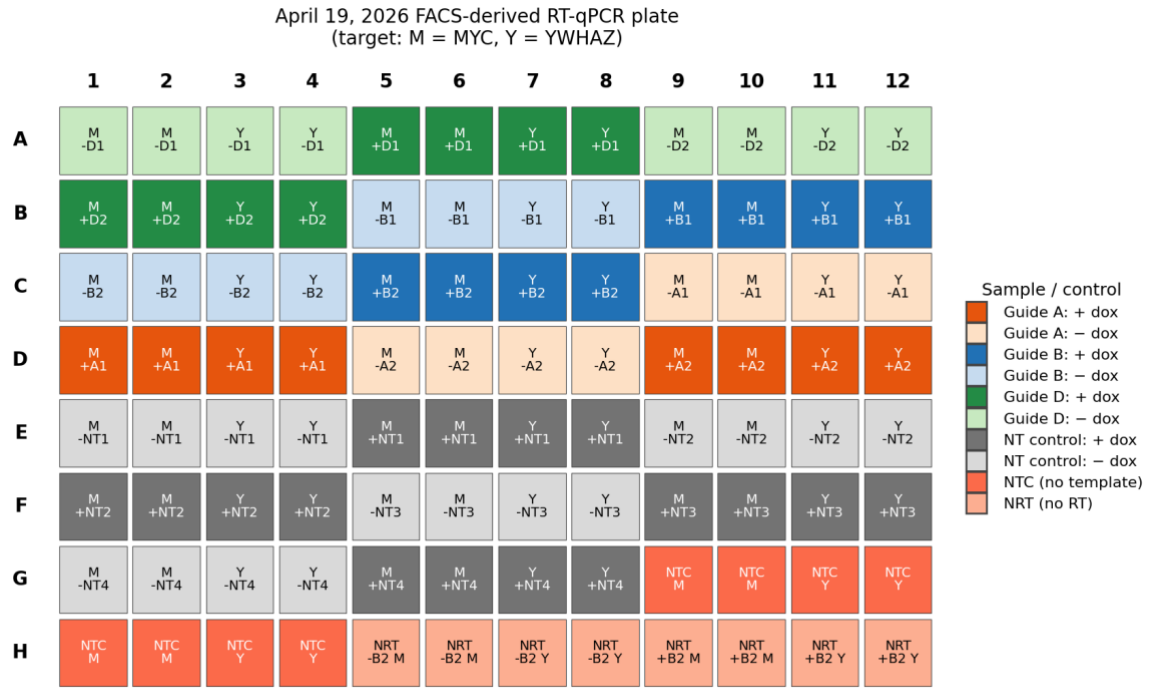


**Figure B.1.** April 19, 2026 FACS-derived RT-qPCR plate layout. Color encoding as described in the Appendix B introduction. NRT controls cover only the +B2 and −B2 conditions (rows G–H, columns 5–12).

**Table B.1. April 19 FACS-derived plate — sample design summary. Each sample-by-target combination is loaded in technical duplicate (two adjacent wells) unless otherwise noted.**

| Sample group | − dox | + dox | Targets (per condition) | NRT controls included |
|---|---|---|---|---|
| A1, A2 | ✓ | ✓ | MYC, YWHAZ | — |
| B1, B2 | ✓ | ✓ | MYC, YWHAZ | B2 only (MYC, YWHAZ; both ± dox) |
| D1, D2 | ✓ | ✓ | MYC, YWHAZ | — |
| NT1, NT2, NT3, NT4 | ✓ | ✓ | MYC, YWHAZ | — |
| NTC | n/a | n/a | MYC × 4 wells, YWHAZ × 4 wells | n/a |

## B.2 April 21, 2026 H100 plate

RNA input: 20 ng per well. Targets: MYC, YWHAZ, B2M, and Cas9. Four-guide design (A, B, D, NT) with each guide in two biological replicates and NT in two replicates. Cas9 wells were included on the right side of rows E–H as a platform-induction check.

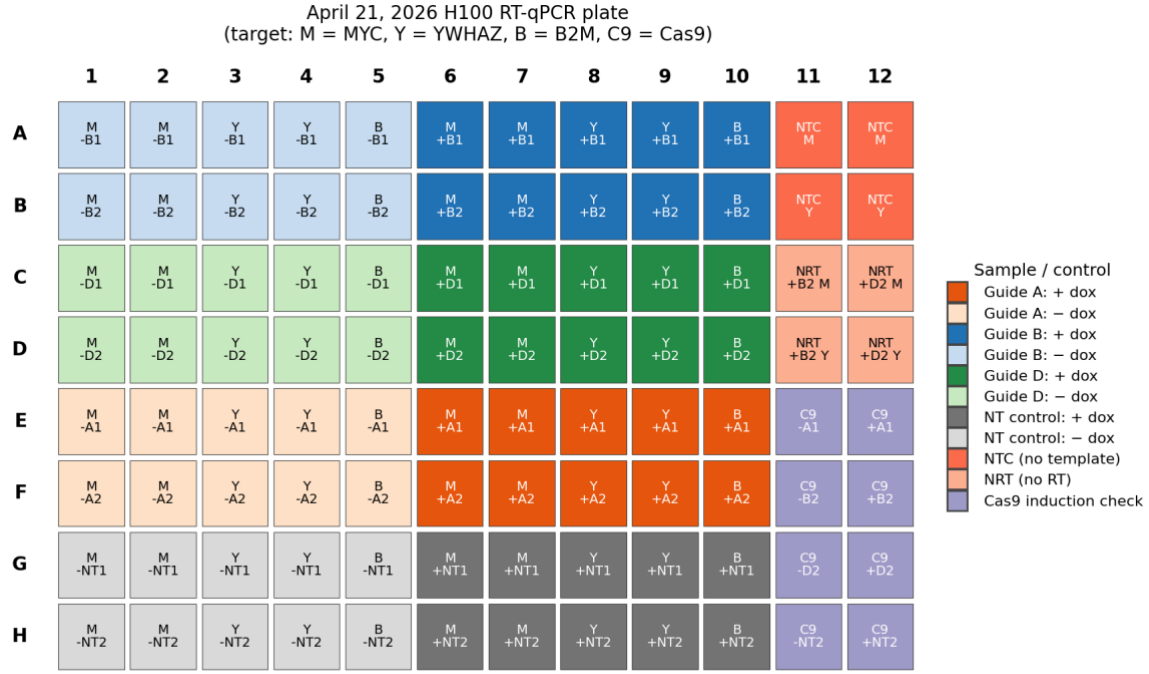


**Figure B.2.** April 21, 2026 H100 RT-qPCR plate layout. Color encoding as described in the Appendix B introduction. Right edge (columns 11–12) carries a mix of NTC, NRT, and Cas9 induction-check wells across rows; the colored cells make the irregular structure scannable at a glance.

**Table B.2. April 21 H100 plate — sample design summary. Each sample-by-target combination is loaded in technical duplicate (two adjacent wells) for MYC and YWHAZ, and as a single well for B2M.**

| Sample group | − dox | + dox | RT-qPCR targets | NRT controls included | Cas9 induction-check wells |
|---|---|---|---|---|---|
| A1, A2 | ✓ | ✓ | MYC (dup), YWHAZ (dup), B2M (single) | — | A1 only (− and +) |
| B1, B2 | ✓ | ✓ | MYC (dup), YWHAZ (dup), B2M (single) | B2 only (MYC, YWHAZ; + dox) | B2 only (− and +) |
| D1, D2 | ✓ | ✓ | MYC (dup), YWHAZ (dup), B2M (single) | D2 only (MYC, YWHAZ; + dox) | D2 only (− and +) |
| NT1, NT2 | ✓ | ✓ | MYC (dup), YWHAZ (dup), B2M (single) | — | NT2 only (− and +) |
| NTC | n/a | n/a | MYC × 2 wells, YWHAZ × 2 wells | n/a | — |

## B.3 May 1, 2026 H100 DNase rerun

RNA input: 20 ng per well. Targets: MYC, B2M, YWHAZ. The plate retained the April 21 four-guide H100 design but used DNase-treated RNA, a previously unopened NZYRT mix aliquot, and freshly diluted MYC, B2M, and YWHAZ primer working stocks. Wells

in column 11 (rows A–D) contained aliquots of the original (non-DNase-treated) April 21 RNA, run alongside the DNase-treated samples as the “OLD” control for separating NZYRT-mix effects from DNase-treatment effects (§3.2.3).

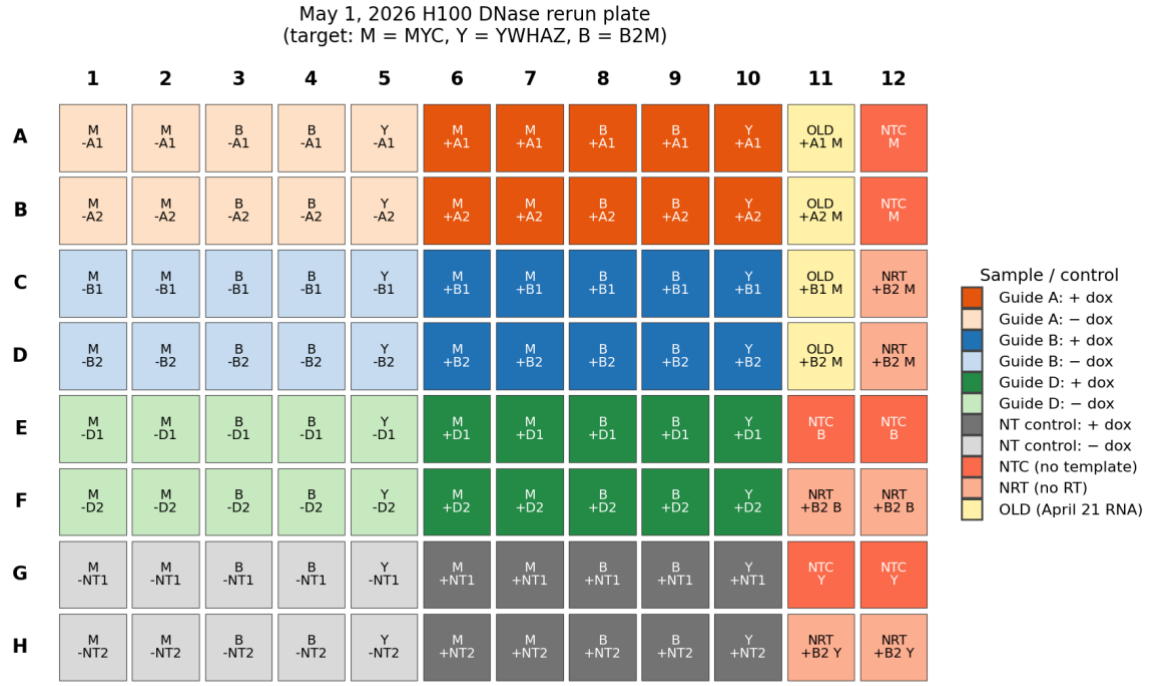


**Figure B.3.** May 1, 2026 H100 DNase rerun plate layout. Color encoding as described in the Appendix B introduction. OLD wells (pale yellow) in column 11, rows A–D, hold non-DNase-treated April 21 RNA and serve as the within-plate comparator for the NZYRT-vs-DNase contrast.

**Table B.3. May 1 H100 DNase rerun plate — sample design summary. Each sample-by-target combination is loaded in technical duplicate (two adjacent wells) for MYC and B2M, and as a single well for YWHAZ.**

| Sample group | − dox | + dox | RT-qPCR targets | NRT controls included | OLD wells (April 21 RNA, + dox MYC) |
|---|---|---|---|---|---|
| A1, A2 | ✓ | ✓ | MYC (dup), B2M (dup), YWHAZ (single) | — | A1, A2 |
| B1, B2 | ✓ | ✓ | MYC (dup), B2M (dup), YWHAZ (single) | B2 only (MYC, B2M, YWHAZ; + dox) | B1, B2 |
| D1, D2 | ✓ | ✓ | MYC (dup), B2M (dup), YWHAZ (single) | — | — |
| NT1, NT2 | ✓ | ✓ | MYC (dup), B2M (dup), YWHAZ (single) | — | — |
| NTC | n/a | n/a | MYC × 2 wells, B2M × 2 wells, YWHAZ × 2 wells | n/a | — |

Together, these plate-layout records document the physical RT-qPCR design underlying the main fold-change summaries and control interpretations in Chapter 3.

## Appendix C. Per-sample Cq tables

This appendix provides per-sample Cq summaries for the three RT-qPCR runs that carry the main quantitative interpretation in Chapter 3: April 19 FACS-derived (§3.2.2), April 21 H100 (§3.2.3), and May 1 H100 DNase rerun (§3.2.3). Cq values are the mean of technical replicates where available, with the technical-replicate standard deviation shown when both replicates produced a valid Cq. NaN denotes a well with no Cq called within 40 cycles. NRT and NTC controls are shown after the sample wells. Plate layouts for these runs are given in Appendix B; raw export files are stored alongside the run folders.

Two flagging conventions defined in Chapter 3 are summarized per run below each table to make the per-sample audit trail mechanical: (i) inhibitor-affected samples, identified by combined post-DNase 260/230 <= 0.5 and simultaneous Cq suppression across MYC, B2M, and YWHAZ (§3.2.3, Table 3.6), and (ii) MYC melt-window status, scored as a called melt peak inside the 88.5–90.5 °C MYC amplicon window in unknown MYC sample wells (§3.2.1, Table 3.3). NTC and NRT wells are flagged as in-window only when a called peak fell inside the same target window; otherwise their Cq values are treated as non-specific (§2.8).

## C.1 April 19, 2026 FACS-derived plate

Targets: MYC (89.0–89.5 °C melt) and YWHAZ (82 °C melt). RNA input: 8 ng per well.

**Table C.1. April 19 FACS-derived per-sample Cq summary.**

| Sample | MYC Cq mean | MYC SD | YWHAZ Cq mean | YWHAZ SD |
|---|---|---|---|---|
| -D1 | 31.08 | 0.04 | 26.04 | 0.02 |
| +D1 | 26.53 | 2.79 | 21.54 | 2.83 |
| -D2 | 28.76 | 0.35 | 26.59 | 0.02 |
| +D2 | 23.33 | 0.01 | 18.57 | 0.07 |
| -B1 | 24.18 | 0.12 | 20.21 | 0.08 |
| +B1 | 25.97 | 0.03 | 19.98 | 0.11 |
| -B2 | 24.29 | 0.14 | 20.48 | 0.14 |
| +B2 | 25.36 | 0.12 | 19.24 | 0.25 |
| -A1 | 26.34 | 0.16 | 20.32 | 0.03 |
| +A1 | 25.36 | 0.14 | 20.90 | 0.10 |
| -A2 | 25.79 | 0.60 | 19.38 | 0.21 |
| +A2 | 25.01 | 0.22 | 19.99 | 0.04 |
| -NT1 | 25.16 | 0.12 | 20.29 | 0.15 |
| +NT1 | 26.15 | 0.65 | 19.34 | 0.08 |
| -NT2 | 24.69 | 0.21 | 20.58 | 0.23 |
| +NT2 | 25.90 | 0.06 | 19.41 | 0.04 |
| -NT3 | 24.66 | 0.04 | 20.06 | 0.07 |
| +NT3 | 25.78 | 0.70 | 19.06 | 0.05 |
| -NT4 | 26.80 | 0.01 | 20.83 | 0.20 |
| +NT4 | 27.67 | 1.02 | 19.28 | 0.12 |
| MYC NTC | 33.40 | 0.40 | — | — |
| YWHAZ NTC | — | — | 33.07 | 2.12 |
| -B2 MYC NRT | 39.53 (n=1) | — | — | — |
| -B2 YWHAZ NRT | — | — | 25.59 | 0.04 |
| +B2 MYC NRT | 34.65 | 1.81 | — | — |
| +B2 YWHAZ NRT | — | — | 25.80 | 0.74 |

**Flag summary (C.1).** Inhibitor-affected samples: none on this plate (the April 19 prep did not enter the inhibitor-flagging exercise, which was developed for the April 3 H100 prep used on April 21 / May 1). MYC melt window: 37/40 unknown MYC sample wells inside the 88.5–90.5 °C window (Table 3.3); per-sample window assignment was uniformly inside across the 40 wells with the three excluded wells distributed across the panel (§3.2.2). MYC NTC was at Cq 33.40 outside the MYC window. YWHAZ NTC at Cq 33.07 was outside the YWHAZ window; -B2 YWHAZ NRT at Cq 25.59 and +B2 YWHAZ NRT at Cq 25.80 fell close to the YWHAZ sample window and limit YWHAZ-normalized interpretation for guide B in this run.

## C.2 April 21, 2026 H100 plate

Targets: MYC (no called melt peaks; see §3.2.1 and §3.2.3), YWHAZ (82–83.5 °C melt), B2M (80 °C melt), and Cas9 (83–84 °C melt). RNA input: 20 ng per well.

**Table C.2. April 21 H100 per-sample Cq summary.**

| Sample | MYC Cq mean | MYC SD | YWHAZ Cq mean | YWHAZ SD | B2M Cq | Cas9 Cq |
|---|---|---|---|---|---|---|
| -B1 | 36.77 | 4.01 | 24.71 | 0.08 | 17.61 | — |
| +B1 | 39.16 | 0.32 | 23.15 | 0.05 | 16.23 | — |
| -B2 | 34.14 | 0.50 | 22.76 | 0.03 | 16.84 | 21.44 |
| +B2 | 35.63 | 0.35 | 23.36 | 0.01 | 16.65 | 20.20 |
| -D1 | 34.63 | 0.52 | 24.06 | 0.01 | 18.04 | — |
| +D1 | 34.93 | 0.73 | 22.12 | 0.20 | 16.36 | — |
| -D2 | NaN | — | 22.69 | 0.07 | 16.27 | 22.33 |
| +D2 | 34.20 (n=1) | — | 23.19 | 0.51 | 16.63 | 20.22 |
| -A1 | 32.27 | 0.37 | 22.17 | 0.22 | 16.30 | 21.02 |
| +A1 | 34.92 | 0.82 | 22.69 | 0.19 | 16.21 | 19.80 |
| -A2 | 33.93 | 0.23 | 22.57 | 0.01 | 15.31 | — |
| +A2 | 37.34 (n=1) | — | 23.09 | 0.12 | 14.62 | — |
| -NT1 | 33.56 | 0.61 | 19.86 | 4.85 | 16.25 | — |
| +NT1 | 34.91 | 2.13 | 22.03 | 0.01 | 16.07 | — |
| -NT2 | 33.92 | 0.74 | 22.50 | 0.22 | 15.34 | 22.07 |
| +NT2 | 34.76 (n=1) | — | 22.19 | 0.03 | 16.00 | 19.42 |
| MYC NTC | 34.02 | 0.33 | — | — | — | — |
| +B2 MYC NRT | 31.91 (n=1) | — | — | — | — | — |
| +D2 MYC NRT | 31.00 (n=1) | — | — | — | — | — |
| +B2 YWHAZ NRT | — | — | 22.33 (n=1) | — | — | — |
| +D2 YWHAZ NRT | — | — | 22.34 (n=1) | — | — | — |

The G03 -NT1 YWHAZ well (Cq 16.43) was excluded as an outlier from the -NT1 YWHAZ summary because the matched G04 well (Cq 23.29) gave a Cq that fits the rest of the YWHAZ panel; the SD shown reflects the raw two-well spread before the outlier judgment. -D2_MYC failed in both replicates, and one replicate failed for +D2_MYC, +A2_MYC, and +NT2_MYC.

**Flag summary (C.2).** Inhibitor-affected samples: -B1 (pre-DNase 260/230 = 0.10) and -B2 (0.39) carried localized extraction-buffer carryover from the April 3 prep (Appendix A.1); on this plate the inhibitor effect manifested as late MYC Cq and failed melt peaks. The inhibitor-flagging rule was finalized after the May 1 rerun and is applied prospectively to the May 1 plate (Table C.3); the April 21 panel is reported

here for traceability. MYC melt window: 2/32 unknown MYC sample wells inside the 88.5–90.5 °C MYC amplicon window (Table 3.3); the failure was plate-wide and is interpreted as a run-level reverse-transcription / NRT-proximity limitation rather than per-sample biology (§3.2.1, §3.2.3). MYC NTC at Cq 34.02 was outside the MYC window. Both +B2 MYC NRT (Cq 31.91) and +D2 MYC NRT (Cq 31.00) sat close to the failing sample MYC Cq window and contribute to the run-level NRT-proximity concern.

## C.3 May 1, 2026 H100 DNase rerun

Targets: MYC (89.5 °C melt), B2M (80–80.5 °C melt), YWHAZ (82 °C melt). RNA input: 20 ng per well, prepared from DNase-treated April 3 H100 RNA. OLD wells contained aliquots of the same April 3 RNA without DNase treatment, run with the same fresh NZYRT and primers.

**Table C.3. May 1 H100 DNase rerun per-sample Cq summary.**

| Sample | MYC Cq mean | MYC SD | B2M Cq mean | B2M SD | YWHAZ Cq |
|---|---|---|---|---|---|
| -A1 | 24.82 | 0.65 | 23.44 | 0.34 | 21.51 |
| +A1 | 26.92 | 0.57 | 24.66 | 0.18 | 22.38 |
| -A2 | 24.36 | 0.73 | 23.32 | 0.19 | 22.10 |
| +A2 | 27.31 | 0.05 | 25.57 | 0.02 | 23.11 |
| -B1 | 28.02 | 0.25 | 26.51 | 0.07 | 25.16 |
| +B1 | 26.83 | 0.45 | 25.72 | 0.19 | 23.70 |
| -B2 | 27.54 | 0.03 | 23.48 | 0.04 | 22.05 |
| +B2 | 28.30 | 0.18 | 27.02 | 0.16 | 24.88 |
| -D1 | 30.39 | 0.37 | 26.20 | 0.17 | 24.78 |
| +D1 | 27.34 | 0.03 | 23.96 | 0.21 | 21.44 |
| -D2 | 24.98 | 0.77 | 23.56 | 0.20 | 22.30 |
| +D2 | 28.26 | 0.15 | 26.44 | 0.14 | 23.96 |
| -NT1 | 24.78 | 0.58 | 23.79 | 0.36 | 22.64 |
| +NT1 | 26.10 | 0.91 | 22.54 | 0.11 | 20.71 |
| -NT2 | 25.32 | 0.04 | 22.64 | 0.58 | 30.63 (outlier) |
| +NT2 | 27.07 | 0.03 | 21.85 | 1.58 | 20.66 |
| +A1 MYC OLD | 24.33 (n=1) | — | — | — | — |
| +A2 MYC OLD | 23.41 (n=1) | — | — | — | — |
| +B1 MYC OLD | 25.18 (n=1) | — | — | — | — |
| +B2 MYC OLD | 25.56 (n=1) | — | — | — | — |
| MYC NTC | 34.07 | 0.92 | — | — | — |
| B2M NTC | — | — | 32.42 | 0.01 | — |
| YWHAZ NTC | — | — | — | — | 34.20 (mean) |
| +B2 MYC NRT | NaN | — | — | — | — |
| +B2 B2M NRT | — | — | 29.86 | 1.29 | — |
| +B2 YWHAZ NRT | — | — | — | — | 36.00 (mean) |

Inhibitor-affected samples (-B1, -B2, +B2, -D1; §3.2.3, Appendix A.3) show simultaneous Cq suppression across MYC, B2M, and YWHAZ. The -NT2 YWHAZ well at Cq 30.63 was excluded from interpretation as an outlier; +NT2 YWHAZ at Cq 20.66 was used. MYC NRT was undetermined for +B2, confirming effective DNase-mediated removal of gDNA-derived signal in the MYC channel. YWHAZ NRT shifted from approximately Cq 22 on April 21 to Cq 36 on May 1 for the +B2 sample.

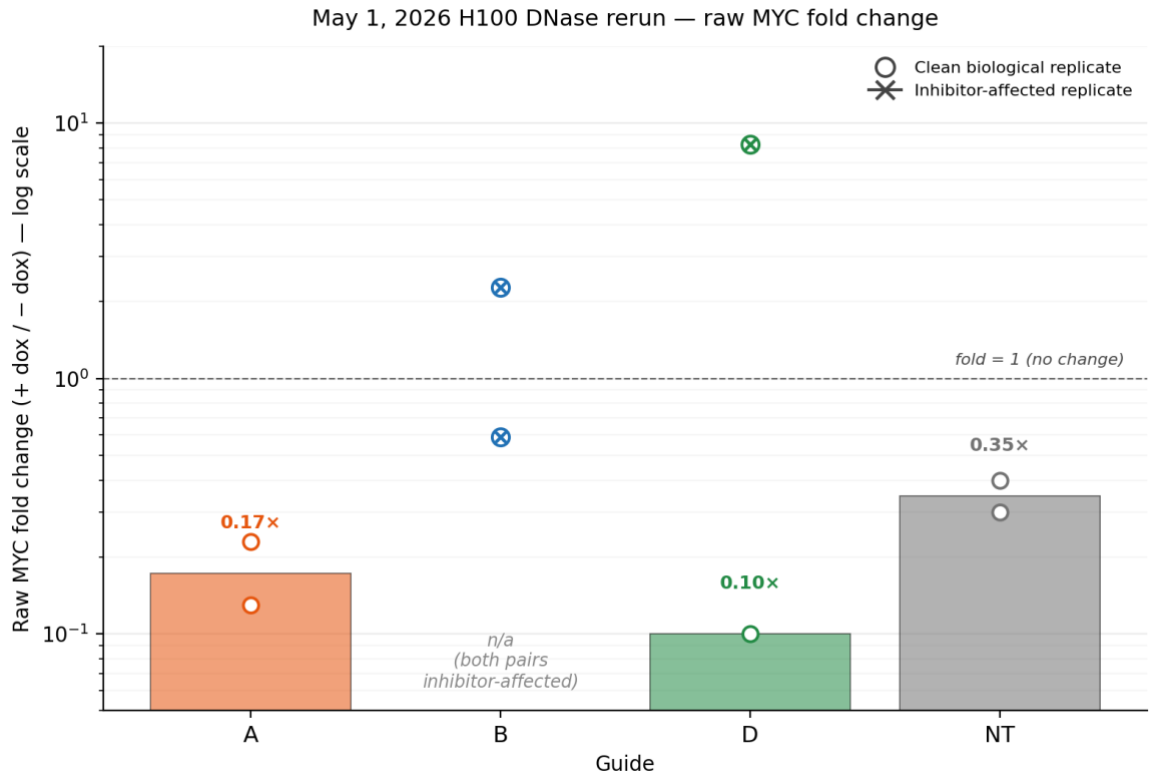


**Figure C.1.** Raw MYC fold change in the May 1, 2026 H100 DNase rerun (directional readout for §3.2.3 because NT reference-gene shifts made normalized values non-specific). Fold change was calculated as +dox/−dox from raw MYC Cq values and plotted on a log y-axis; values below 1 indicate lower MYC in the induced condition. Bars show guide-level geometric means computed from non-flagged biological replicates only, and the dashed line marks fold change = 1. Open circles show individual biological replicate pairs (A1/A2, B1/B2, D1/D2, NT1/NT2). Replicates marked with an X were inhibitor-affected (B1, B2, and D1; Table 3.6) and excluded from the geometric means. Guide B is shown as “n/a” because both B replicate pairs were inhibitor-affected; guide D is represented by D2 alone.

**Flag summary (C.3).** Inhibitor-affected samples were identified using the combined 260/230 <= 0.5 and multi-target Cq suppression rule described in §3.2.3. The affected samples were −B1, −B2, −D1, and +B2. These four samples were excluded from the clean-pair interpretation in §3.2.3 and from the geometric means in Figure C.1. MYC melt window: 27/32 unknown MYC sample wells inside the 89.5 °C MYC window by manual derivative-curve review (CFX auto-call returned no peaks on this plate; Table 3.3). The five sample wells without called peaks at the auto-detection threshold (-B1, +B2, and one -D1 replicate; §3.2.3) correspond to the inhibitor-

affected samples, and manual inspection of the raw melt curves confirmed subthreshold 89.5 °C peaks rather than absent product. MYC NTC at Cq 34.07 was outside the MYC window with a 79 °C primer-dimer-like peak. +B2 MYC NRT was undetermined (effective DNase removal of gDNA-derived MYC signal); +B2 B2M NRT and +B2 YWHAZ NRT are documented above as cycle-shifted ~14 cycles from the April 21 plate.

**OLD-wells attribution analysis (C.3).** The May 1 plate included four control wells (+A1, +A2, +B1, +B2; wells A11–D11) loaded with the same April 21 RNA aliquots but without DNase treatment, run with the fresh NZYRT and freshly diluted primers used elsewhere on the May 1 plate. These OLD wells separate the contributions of NZYRT freshness and DNase treatment to the April 21-to-May 1 MYC Cq recovery. The four OLD-well MYC Cq values (24.3, 23.4, 25.2, 25.6 for +A1, +A2, +B1, +B2) were approximately 10–14 cycles earlier than the matched April 21 wells (34.9, 37.3, 39.2, 35.6) and approximately 2–3 Cq earlier than the matched DNase-treated May 1 wells. This pattern is most consistent with fresh NZYRT activity as the main contributor to the April 21-to-May 1 MYC recovery, with DNase treatment providing the expected separate effect of removing gDNA-derived signal from the cDNA-specific readout. The per-sample comparison is given in Table C.4.

**Table C.4. May 1 OLD-well comparison for MYC Cq recovery.** OLD wells used April 21 RNA aliquots without DNase treatment, run on the May 1 plate with fresh NZYRT. April 21 values are the corresponding MYC Cq values for the same samples on the April 21 run.

| Sample | April 21 MYC Cq | May 1 OLD-well MYC Cq | Change |
|---|---|---|---|
| +A1 | 34.9 | 24.3 | ~10.6 Cq earlier |
| +A2 | 37.3 | 23.4 | ~13.9 Cq earlier |
| +B1 | 39.2 | 25.2 | ~14.0 Cq earlier |
| +B2 | 35.6 | 25.6 | ~10.0 Cq earlier |

Together, these per-sample Cq summaries provide the audit trail behind the RT-qPCR fold-change interpretations, melt-support assessments, and inhibitor/control-behavior flags used in Chapter 3.

# Appendix D. ChIP-qPCR plate layouts and Cq summaries

This appendix supports §3.3 by documenting the ChIP-qPCR plate layouts and the per-condition mean Cq values that underlie the percent-input summaries reported in Tables 3.10 and 3.11. The main results focus on interpreted readouts (percent input and guide-level occupancy conclusion), while this appendix records the physical qPCR layout, upstream Cq numbers, curve-review plots, chemistry side comparison, and gel check so a reader can audit the negative ChIP-qPCR conclusion. Two separate ChIP runs were carried out as direct guide-versus-control occupancy tests (April 30 and May 6); the earlier April 20 run was an IP-optimization plate and its underlying Cq values are already reported as Table 3.8 in §3.3. Mean Cq is given as mean±population SD across technical triplicates; CTCF % input is recomputed from the same mean Cq values via the formula in §2.10 (`%input = 100 × 2^(Cq_input − log2(100) − Cq_IP)`) and matches Tables 3.10 / 3.11 within rounding except where noted.

Per-sample post-cleanup NanoDrop measurements were also recorded for the April 28 B/NT2 and May 5 A/D/NT3 chromatin preps (project documentation), but are not tabulated here because percent input was calculated from matched input/IP Cq values rather than from NanoDrop-based DNA mass, and NanoDrop measurements on ChIP DNA showed low 260/230 ratios consistent with cleanup-buffer carryover (§3.3). The NanoDrop records are retained as documentation of DNA recovery only.

## D.1 ChIP-qPCR run designs

**Table D.1. ChIP-qPCR run designs across the thesis.** The same crosslinking/IP/qPCR protocol (§2.10) was used in all three runs. The April 30 and May 6 runs were the two direct guide-versus-control occupancy tests; the earlier April 20 run was an IP-optimization plate.

| Run | Purpose | Conditions | IP fractions per condition | qPCR assays | Reference |
|---|---|---|---|---|---|
| April 20 | IP optimization on shared HCT116-derived chromatin | single chromatin pool | 1% input, anti-CTCF IP, IgG IP, anti-Pol II IP (GAPDH only) | `mycP_CTCF`, `OSE_CTCF`, `negC_CTCF`, `GAPDH` | Tables 3.8, 3.9; Figure 3.8; Figure D.1 |
| April 30 | B / NT2 occupancy test | B−, B+, NT2−, NT2+ | 1% input, anti-CTCF IP, IgG IP | `mycP_CTCF`, `negC_CTCF` | Table 3.10; Figure D.2; Figures D.5-D.6; Table D.2 |
| May 6 | A / D / NT3 occupancy test (separate plates per assay) | A−, A+, D−, D+, NT3−, NT3+ | 1% input, anti-CTCF IP, IgG IP | `mycP_CTCF` (separate plate); `OSE_CTCF` (separate plate) | Table 3.11; Figure 3.10; Figures D.3-D.4; Figures D.7-D.9; Table D.3 |

## D.2 ChIP-qPCR plate layouts

The plate maps below use the same convention across ChIP-qPCR runs: blue marks input DNA, green marks anti-CTCF IP, orange marks IgG IP, purple marks the anti-Pol II IP used only for the April 20 GAPDH control, and red marks no-template controls. The top line inside each well gives the assay/fraction, and the second line gives the condition where applicable. Empty wells were not used in the exported CFX qPCR run.

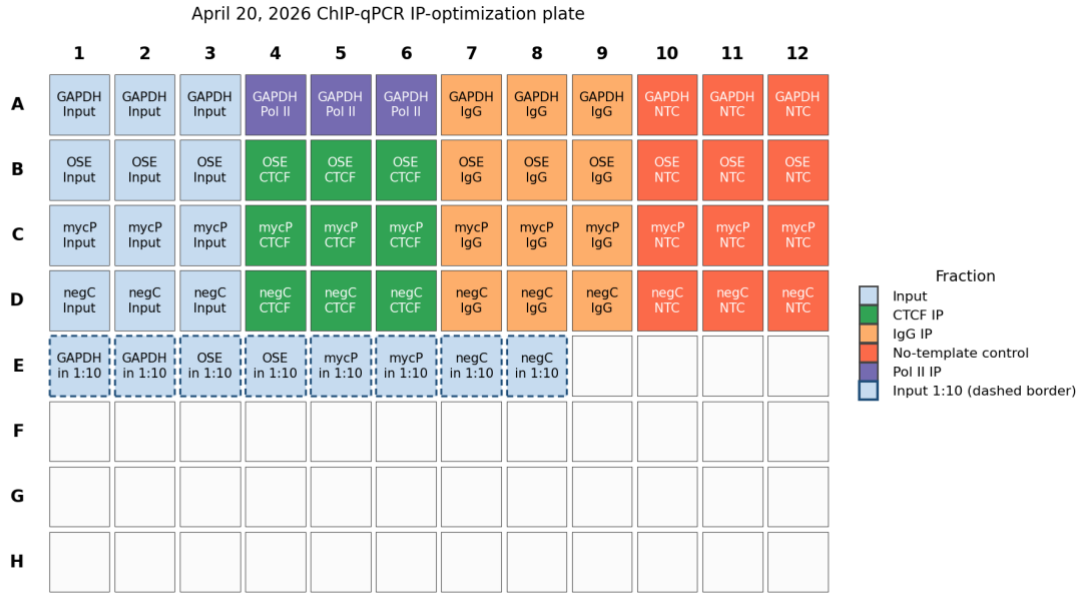


**Figure D.1.** April 20, 2026 ChIP-qPCR IP-optimization plate. The plate tested one shared chromatin pool across GAPDH, `OSE_CTCF`, `mycP_CTCF`, and `negC_CTCF`, with input, antibody IP, IgG, and water controls. This was an assay/IP-validation plate rather than a guide-versus-control occupancy test.


**Figure D.2.** April 30, 2026 B / NT2 ChIP-qPCR occupancy plate. Rows A-C carry the interpretable `mycP_CTCF` assay for B−, B+, NT2−, and NT2+ across input, CTCF IP, IgG IP, and NTC wells. Rows E-H carry the `negC_CTCF` assay, which was retained for traceability but excluded from interpretation because sample and NTC behavior overlapped.

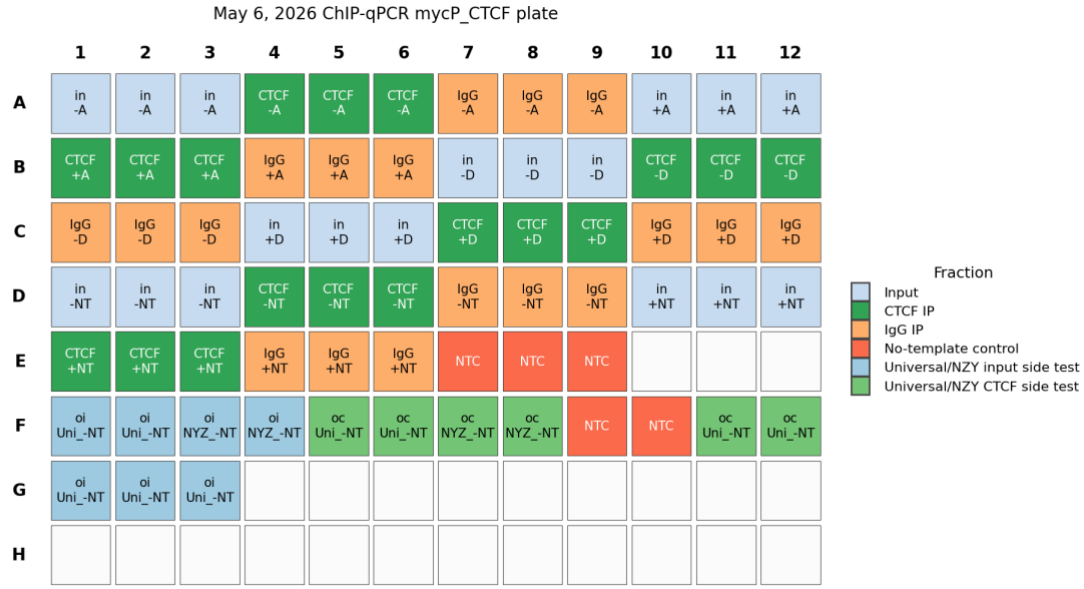


**Figure D.3.** May 6, 2026 `mycP_CTCF` ChIP-qPCR plate. Rows A-E carry the A/D/NT3 occupancy test. Rows F-G contain the Universal-versus-NZY side comparison for the same promoter-proximal amplicon; these wells were used for chemistry comparison and not for the main A/D/NT3 percent-input interpretation.

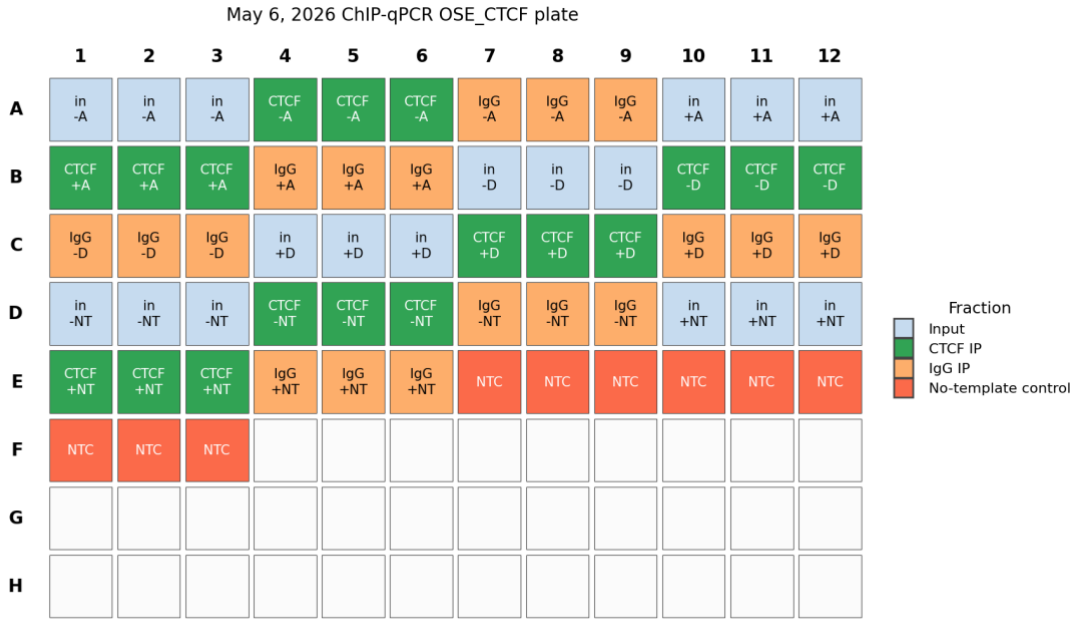


**Figure D.4.** May 6, 2026 OSE_CTCF ChIP-qPCR plate. Rows A-E carry the A/D/NT3 occupancy test at the distal OSE-associated CTCF region, with additional NTC wells in rows E-F. This plate was technically cleaner than the May 6 promoter-proximal plate and is the main basis for the guide-D/NT3-adjusted distal-occupancy interpretation.

## D.3 April 30 ChIP-qPCR mean Cq summary

**Table D.2. April 30 B/NT2 ChIP-qPCR mean Cq values per condition.** Mean Cq±SD across technical triplicates (n=3 throughout) for each condition × assay × IP fraction, with NTC behavior summarized at the assay level (mean Cq across detected NTC wells, with detected/total). CTCF % input is recomputed from the mean Cq values shown in this table; the corresponding interpreted summary is in Table 3.10. The NT2+ row reproduces the "raw" NT2+ mean that includes the C04 outlier (Cq 30.19 in the input wells). Table 3.10 reports a corrected NT2+ value (4.94% input) computed from the C05/C06 input mean alone (per the C04-outlier note under that table); the 10.31% value here is the raw uncorrected mean for traceability and is not the value used in §3.3. The negC_CTCF rows are shown for completeness only: across all four conditions, neither the sample wells nor the eight NTC wells produced an accepted melt peak, so the listed % input values do not reflect specific PCR product (see §3.3 and Figures D.5-D.6).

| Condition | Assay | Input mean Cq | CTCF IP mean Cq | IgG mean Cq | NTC behavior | CTCF % input |
|---|---|---|---|---|---|---|
| B- | mycP_CTCF | 27.99±0.13 | 25.43±0.01 | 26.16±0.06 | undetected (6/6) | 5.91% |
| B- | negC_CTCF | 24.45±0.14 | 24.43±0.06 | 24.42±0.06 | Cq 23.96 (8/8 det.) | 1.02% |
| B+ | mycP_CTCF | 28.28±0.10 | 25.78±0.03 | 27.98±0.06 | undetected (6/6) | 5.66% |
| B+ | negC_CTCF | 24.30±0.05 | 24.47±0.12 | 24.30±0.07 | Cq 23.96 (8/8 det.) | 0.89% |
| NT2- | mycP_CTCF | 26.45±0.11 | 23.95±0.09 | 29.55±0.01 | undetected (6/6) | 5.65% |

| Condition | Assay | Input mean Cq | CTCF IP mean Cq | IgG mean Cq | NTC behavior | CTCF % input |
|---|---|---|---|---|---|---|
| NT2- | negC_CTCF | 24.33±0.06 | 24.28±0.09 | 24.24±0.11 | Cq 23.96 (8/8 det.) | 1.03% |
| NT2+ | mycP_CTCF | 28.06±1.50 | 24.69±0.05 | 27.26±0.08 | undetected (6/6) | 10.31% (raw; see caption) |
| NT2+ | negC_CTCF | 24.15±0.12 | 22.94±1.87 | 21.28±2.85 | Cq 23.96 (8/8 det.) | 2.30% |

## D.4 May 6 ChIP-qPCR mean Cq summary

**Table D.3. May 6 A/D/NT3 ChIP-qPCR mean Cq values per condition.** The May 6 run was split across two qPCR plates: mycP_CTCF was run on one plate and OSE_CTCF on a separate plate, each carrying its own NTC wells. Mean Cq±SD is reported across technical triplicates (n=3 throughout) per condition × assay × IP fraction, with NTC behavior summarized at the assay level. CTCF % input is recomputed from the mean Cq values shown here and reproduces Table 3.11 within rounding. The mycP_CTCF plate had three NTC wells, all of which produced weak expected-temperature signal at Cq ~33-36 (not undetected, but well below the sample Cq window of ~25-29); the OSE_CTCF plate had nine NTC wells, of which five produced amplification at Cq ~39.4-39.9, near the assay detection floor and well above the sample Cq window of ~28-30 (see §3.3 and Figure D.7).

| Assay | Condition | Input mean Cq | CTCF IP mean Cq | IgG mean Cq | NTC behavior | CTCF % input |
|---|---|---|---|---|---|---|
| mycP_CTCF | A- | 28.77±0.22 | 27.35±0.31 | 31.57±0.16 | Cq 35.20 (3/3 det.) | 2.69% |
| mycP_CTCF | A+ | 28.99±0.10 | 26.67±0.37 | 31.08±0.14 | Cq 35.20 (3/3 det.) | 4.98% |
| mycP_CTCF | D- | 29.38±0.12 | 27.56±0.08 | 33.30±0.39 | Cq 35.20 (3/3 det.) | 3.55% |
| mycP_CTCF | D+ | 29.15±0.15 | 26.46±0.04 | 31.08±0.10 | Cq 35.20 (3/3 det.) | 6.45% |
| mycP_CTCF | NT3- | 29.52±0.33 | 27.22±0.30 | 32.36±0.22 | Cq 35.20 (3/3 det.) | 4.92% |
| mycP_CTCF | NT3+ | 28.34±0.10 | 25.50±0.07 | 30.91±0.22 | Cq 35.20 (3/3 det.) | 7.16% |
| OSE_CTCF | A- | 29.71±0.12 | 29.46±0.09 | 32.39±0.05 | Cq 39.64 (5/9 det.) | 1.19% |
| OSE_CTCF | A+ | 29.80±0.15 | 29.69±0.06 | 32.41±0.09 | Cq 39.64 (5/9 det.) | 1.08% |
| OSE_CTCF | D- | 30.40±0.05 | 30.03±0.05 | 34.23±0.40 | Cq 39.64 (5/9 det.) | 1.29% |
| OSE_CTCF | D+ | 30.02±0.00 | 28.97±0.07 | 31.79±0.09 | Cq 39.64 (5/9 det.) | 2.07% |
| OSE_CTCF | NT3- | 30.04±0.23 | 29.62±0.13 | 33.40±0.21 | Cq 39.64 (5/9 det.) | 1.34% |
| OSE_CTCF | NT3+ | 29.44±0.04 | 28.34±0.06 | 31.78±0.08 | Cq 39.64 (5/9 det.) | 2.14% |

## D.5 ChIP-qPCR curve, chemistry, and gel QC

The detailed ChIP-qPCR QC plots below support the assay-level statements in §3.3 while keeping raw curve review out of the main Results narrative.

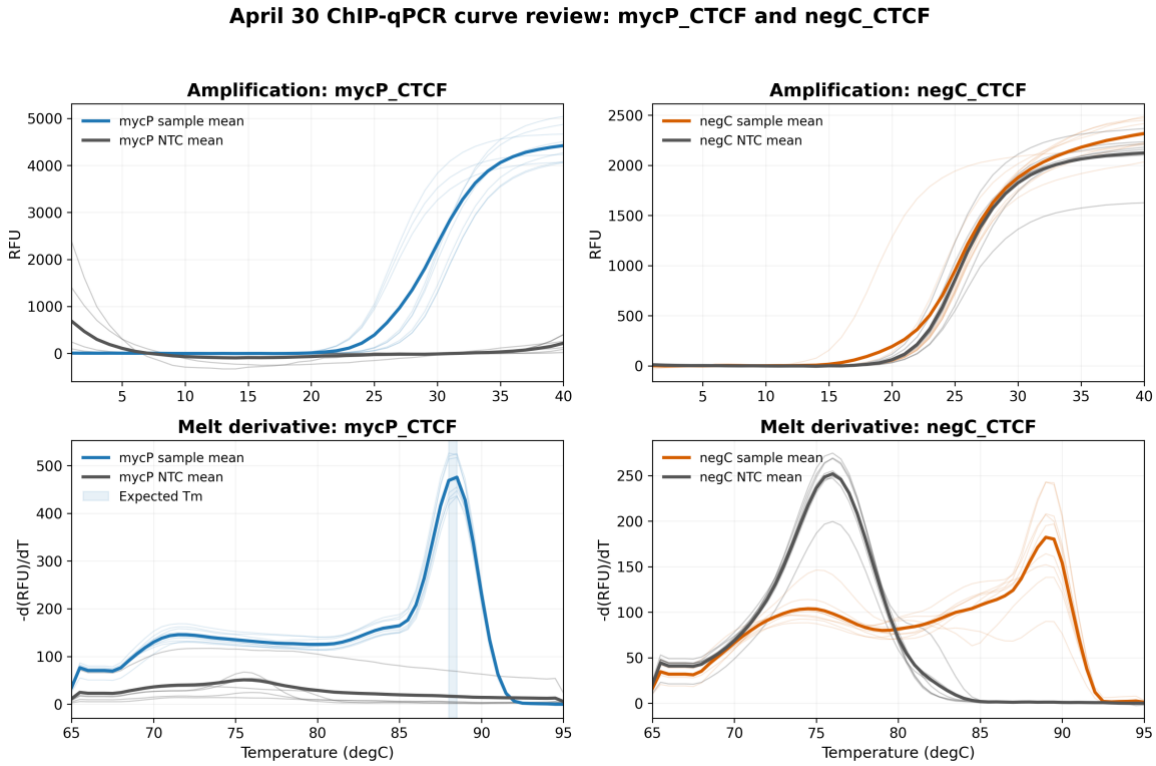


**Figure D.5.** Raw curve review for the April 30 ChIP-qPCR run. Amplification and melt-derivative traces are shown for the mycP_CTCF assay and the negC_CTCF negative-region assay, with sample and NTC traces plotted separately.

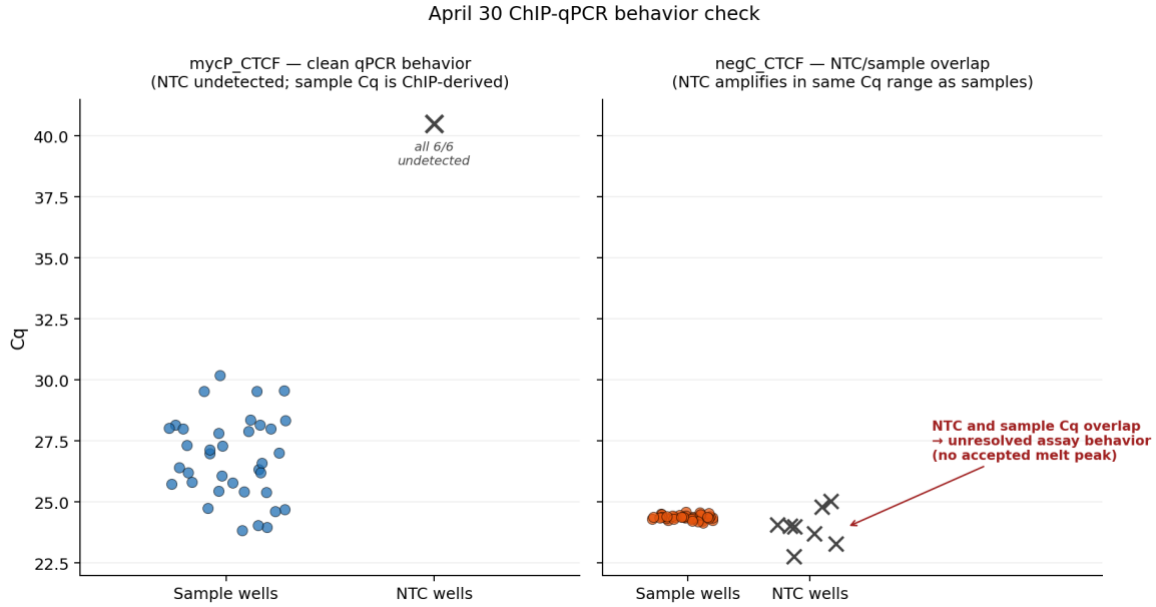


**Figure D.6.** April 30 ChIP-qPCR per-well Cq distributions for mycP_CTCF and negC_CTCF. Sample wells and NTC wells are plotted separately; X markers indicate undetected wells.

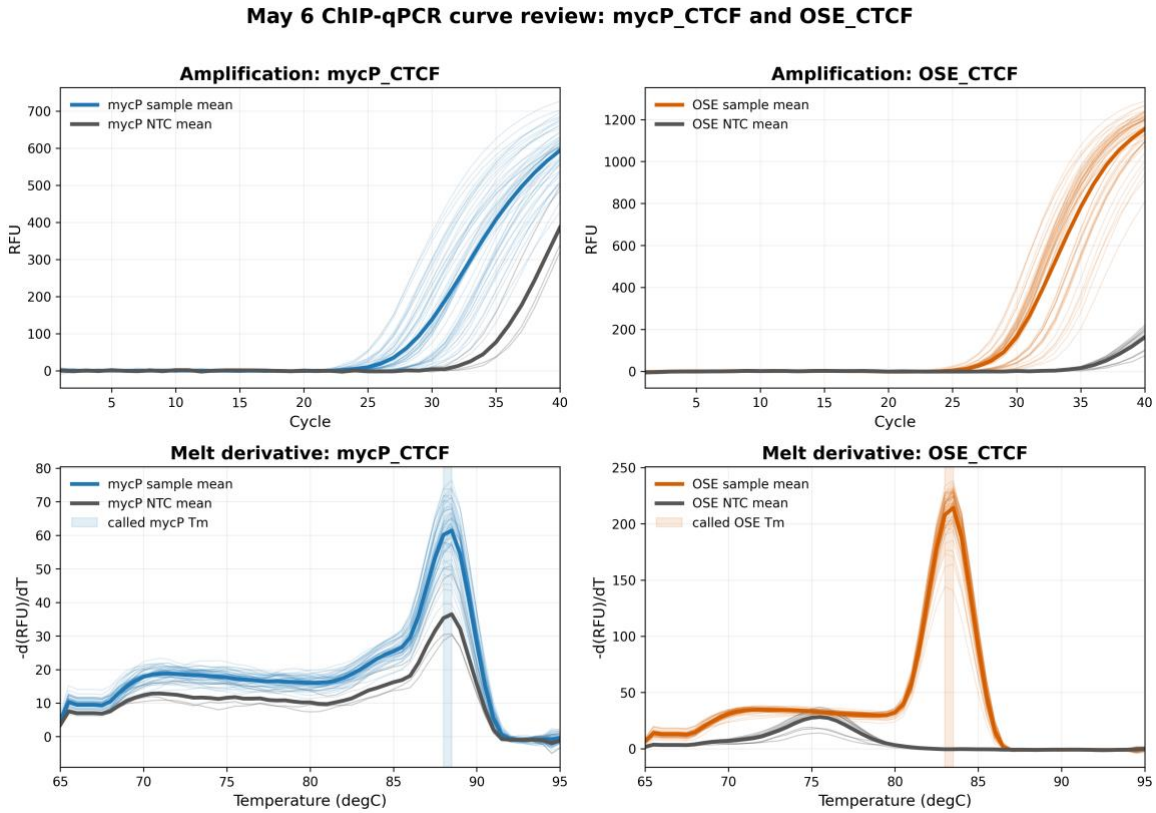


**Figure D.7.** May 6 ChIP-qPCR curve review for `mycP_CTCF` and `OSE_CTCF`. Amplification traces are shown above and melt-derivative traces below. Thin lines show individual sample or NTC wells, thick lines show the corresponding mean traces, and shaded regions mark the expected product melt-temperature windows.

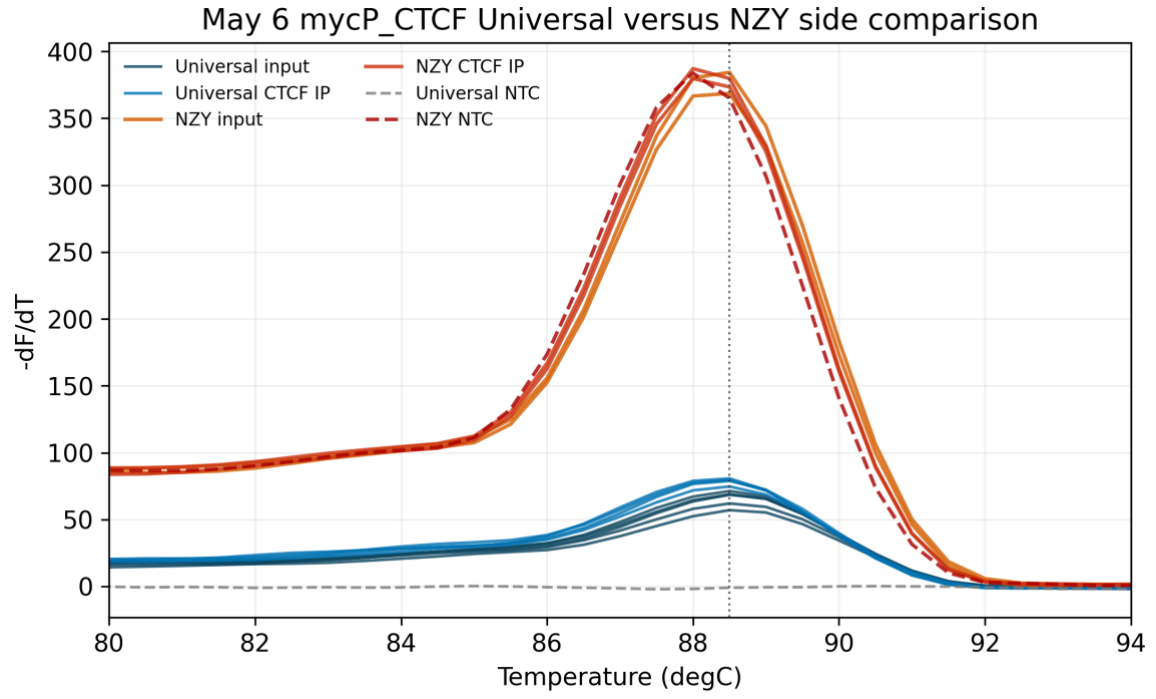


**Figure D.8.** May 6 `mycP_CTCF` Universal/NZY chemistry side comparison using April 30 -NT material. Curves show melt-derivative traces for April 30 input DNA, April 30 CTCF IP DNA, and no-template controls amplified with Universal or NZY chemistry.

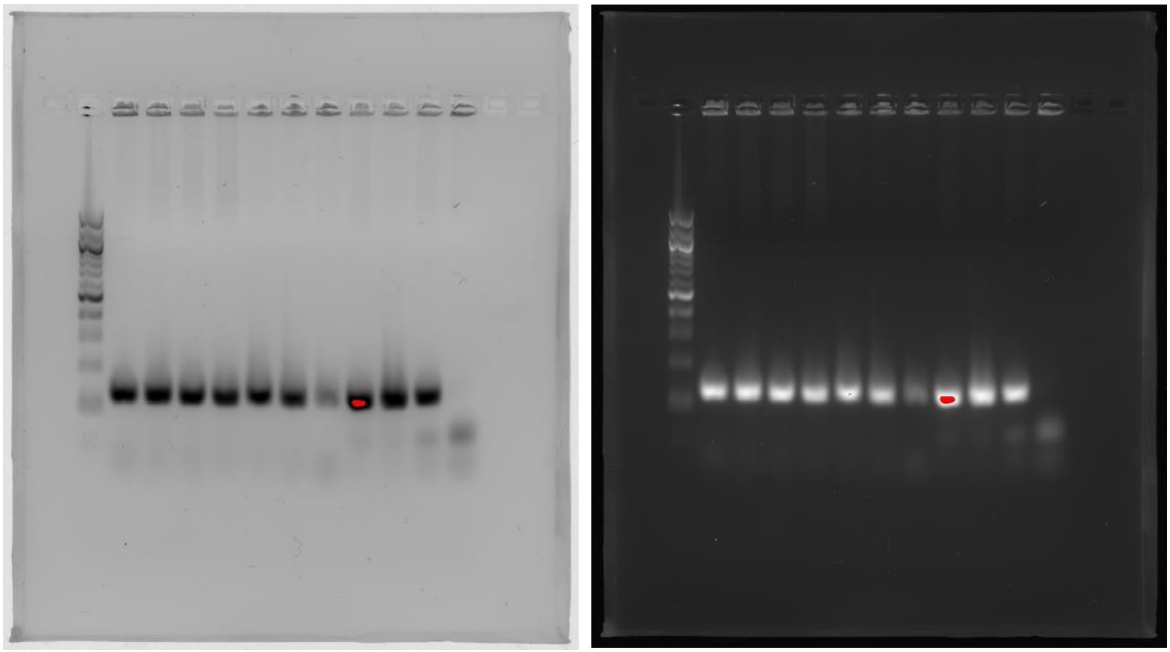

**Figure D.9.** Agarose gel verification of selected May 6 ChIP-qPCR products. The same gel is shown under two transilluminator settings: white-background acquisition (left) and dark-background acquisition (right). Lane 1 shows a NEB 100 bp ladder. Lanes 2-8 show mycP_CTCF qPCR products from input, A- CTCF IP, A+ CTCF IP, NT3- CTCF IP, NT3+ CTCF IP, IgG, and NTC material. Lanes 9-12 show OSE_CTCF qPCR products from input, CTCF IP, IgG, and NTC material. The expected product sizes were approximately 131 bp for the promoter-proximal assay and 143 bp for the distal OSE assay.

## D.6 ChIP-qPCR interpretation checkpoints

**Table D.4. Practical interpretation checkpoints for the ChIP-qPCR series.** This table summarizes which parts of the ChIP-qPCR series were interpretable and which remained developmental or control-limited.

| Run | Interpretable material | Main limitation | Consequence for thesis interpretation |
|---|---|---|---|
| April 20 IP optimization | mycP_CTCF showed strong CTCF enrichment over IgG; OSE_CTCF showed weaker but detectable enrichment. | GAPDH/Pol II and negC_CTCF controls failed, so this run validates the CTCF target assays only partly. | Supports moving to direct occupancy tests, but does not by itself test guide-dependent CTCF loss. |
| April 30 B / NT2 | mycP_CTCF behaved cleanly, with B+ close to B− and NT2 controls. | negC_CTCF failed and IgG background was variable. | No bulk-detectable B-specific CTCF depletion was observed at the promoter-proximal assay in this single run. |
| May 6 A / D / NT3 | OSE_CTCF was the cleanest A/D/NT3 readout; mycP_CTCF was still usable but had weak NTC features. | The +dox shift at OSE occurred similarly for D and NT3, and the promoter plate had weak NTC amplification. | No guide-specific A or D CTCF depletion was detected; direct dCas9 ChIP-qPCR remains the decisive next occupancy experiment. |

**Practical limit of detection across the guide-versus-control runs.** Each of the April 30 and May 6 follow-ups represents a single biological IP per condition read out in technical triplicate qPCR wells, so the resolving power of the series is bounded by between-condition technical variation rather than by within-triplicate variance. The matched −dox `mycP_CTCF` percent input across all four guide/control conditions (B− 5.91% from April 30; A− 2.69%, D− 3.55%, NT3− 4.92% from May 6) spans more than two-fold even before induction, and the matched −/+ input mean Cq values in Table D.3 shift by ≈ 0.4–0.6 cycles between paired conditions at `0SE_CTCF`. Taken together, these baseline shifts place the practical limit of detection for guide-specific CTCF loss at approximately a two-fold percent-input reduction at the mapped target assay (§3.3). The negative occupancy results therefore do not support a strong (≥2×) bulk CTCF eviction at `mycP_CTCF` for guides A/B or at `0SE_CTCF` for guide D under the tested conditions, but they do not exclude smaller, partial, transient, or cell-heterogeneous occupancy changes. Recovering finer occupancy resolution would require biological replicate IPs per condition (>=3 independent chromatin preparations), a working negative-region assay to anchor IgG/non-specific drift, and ideally a quantitative spike-in normalization to control between-condition input-Cq shifts.

## D.7 Reverse-crosslinking and DNA-cleanup protocol

This section gives the full procedural detail referenced from §2.10.3. For all samples (IP eluates and matched 10 % inputs, the latter brought to 150 µL by adding 1× IP Elution Buffer), reverse crosslinking was performed by adding 6 µL 5 M NaCl and 2 µL Proteinase K and incubating at 65 °C for 1.5 h. DNA was purified using the Pierce kit's DNA cleanup columns: 750 µL DNA Binding Buffer per sample loaded onto the column, washed with 750 µL DNA Column Wash Buffer, dried by centrifugation, and eluted in 50 µL DNA Column Elution Solution. Purified DNA was stored at −20 °C.

Together, these ChIP-qPCR supporting data define which occupancy conclusions are supported by the present assays and why direct dCas9 ChIP-qPCR remains the decisive next experiment.

# Appendix E — Full sgRNA Sanger-sequencing summary

## E.1 Per-clone Sanger trace

This appendix gives the full per-clone Sanger summary referenced in §2.3.4 / Table 2.1. It includes the constructs taken forward to mammalian-cell work, the additional sequence-confirmed clones that were not selected as the downstream representative, and the excluded or unreadable clones (including the 2025 first-batch entries that were later rescued by replating).

**Table E.1. Full per-clone Sanger summary for the sgRNA clones screened during this work (Eurofins LightRun service).** "Origin" distinguishes 2025 first-batch clones, replated 2026 colonies, and fresh 2026 clones. "Status" indicates whether each clone was used downstream, sequence-confirmed but not selected, discarded, or unreadable. The compact summary of constructs taken forward is given in Table 2.1. NanoDrop values were transcribed from the handwritten Eurofins LightRun submission records. Because some clone labels were reused between batches, entries are distinguished by both clone label and LightRun sequence ID.

| Guide | Clone | Origin | LightRun Seq. ID | Concentration | A260/280 | A260/230 | Status |
|---|---|---|---|---|---|---|---|
| A | A4 | Replated 2026 colony from 2025 batch | JTJ522 | 3879.5 ng/µL | 1.89 | 2.22 | Used downstream (sequence-confirmed) |
| B | B2 | 2026 cloning | JTJ512 | 365.0 ng/µL | 1.94 | 2.15 | Used downstream |
| D | D1 | 2026 cloning | JTJ519 | 2687.0 ng/µL | 1.92 | 2.25 | Used downstream |
| NT | NT2 | 2026 cloning | JTJ523 | 4137.0 ng/µL | 1.90 | 2.21 | Used downstream |
| NT | NT3 | 2026 cloning | JTJ524 | 1883.3 ng/µL | 1.93 | 2.28 | Used downstream |
| A | A1 | 2026 cloning (new) | JTJ525 | 1346.2 ng/µL | 1.96 | 2.28 | Sequence-confirmed but not selected (A4 used downstream) |
| A | A3 | Replated 2026 colony from 2025 batch | JTJ527 | 35.1 ng/µL | 2.10 | 2.05 | Sequence-confirmed but not selected (A4 used downstream) |
| A | A2 | 2026 cloning (new) | JTJ526 | 2229.5 ng/µL | 1.94 | 2.28 | Discarded; one-nucleotide deletion in sgRNA insert |
| D | D2 | 2026 cloning | JTJ520 | 1318.6 ng/µL | 1.91 | 1.74 | Discarded; one-nucleotide deletion in sgRNA insert |
| B | B1 | 2026 cloning | JTJ511 | 73.8 ng/µL | 2.01 | 2.14 | Not used; only partially readable Sanger sequence |

| Guide | Clone | Origin | LightRun Seq. ID | Concentration | A260/280 | A260/230 | Status |
|---|---|---|---|---|---|---|---|
| A | A1 | 2025 first batch | JTJ508 | 205.5 ng/µL | 1.98 | 2.13 | Not used; no readable Sanger sequence on first read (later rescued by replating, see A3/A4) |
| A | A2 | 2025 first batch | JTJ507 | 128.1 ng/µL | 1.92 | 1.86 | Not used; no readable Sanger sequence on first read (later rescued by replating, see A3/A4) |

Together, these Sanger-verification records document which sgRNA constructs were sequence-confirmed, which were excluded, and which clones were used for downstream perturbation experiments.

# Appendix F — RNA-FISH sample preparation and image QC

## F.1 First experiment: six-channel ibidi slide layout (D, B, NT)

This appendix documents the physical layout of the two RNA-FISH experiments described in §2.11 and analyzed in §3.4.1–§3.4.2, together with the direct image-QC evidence used to interpret the second-experiment E3 failure. The first experiment is the source of the FACS-derived single-cell results in §3.4.1; the second experiment extended the panel to guide A, used a longer four-day hybridization, and contributed the H100 guide-A and rescued guide-D results in §3.4.2. In the first experiment, six matched conditions were prepared in separate channels of a six-channel ibidi µ-slide before fixation and imaging, so that all conditions experienced the same staining, washing, and imaging steps in parallel. Cells from the FACS-derived BFP-enriched H100 subpopulation were seeded into the six channels in matched −dox and +dox pairs for guide D, guide B, and the non-targeting control. The +dox channels received doxycycline together with Shield-1 to induce dCas9 expression, while the matched −dox channels received the vehicle treatment used elsewhere in the project, so that each guide identity contributed one uninduced and one induced channel that differed only in the inducer.

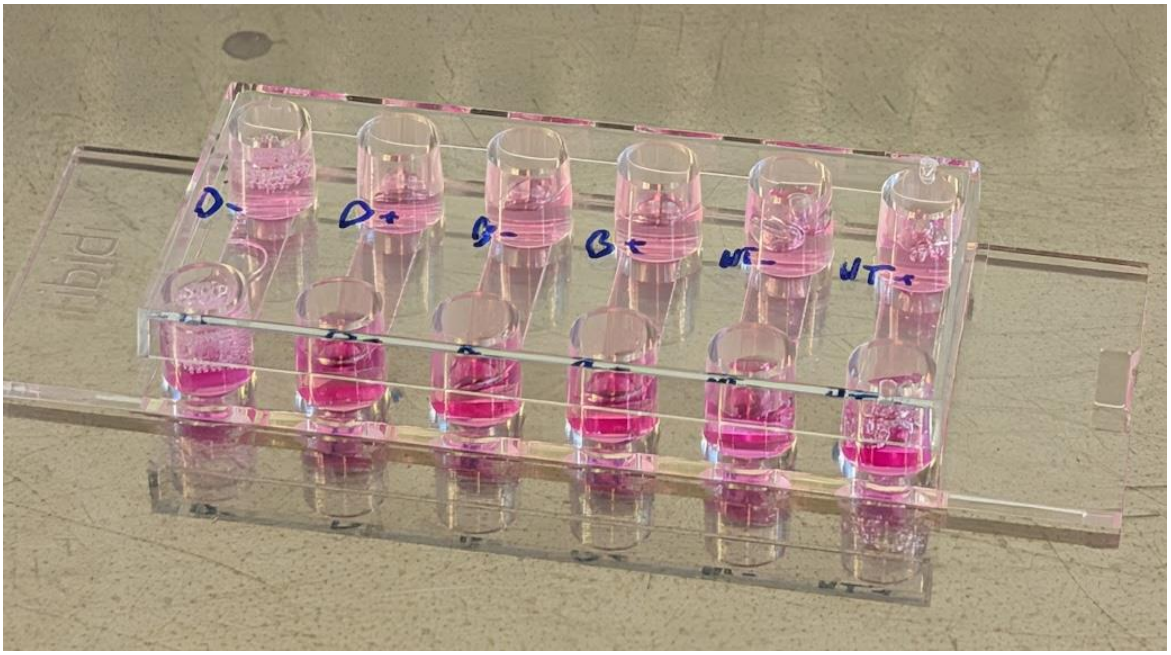


**Figure F.1. Six-channel ibidi µ-slide used for RNA-FISH sample preparation.** The six RNA-FISH conditions were prepared in separate channels before fixation and imaging, with matched uninduced and doxycycline/Shield-1-induced pairs for guide D, guide B, and the non-targeting control. Channel labels are written on the upper reservoirs in the photograph and read from left to right as D−, D+, B−, B+, NT−, NT+. Pink color reflects the medium phenol red rather than any condition-specific reagent.

**Table F.1.** Channel-to-condition mapping for the six-channel ibidi µ-slide shown in Figure F.1. Each channel was imaged as 10 fields of view per condition (Chapter 3, §3.4.1). Probes D1 and D2 detected GAPDH and MYC respectively in every channel.

| Channel | Condition | Guide identity | Induction state |
|---|---|---|---|
| 1 | D− | Guide D (CTCF-associated distal site) | Uninduced (vehicle) |
| 2 | D+ | Guide D (CTCF-associated distal site) | Doxycycline + Shield-1 induced |
| 3 | B− | Guide B (promoter-proximal CTCF site) | Uninduced (vehicle) |
| 4 | B+ | Guide B (promoter-proximal CTCF site) | Doxycycline + Shield-1 induced |
| 5 | NT− | Non-targeting control | Uninduced (vehicle) |
| 6 | NT+ | Non-targeting control | Doxycycline + Shield-1 induced |

## F.2 Second experiment: ibidi + 96-well glass-bottom plate layout (A, B, D, NT)

A second RNA-FISH experiment was carried out as a follow-up that extended the guide panel to include guide A and used a four-day primary-hybridization at a lower probe concentration (1 nM per target), as described in §2.11 and Table 2.9. The second experiment was performed in the H100 platform population (§2.2), in contrast to the first experiment which used the FACS-derived BFP-enriched H100 subpopulation. In this run, guide A, guide B, and the −dox NT control were prepared on a fresh six-channel ibidi µ-slide; guide D and the matched −dox/+dox NT pair were prepared in matched wells of a 96-well glass-bottom plate so that the +dox NT control could be recovered after a contamination event in the previously opened ibidi slide caused the +dox NT cells in channel 6 to die before fixation. The split layout means that the second experiment used two physical sample carriers in parallel; both were processed with identical fixation, hybridization, and post-hybridization handling.

**Table F.2.** Channel- and well-to-condition mapping for the second RNA-FISH experiment. Channel codes C1–C6 refer to the channels of the ibidi µ-Slide VI 0.5 Glass Bottom; well codes (e.g. B2) refer to the named wells of the 96-well glass-bottom plate. Channel C6 of the ibidi slide is listed as “not used” because the previously opened slide had a contamination in this channel that killed the +dox NT cells before fixation; the +dox NT condition was recovered on the 96-well plate. The probe-detection assignment was the same as in the first experiment (D1 → GAPDH, D2 → MYC).

| Carrier | Position | Condition | Guide identity | Induction state |
|---|---|---|---|---|
| ibidi 6-channel slide | C1 | B− | Guide B (promoter-proximal CTCF site) | Uninduced (vehicle) |
| ibidi 6-channel slide | C2 | B+ | Guide B (promoter-proximal CTCF site) | Doxycycline + Shield-1 induced |

| Carrier | Position | Condition | Guide identity | Induction state |
|---|---|---|---|---|
| ibidi 6-channel slide | C3 | A− | Guide A (promoter-proximal CTCF site, opposite strand to B) | Uninduced (vehicle) |
| ibidi 6-channel slide | C4 | A+ | Guide A (promoter-proximal CTCF site, opposite strand to B) | Doxycycline + Shield-1 induced |
| ibidi 6-channel slide | C5 | NT− | Non-targeting control | Uninduced (vehicle) |
| ibidi 6-channel slide | C6 | not used (contamination, +dox NT cells died) | — | — |
| 96-well glass-bottom plate | B2 | D− | Guide D (CTCF-associated distal site) | Uninduced (vehicle) |
| 96-well glass-bottom plate | B3 | D+ | Guide D (CTCF-associated distal site) | Doxycycline + Shield-1 induced |
| 96-well glass-bottom plate | E2 | NT− | Non-targeting control | Uninduced (vehicle) |
| 96-well glass-bottom plate | E3 | NT+ | Non-targeting control | Doxycycline + Shield-1 induced |

## F.3 E3 (NT+, plate) failure mode — direct image inspection

The +dox NT well on the 96-well plate (E3) was the only +dox NT condition in the second experiment after the ibidi C6 contamination loss, and it could not be used as a clean +dox NT baseline. Direct image inspection of E3 (Figure F.2) showed two compounding factors. First, Concanavalin A membrane staining failed across the well: instead of the per-cell membrane outlines required for the standard cell-segmentation step, the ConcA channel showed a uniform diffuse signal with no distinguishable cell boundaries. The DAPI nuclear channel and the GAPDH RNA-FISH channel in the same fields were healthy, so the failure was specific to ConcA, not a generic acquisition or staining problem. Second, the MYC RNA-FISH signal in E3 was genuinely lower per FOV than in the matched-protocol E2 well, independent of any cell-counting step: a segmentation-independent re-detection returned ~4× fewer MYC spots per FOV in E3 than in E2 (E3 / E2 density ratio 0.23), with per-FOV E3 counts tightly clustered, indicating a well-wide reduction rather than a localized technical artifact. A plausible explanation for the well-specific ConcA failure is cell-surface stress: Concanavalin A binds alpha-mannose / alpha-glucose residues on cell-surface glycoproteins, and stressed or dying cells can present an altered glycocalyx that gives diffuse rather than membrane-localized lectin signal. This remains an inference from the image phenotype, but it is consistent with the simultaneous ~4× per-FOV MYC reduction. The combined failure mode (ConcA broken + per-FOV MYC genuinely reduced) is what makes the E3 +dox NT condition unusable as a single-cell baseline in §3.4.2 (decision summarized in §F.5, Table F.4).

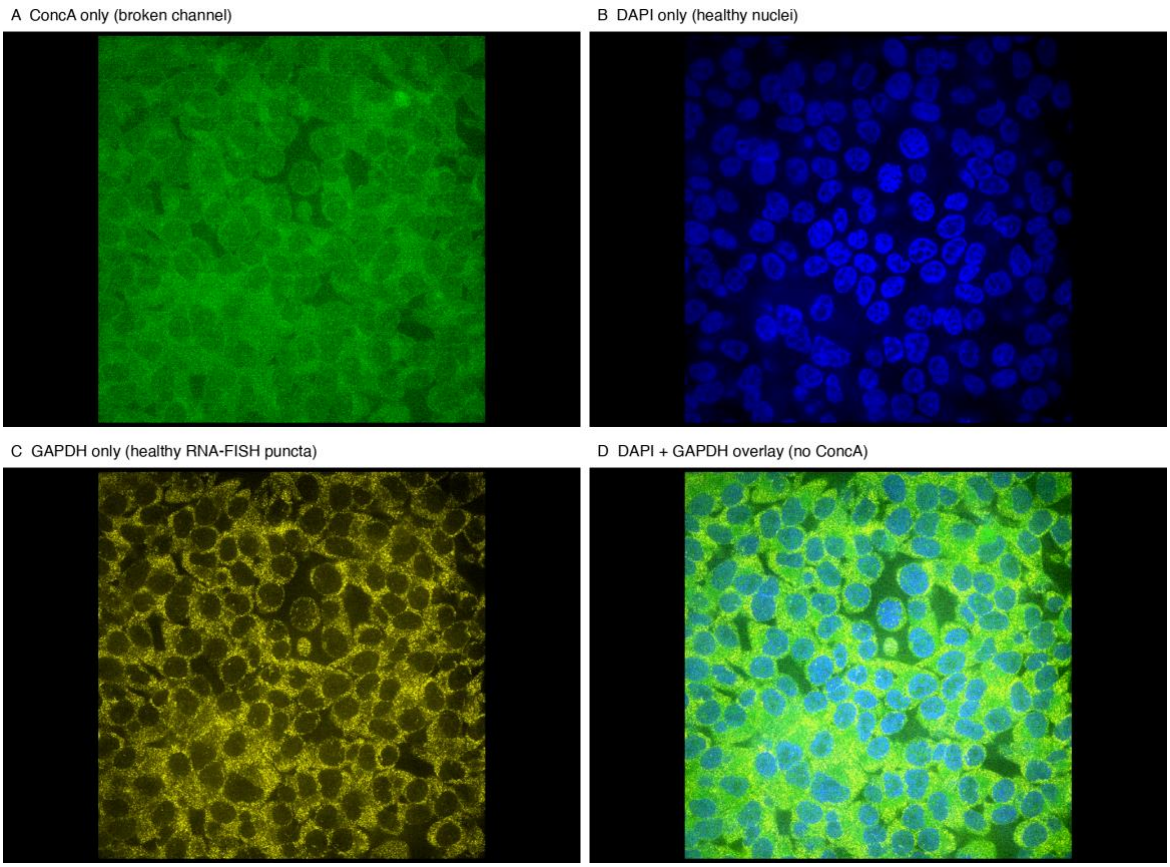


**Figure F.2. Direct image inspection of E3 (NT+, plate) confirming the ConcA segmentation failure.** Four-panel view of the same representative field of view from the `E3_D1.nd2` acquisition, with each napari layer shown in isolation: **(A)** ConcA-Alexa488 membrane channel — uniform diffuse green signal with no distinguishable cell boundaries (the failure mode that breaks the cell-mask watershed). **(B)** DAPI channel — densely-packed, well-segmented nuclei, confirming that cells are physically present and the DAPI staining worked normally. **(C)** GAPDH RNA-FISH channel — sparse, well-defined puncta in cytoplasm and perinuclear regions, characteristic of healthy single-molecule FISH signal. **(D)** DAPI + GAPDH overlay (no ConcA) — cells are clearly resolved by the combination of nuclear and cytoplasmic-RNA channels, demonstrating that the per-cell biology is recoverable by the imaging step itself; only the ConcA channel — the standard-pipeline input for cell-membrane segmentation — failed.

The ConcA failure was specific to the E3 well, not a generic property of the 96-well plate format or of the second-experiment imaging session. Direct image inspection of the matched −dox NT well on the same plate (E2; Figure F.3) and of one of the second-experiment ibidi channels (C1, B−; Figure F.4) shows ConcA producing the well-defined per-cell membrane outlines required for cell-mask watershed segmentation in both formats. Together with Figure F.2, these confirm that the failure mode noted in §3.4.2 (and audited in §F.5, Table F.4) for the +dox NT comparator is a per-well event in E3 specifically, not a systematic loss of signal in the second experiment.

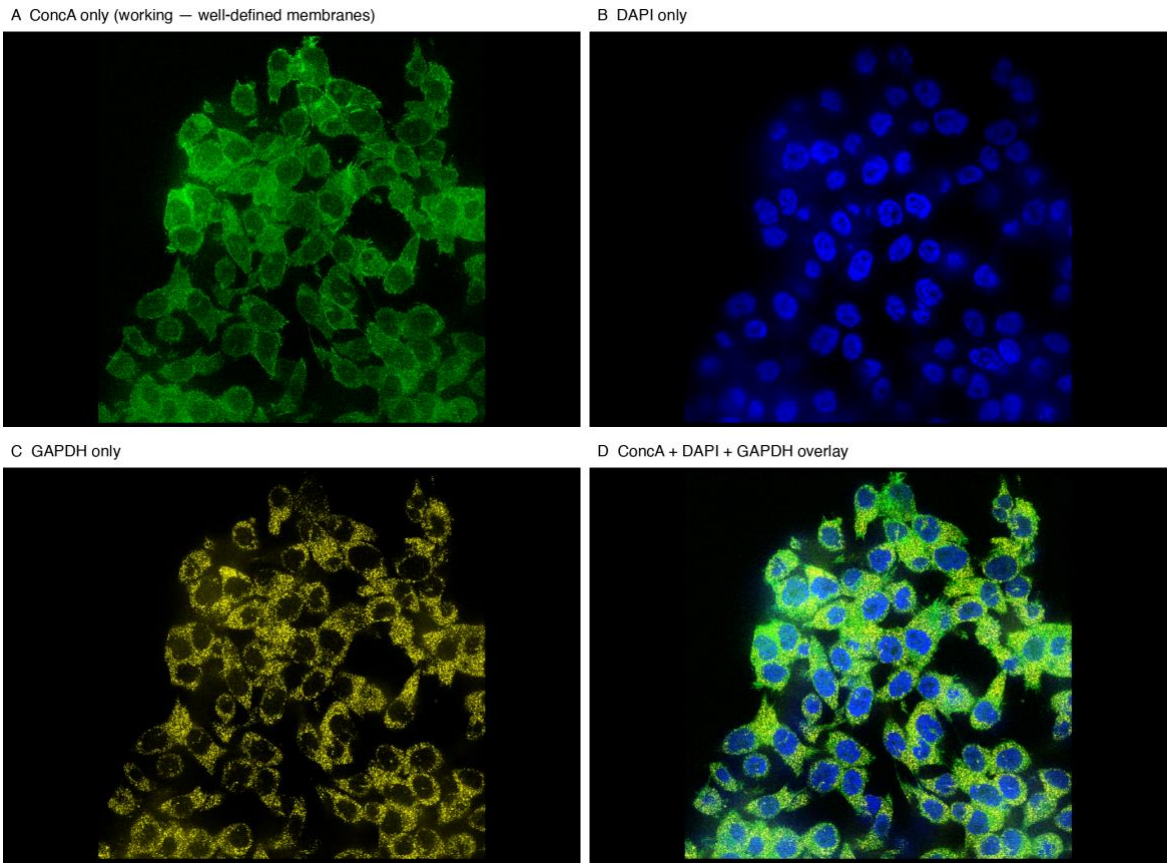


**Figure F.3. Working ConcA on the same 96-well plate format as E3.** Same four-panel layout as Figure F.2, applied to a representative field of view from the `E2_D1.nd2` acquisition (NT−, plate). Panel **(A)** shows ConcA-Alexa488 membrane staining with crisp per-cell outlines — the working membrane signal that supports cell-mask segmentation in the standard pipeline, in contrast to Figure F.2 panel A. Panels **(B)** and **(C)** show the matched DAPI and GAPDH channels; panel **(D)** is the tri-channel overlay (ConcA + DAPI + GAPDH).

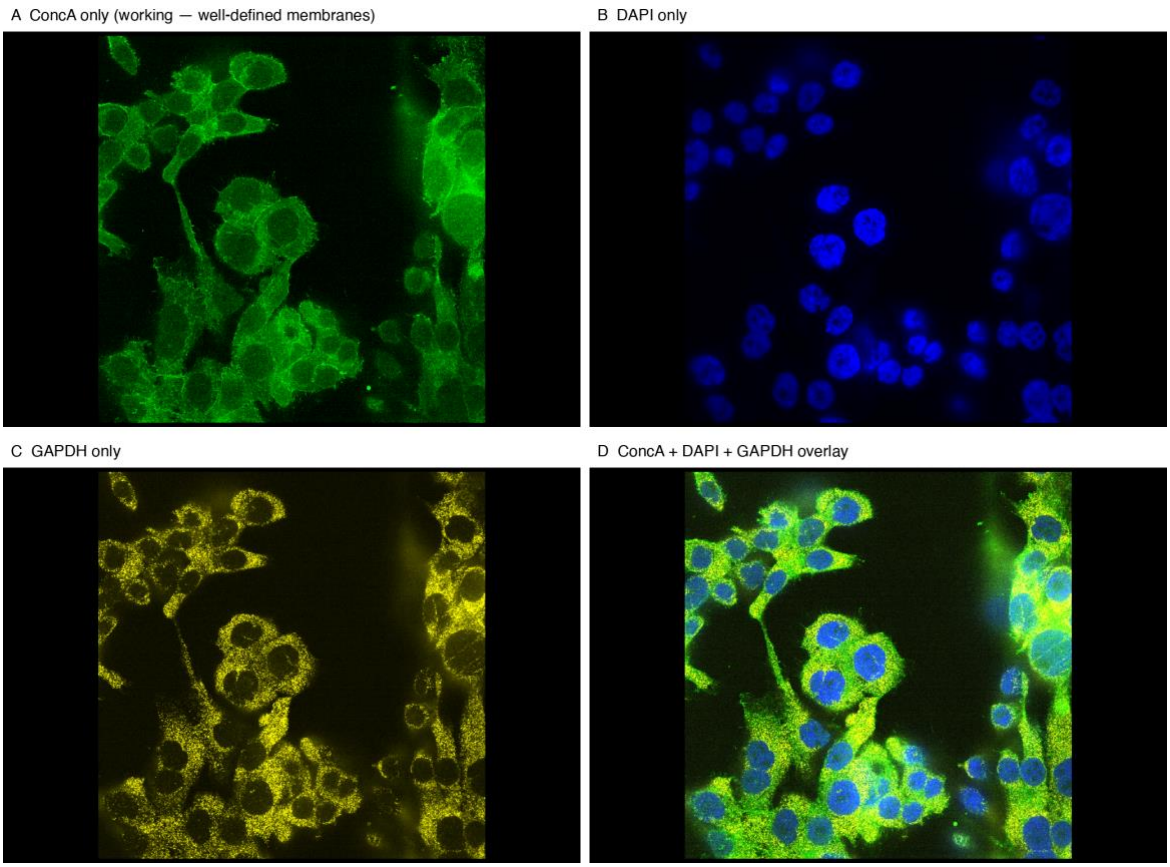


**Figure F.4. Working ConcA on the second-experiment ibidi slide.** Same four-panel layout as Figure F.2, applied to a representative field of view from the `C1_D1.nd2` acquisition (B−, ibidi). Panel **(A)** shows ConcA-Alexa488 membrane staining with crisp per-cell outlines on the ibidi format. Panels **(B)** and **(C)** show the matched DAPI and GAPDH channels; panel **(D)** is the tri-channel overlay.

Therefore, E3 was not used as a matched +dox NT single-cell comparator in the second RNA-FISH experiment. NT− is shown only as a parallel −dox baseline.

## F.4 Guide-D plate-well channel-order rescue

The guide-D wells in the second experiment (B2 = D−, B3 = D+) were initially suspicious because the standard exported tables contained ~30–70× fewer RNA-FISH spots than the other conditions, despite normal segmented-cell counts. The later diagnosis was a file-level channel-order mismatch rather than a biological or plate-format failure. In the morning-batch files, the RNA-FISH channel was channel index 0; in the B2 / B3 acquisitions, DAPI was channel index 0 and MYC was channel index 2. The standard pipeline therefore detected bright DAPI structures as if they were RNA-FISH spots until the channel order was corrected.

An initial in-house corrected-channel rescue showed that re-running B2 and B3 with the correct channel indices recovered morning-batch-like single-molecule FISH profiles and produced a quantitative guide-D contrast in the H100 platform population. Jonas Grini subsequently re-processed the same B2 / B3 acquisitions

with the corrected channel order using the laboratory image-analysis workflow. This corrected Jonas output is treated as the primary guide-D analysis in §3.4.2 because it follows the laboratory workflow, while the in-house rescue is retained as a supporting sensitivity analysis. During Jonas's re-processing, an initial May 14 export revealed a B3 D1/D2 assignment issue in which MYC-derived values had been assigned to GAPDH; this was corrected on May 15, and the corrected May 15 output is the primary analysis shown in Table F.3. Both corrected analyses supported reduced per-cell MYC after induction for guide D and agreed closely in direction and approximate magnitude: Jonas corrected re-processing gave a D+ / D− per-cell mean MYC fold change of 0.48, while the in-house corrected-channel rescue gave 0.52.

**Table F.3. Guide-D second-experiment corrected-channel analysis summary.** Jonas Grini's corrected re-processing is used as the primary guide-D analysis in §3.4.2 because it follows the laboratory image-analysis workflow. The in-house corrected-channel rescue was performed first and is retained as a supporting sensitivity analysis. Both analyses recovered the same direction and similar magnitude of MYC reduction after induction; absolute counts differ between pipelines because segmentation and spot assignment differ, but the D+ / D− fold-change direction is stable.

| Analysis | Role | D− mean MYC | D+ mean MYC | MYC FC | MYC/GAPDH FC |
|---|---|---|---|---|---|
| Jonas corrected re-processing (May 15) | Primary corrected guide-D analysis | 61.8 | 29.9 | 0.48 | 0.35 |
| In-house corrected-channel rescue | Supporting sensitivity analysis | 34.8 | 18.1 | 0.52 | 0.43 |

## F.5 RNA-FISH QC and rescue decision summary

The RNA-FISH analysis contains several exclusions and rescues, but they fall into a small number of decision types. Table F.4 summarizes how each issue was handled and what it changes in the interpretation.

**Table F.4. RNA-FISH QC and rescue decision audit (§3.4.1–§3.4.2).** FOV-level exclusions were applied by the pre-declared technical criteria (GAPDH/reference-channel failure, MYC-to-cell assignment failure, segmentation/focus failure, coherent within-channel acquisition artifact) — never by MYC outcome.

| Dataset / condition | Issue | Decision | Interpretive consequence |
|---|---|---|---|
| Experiment 1, D+ C2 FOV6 | MYC detection / assignment artifact | excluded from headline; rescued as sensitivity check | D direction unchanged; MYC-only FC weakens slightly |
| Experiment 1, NT FOVs | weak GAPDH or MYC-to-cell assignment failure | excluded before fold-change calculation | QC-filtered NT does not mimic B/D decrease |

| Dataset / condition | Issue | Decision | Interpretive consequence |
|---|---|---|---|
| Experiment 2, B− C1 FOVs 0–6 | coherent low-signal block in GAPDH and MYC | excluded from guide-B FC calculation | B in H100 remains conditional |
| Experiment 2, D B2/B3 | wrong channel read as RNA-FISH | Jonas corrected re-processing used as primary guide-D analysis; in-house corrected-channel rescue retained as supporting sensitivity analysis | Both analyses support reduced per-cell MYC after induction (Table F.3) |
| Experiment 2, NT+ E3 | ConcA failure plus ~4× lower MYC density | QC-only; excluded from NT +/− interpretation | no clean matched +dox NT comparator (§F.3) |
| Experiment 2, NT− E2 | working plate-format NT− profile | retained as plate reference only | confirms E3 was a per-well failure |

## F.6 Compact H100 ibidi RNA-FISH summary

Table F.5 is the compact per-cell summary for the ibidi part of the second RNA-FISH experiment (guides A and B and the parallel NT− baseline). Plate-format conditions are not included here: rescued guide D is summarized in Appendix F.4 (Table F.3), and the failed E3 +dox NT comparator is documented in Appendix F.3 and audited in Appendix F.5 (Table F.4).

**Table F.5. Compact ibidi-channel summary for the second H100 RNA-FISH experiment.** Per-cell MYC is the headline biological readout. Guide B is shown using the retained B− FOVs 7–9 subset because C1 FOVs 0–6 were excluded as a within-channel acquisition artifact (§2.12; Table F.4). NT− is shown as a parallel −dox baseline only because the matched +dox NT condition was not recovered as a usable single-cell comparator (§F.3).

| Guide | Condition | Cells | Median per-cell MYC | Headline MYC FC | Interpretation |
|---|---|---|---|---|---|
| A | A− (C3) | 478 | 46 | — | matched uninduced baseline |
| A | A+ (C4) | 662 | 33 | 0.64 | reduced per-cell MYC after induction |
| B | B− (C1, retained FOVs 7–9) | 149 | 32 | — | conditional uninduced baseline |
| B | B+ (C2) | 733 | 22 | 0.70 | weaker conditional reduction |
| NT | NT− (C5) | 605 | 40 | — | parallel −dox baseline only |

Together, these RNA-FISH setup, QC, exclusion, and rescue records provide the audit trail behind the single-cell MYC expression conclusions in §3.4.

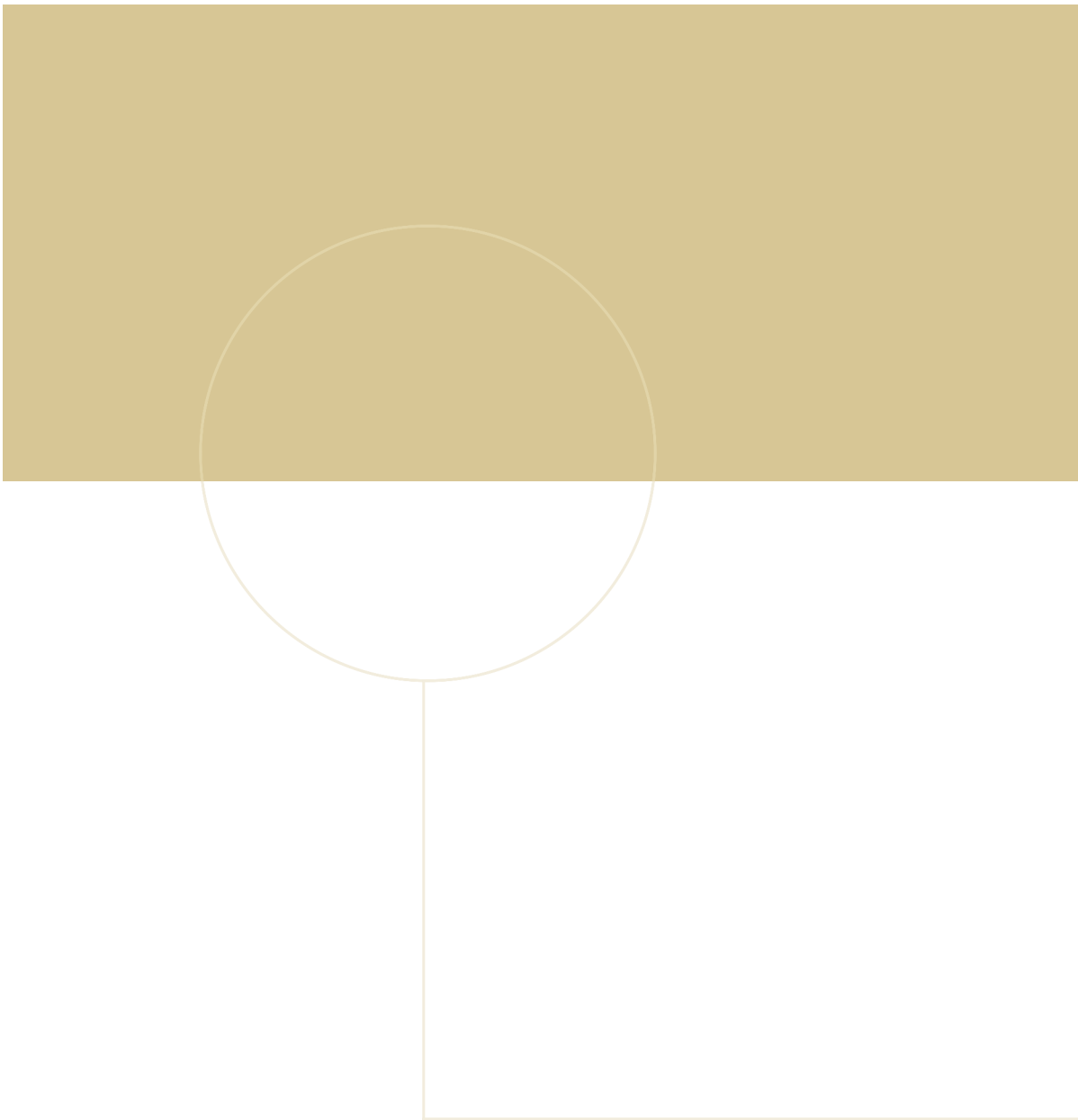

NTNU

Norwegian University of
Science and Technology